MINERALOGICAL CHARACTERISATION OF BRITTLENESS INDICES OF PLATINUM-BEARING REEFS (UG 2), LOCATED IN THE EASTERN LIMB OF THE BUSHVELD IGNEOUS COMPLEX

BY

NCEDO MATRICIA MATUKANE

DISSERTATION SUBMITTED FOR THE DEGREE OF MASTER OF SCIENCE IN GEOLOGY IN THE DEPARTMENT OF GEOLOGY AND MINING, SCHOOL OF PHYSICAL AND MINERAL SCIENCES, FACULTY OF SCIENCE AND AGRICULTURE, UNIVERSITY OF LIMPOPO, SOUTH AFRICA.

MAIN SUPERVISOR: PROF FHATUWANI SENGANI
CO-SUPERVISOR: MS KGOETJA. A. RAMAKADI

2025

DECLARATION

I, **Matukane Ncedo Matricia**, do hereby declare that this dissertation is the result of my investigation and research that has not been submitted in part or full for any other degree to any university or publication houses (journal, conference proceedings, etc).

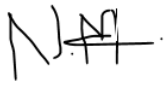

Matukane NM

DEDICATION

I dedicate this work to my beloved parents, Mr Mandla Wiseman Matukane and Mrs Cynthia Sithembile Matukane. Their unwavering emotional support, financial support and love have been the cornerstone of my journey. I am eternally grateful.

To my younger brother, Feza Kuhle Matukane, who has inspired me with his determination and competitive spirit. I am fuelled by your ambition.

ACKNOWLEDGEMENTS

Special thanks go to the Department of Geology and Mining at the University of Limpopo, Turfloop Campus, for allowing me the opportunity to pursue not only this study but also for providing a sturdy foundation from my first year of study. I would like to extend my appreciation for the sponsorship from SAMERDI and the collaboration with the University of Pretoria.

I extend my heartfelt thanks to my supervisor, Prof. Fhatuwani Sengani, and my co-supervisor, Ms. K.A. Ramakadi, for their invaluable guidance and supervision. This work would not have been possible without their input and leadership.

I would also like to acknowledge my master's colleagues for their contributions and emotional support during the initial stages of this study.

Lastly, I express my utmost gratitude to my friends, who have been my emotional pillars throughout this journey.

ABSTRACT

The brittleness of rocks has traditionally been measured utilizing mechanical properties, however, it has been established that the mechanical properties of rock masses strongly depend on their petrographic properties, and mineralogical composition plays a critical role in determining the property of rocks to fail. Despite the existence of established brittleness indices based on the mineralogical composition of rocks, the selection of brittle components in rocks remains subjective and can be contradictory. The effects of porosity, stress state, cement type and strength, pre-consolidation factor, grain size, and external mechanical conditions are also not considered in the existing brittleness indices. This study aims to characterize the brittleness indices of platinum-bearing (UG2) reefs on the eastern limb of the Bushveld Igneous Complex using mineralogical analysis. To this aim, microscopic examinations identified different mineralogical characteristics, laboratory analysis of UG2 samples was performed to obtain the mechanical parameters, and additional parameters were obtained from numerical simulations. Innovative brittleness indexes (B1, B2, B3, B4, and B5) are developed utilizing parameters such as textural variables, contact type, contact nature, and packing density. The brittleness indexes are additionally compared with previous important brittleness indices utilizing fieldwork, laboratory analysis, numerical simulation, and predictions (multivariate linear models). Additionally, a similar approach was applied to the mechanical parameters, developing innovative brittleness indexes B1, B2, B4 and B6 using traditional mechanical parameters. The results revealed that contact type and contact nature were the most significant mineralogical predictors of brittleness, with models B2 and B6 demonstrating strong predictive accuracy (R^2 values of 0.778 and 0.727, respectively) and near-perfect precision (SE = 0.000). Texture and packing variables had a lesser impact on brittleness prediction. While tensile (σt) and compressive strength (σc) emerged as key predictors with high accuracy. Models B2 and B6 were the most reliable, showing near-perfect precision with SE values of 0.000. In contrast, models B1 and B4 were less precise, and B3 lacked statistical significance. The high statistical significance and low SE values of B2 and B6 confirmed their reliability for brittleness prediction. It is recommended that more sophisticated methods be applied as well.

Keywords: Brittleness index, Upper Group 2, mineralogy, predictive models

TABLE OF CONTENTS

List of Figures

List of Tables

List of abbreviations

ANN	Artificial Neural Networks
BI	Brittleness Index
BIC	Bushveld Igneous Complex
BMLR	Backward Multiple Linear Regression Analysis
BMS	Base Metal Sulphide
BTS	Brazilian Tensile Strength
Ga	Giga annum
GPa	Giga Pascals
MG2	Middle Group 2
MG3	Middle Group 3
PGE	Platinum Group Elements
PGM	Platinum Group Metals
PLS	Point Load Strength
SE	Specific Energy
SE	Standard Error
SEE	Standard Error of Estimate
SIPS	Surface Instability Peak Stress
TS	Tensile Strength
UCS	Uniaxial Compressive Strength
UG2	Upper Group 2
USA	United States of America

List of symbols

σ_c	Compressive strength
σ_t	Tensile strength
ep	Peak strain
E	Young's modulus
υ	Poisson's ratio
φ	Angle of internal friction
c	Cohesion
τ	Shear stress
εp	Peak strain
ρ	Roundness
Ψp	Sphericity
∞	Infinity
τ_p	Peak strength
τ_r	Residual strength

CHAPTER ONE

INTRODUCTION

1.1 Introduction

Brittleness is an important characteristic of hard rocks and essential in rock mechanics and rock engineering. Chen et al (2019) have defined the brittleness of rock as "*a material property describing the material loss of carrying capacity with a small deformation*". The previously denoted definition is one of the common definitions provided by different researchers because it is standardized (Meng, Wong, and Zhou, 2020; Zhang et al., 2021; Zhang, Ranjith, and Perera, 2016; Xia et al., 2017; Tao et al., 2020; Kavi, Amer, and Molladavood, 2018; Wang et al., 2020; Xia et al., 2019).

Rock brittleness contributes to multiple failure processes and mechanical responses of rock mass such as rock stability, drillability and cutability associated with rock excavation (Wang et al, 2017). Among the outlined significant effects of brittleness, the safe selection, and design of excavation remains imperative (Meng, Wong and Zhou, 2020). Similar to the definition, multiple brittleness indexes have been developed by scholars across many fields (Meng, Wong and Zhou, 2020; Zhang et al, 2021; Zhang, Ranjith and Perera, 2016; Wang, 2019; Wang et al,2019; Wang et al,2020). As such, there are many brittleness indexes of which the majority are based on the concept of stress-strain relationship (mechanical parameters of a rock), while few are on the mineralogy of the rock unit. The mechanical parameters (deformation characteristics and strength) of rock masses are typically measured using laboratory tests and these parameters strongly depend on their petrographic properties (Nouri et al, 2022). However, most of the brittleness indexes do not consider petrographic characteristics such as grain size, and grain contacts among others when designing the brittleness index. Therefore, the above-mentioned gap motivated the current study that is intended to develop new brittleness indexes for Platreef (Upper Group 2 "UG2") using petrographic characteristics and empirical models.

1.2 Problem statement

It has been indicated in the literature that a standardized measurement of brittleness has not yet been established (Meng, Wong, and Zhou, 2020; Zhang *et al*., 2021; Zhang, Ranjith, and Perera, 2016; Xia *et al*., 2017; Tao *et al*., 2020; Kavi, Amer, and Molladavood, 2018; Wang *et al*., 2020; Xia *et al*., 2019) and brittleness is quantified using a brittleness index (Zhang *et al*., 2016). A standardized method for establishing the brittleness index does not yet exist (Meng, Wong and Zhou, 2020; Zhang *et al*, 2021; Zhang, Ranjith and Perera, 2016; Wang, 2019; Wang *et al*,2019; Wang *et al,*2020). Altindag (2009) pointed out that researchers apply brittleness and the brittleness index differently for different motives. The brittle failure of rocks is influenced by a combination of intrinsic and external factors (Wang *et al*., 2017; Xia *et al*., 2019; Zhang *et al*., 2021). Among the intrinsic factors, the mineralogical composition is critical in determining the property of rocks to fail, as determined by Young's modulus (Zhang, Ranjith and Perera, 2016).

Minerals such as quartz and clay can be classified as brittle or ductile (Xia *et al*., 2019; Hasson *et al*., 2022). Previous studies, including Wang *et al* (2015) and Yongshang *et al* (2020), have established that the mechanical properties of rock masses strongly depend on their mineralogical compositions. In the literature, brittleness indices estimated using mineralogical compositions are denoted by B_{24}–B_{28} (Xia *et al*., 2019). Fractions of strong/brittle minerals, weak/ductile minerals, and carbonate in volume (%) are used to determine the brittleness index B_{24}. In the brittleness index, B_{24}, hard, and strong minerals are the principal constituents of rock brittleness. The varying constituents of rocks are the reason for brittle failure, as determined by the brittleness indices B_{25}–B_{28} (Xia *et al*., 2019). Despite the existence of established brittleness indices based on the mineralogical composition of rocks, the selection of brittle components in rocks remains subjective. For example, carbonates are considered brittle in brittleness index B_{25} and plastic in brittleness index B_{27}, which is contradictory (Xia *et al*., 2019). The effects of porosity, stress state, cement type and strength, pre-consolidation factor, grain size, and external mechanical conditions are also not considered in the existing brittleness indices (Meng *et al*., 2019; Xia *et al*., 2019). Existing methods also do not consider the complex nature of rock formation, including multi-stage tectonic movement and geological evolution over millions of years (Meng

et al., 2019). The lack of consideration of the above-mentioned factors and the subjective nature of the existing brittleness indices that are based on mineralogical composition highlights the need for the development of a new predictive model that considers all factors. This study proposes to determine the brittleness indices of platinum-bearing reefs (UG2) using mineralogical characteristics and therefore develop predictive models.

1.3 Aim of the project

The research project aims to characterize the brittleness indices of platinum-bearing reefs (UG2), located on the eastern limb of the Bushveld Igneous Complex, using mineralogical studies.

1.4 Objectives

The objectives of the study are as follows:

I. To determine the brittleness of the UG2 reef based on empirical formulas (mechanical estimation methods).

II. To estimate the brittleness indexes of the UG2 reef from petrographic characteristics.

III. To develop predictive models for indexes of UG2 reef.

1.5 Justification of the study

South Africa is the main global supplier of PGM (Hughes et al, 2021; Kolbadinejab and Ghaemi, 2023). There is an increase in global demand for platinum (Kolbadinejab and Ghaemi, 2023). Rasmussen et al (2019) projected a possible 240-fold increase in global platinum demand by the year 2050 due to the significant demand for fuel-cell vehicles and green hydrogen (Li *et al* 2023). With the increase in platinum demand, there is a need for South African mines to be globally competitive, safe, and competent, in the wake of the fourth industrial revolution. This presents a need for the design and production of more effective mining machinery. An accurate determination and understanding of the brittleness indices of platinum-bearing reefs (UG2) is essential.

The brittleness of rock masses contributes to many essential rock behaviours, some of which directly impact human life, such as slope instability and mine production. This research therefore contributes to the safety of mine workers, as the brittleness indexes determined will provide essential information that can be used to put safety measures in place as needed and can help engineers in the design and usage of suitable mining machinery for better mine production. It is however anticipated that the study will strive to provide a better description of the mechanical properties of the rock mass that may be needed for future projects in the area.

1.7 Location of the study area

The Bushveld Igneous Complex is the largest layered igneous intrusion on Earth's crust (Huthmann et al,2016; Mukherjee, Latypov and Balakrishna, 2017; Mayer et al,2020; Langa et al,2021). It is located in the Northeastern part of the Kaapvaal Craton in South Africa (Scoon and Viljoen, 2018; Mutele and Hunt, 2022). Traditionally, it was believed to range in size from approximately 60,000 km^2 to 65,000 km^2 (Eales and Cawthorn, 1996; Maier et al., 2013). However, a geophysical study by Finn et al (2015) indicated that the complex covers a total area of more than 90,000 km2. (Figure 1). It is Paleoproterozoic in age, dated at approximately 2.5 Ga (Huthmann et al,2016; Mayer et al,2020; Langa et al,2021). The eastern limb of the Bushveld Igneous Complex is located within the Mpumalanga and Limpopo provinces (figure 2). It outcrops in a distinct physiographic region located in northeastern South Africa, termed the Middleveld region. Layered ultramafic-mafic rocks of the Rustenburg Layered Suite and metamorphic aureole outcrop in local escarpments and arcuate ridges in the mountainous landscape created by the superimposed drainage of the Olifants and Steelpoort Rivers (Scoon and Viljoen 2019).

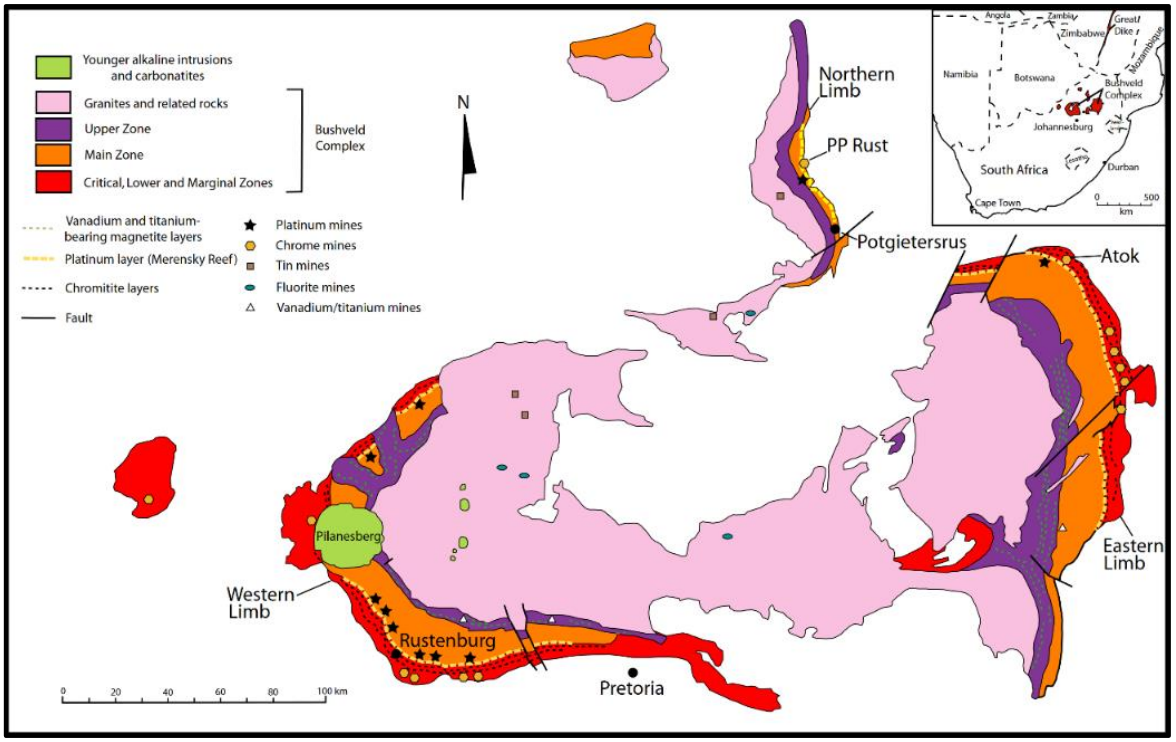

Figure 1. 1 Geological map showing the location of the Bushveld Igneous Complex in South Africa. Taylor et al (2018)

1.8 Layout of the dissertation

Following the introductory chapter, the dissertation is comprised of various chapters with different purposes. The chapter following the introductory chapter is the literature review chapter (Chapter Two). In the literature review, a summary of the geology of the study area is documented, and following that, a detailed literature review of brittleness index methods is documented. The literature chapter revealed that though there are various brittleness index methods, all methods suffer from various disadvantages. As such there is room to explore the use of mineralogical characteristics to develop the brittleness index of the UG2 reef since none of the previous methods can be accurately used to predict the brittleness of the UG2 reef.

Following the knowledge gap, detailed methodologies are reported in chapter three. The methodology incorporates a reconnaissance survey, data collection, laboratory analysis, numerical analysis, and statistical analysis. The collected data led to the analysis of the data in Chapter Four. The first results chapter focuses on developing new brittleness methods with the use of empirical methods (mechanical methods for brittleness index). Indeed, various new methods were developed to accurately

estimate the brittleness of UG2 based on mechanical methods. Similarly, mineralogical characteristics were also implemented to develop new brittleness methods and that was successfully achieved in Chapter Five. Lastly, conclusions and recommendations are reported in Chapter Six.

CHAPTER TWO

LITERATURE REVIEW

2.1 Introduction

This chapter commences with details on the geology of the study area, which incorporates the description of Bushveld Igneous Complex, Rustenburg layered suite, UG2 chromitite layer, among others. The second section of the chapter incorporates a detailed review of the rock brittle index and its methodologies.

2.1 Geology of the study area

2.1.1 The Bushveld Igneous Complex

The Bushveld Igneous Complex outcrops in three distinct limbs: eastern, western, and northern limbs. Some researchers recognize a fourth limb, the far-western limb (Huthmann et al,2016; Mukherjee, Latypov and Balakrishna, 2017; Mayer et al,2020; Scoon and Viljoen 2019). The limbs were traditionally considered separate entities; however, gravity data suggest that the western and eastern limbs are connected at depth under the Bushveld granites and younger sedimentary rocks (Nguuri et al., 2001; Cawthorn and Webb, 2001; Webb et al., 2003; Finn et al., 2015). The western and eastern limbs intruded entirely into rocks of the Transvaal Supergroup, and the northern limb lapsed into Archaean basement rocks (Mukherjee, Latypov and Balakrishna, 2017; Scoon and Viljoen 2019; Mayer et al,2020; Langa et al,2021). The Bushveld Igneous Complex is composed of three main components: the Lebowa Granite Suite, the Rashoop Granophyre Suite and the Rustenburg Layered Suite (Scoon and Viljoen 2019; Mayer et al, 2020).

2.1.2 The Rustenburg Layered Suite

The Rustenburg Layered Suite is the mafic-ultramafic phase of the larger Bushveld Igneous Complex (Huthmann et al,2016; Mayer et al,2020; Roelofse et al,2022; Setera et al,2023). It is the largest layered mafic-ultramafic complex in the world and the most studied part of the Bushveld Igneous Complex (Mungall, Kamo and McQuade, 2016; Langa et al,2021; Skursch et al,2022). The approximately 9 km-thick assemblage of intrusive magmatic and associated rocks stretches approximately 450 km east to west and 350 km north to south (Vermaak 1976; Eales and Cawthorn 1996). It is dated c.

2055.91 ± 0.26 Ma (Zeh et al., 2015). The stratigraphy is complex but ultimately conveys an upward evolution of rocks into progressively more chemically and lithologically evolved rocks (Setera et al,2023). It is vertically divided into five stratigraphic zones: marginal, lower, critical, main, and upper zones, based on the cumulus mineral assemblages (Figure 2.1). The five zones contain varying groups of cumulates with distinctive marker layers (Huthmann et al,2016; Mungall, Kamo and McQuade, 2016; Mukherjee, Latypov and Balakrishna, 2017; Scoon and Costin, 2018; Scoon and Viljoen 2019; Mayer et al,2020; Langa et al,2021; Skursch et al,2022; Setera et al,2023). Although lateral facies are prevalent, not all zones are always present. Individual layers of the Rustenburg Layered Suite are relatively consistent in the western and eastern lobes and can vary in thickness from millimetres to tens of metres (Huthmann et al,2016; Mukherjee, Latypov and Balakrishna, 2017; Scoon and Viljoen, 2019).

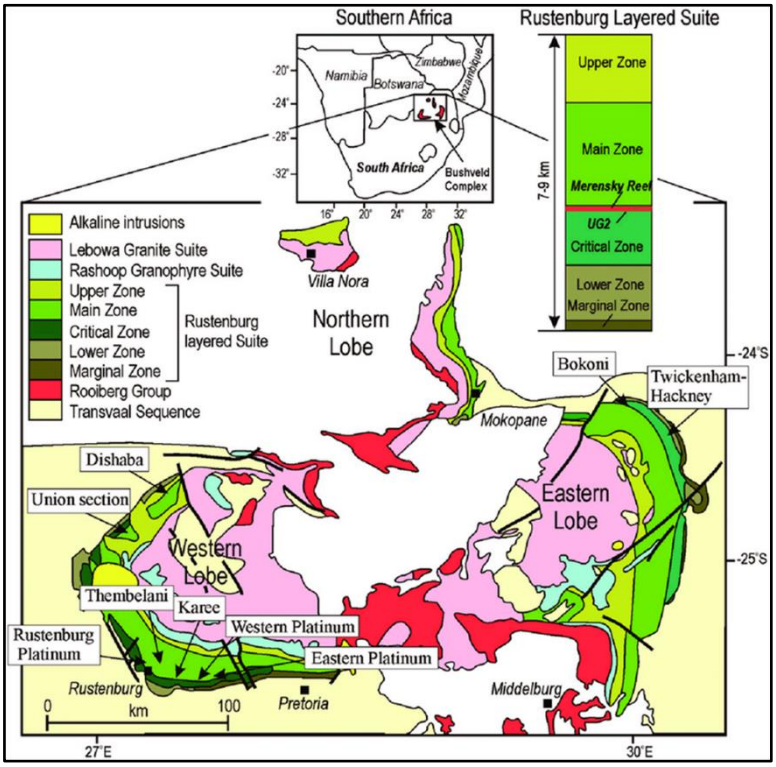

Figure 2. 1 location and schematic diagram of the Bushveld Igneous Complex (Rustenburg layered suite), showing the location of the UG2 chromitite layer (Latypov *et al*., 2015).

2.1.3 Zones of the Rustenburg Layered Suite

In accordance with the stratigraphic law of superposition, the layers of the Rustenburg Layered Suite are assumed to occur in chronological order from oldest to youngest (Mungall, Kamo and McQuade, 2016).

The marginal zone is considered to be the result of quenching of the intruding magma against the floor rocks. It contains units that range in thickness between 0-100 mm (Maier et al., 2013) and is composed of fine-grained norite to gabbronorite and pyroxenites. Xenoliths of anorthosite, dolostone, and quartzite are also present. The zone is classified into three suites, B1, B2, and B3, based on their contact with the lower zone, critical zone, or main zone. (Mukherjee, Latypov and Balakrishna, 2017; Mayer et al,2020).

The lower zone outcrops as through-like bodies that are unconnected. Because of variations in floor topography, the thickness of the zone varies, with the thickest parts reaching up to 13 mm (Wilson, 2012). It is ultramafic in composition and mainly composed of orthopyroxenite, harzburgite, and dunite. The appearance of chromitite seams marks a transition to the critical zone (Mungall, Kamo and McQuade, 2016; Mukherjee, Latypov and Balakrishna, 2017; Mayer et al,2020).

The critical zone occurs in multiple compartments and sectors and is segregated from each other along the strike. The main characteristic of the critical zone is the occurrence of chromitite layers. The chromitites are divided into three distinct clusters: seven lower group (LG) chromitites, four middle group (MG) chromitites and three upper group (UG) chromitites, numbered in sequence from top to bottom (Mungall, Kamo and McQuade, 2016; Mukherjee, Latypov and Balakrishna, 2017; Mayer et al,2020). It is divided into lower and upper critical zones.

The lower critical zone is 700-800 m in thickness (Maier et al., 2013). It is ultramafic in composition and primarily composed of orthopyroxenite with some olivine-rich intervals (Kruger 2005; Mukherjee, Latypov and Balakrishna, 2017; Mayer et al,2020; Mayer et al,2020). An anorthosite layer between MG2 and MG3 is used as a marker to separate the upper and lower critical zones (Mayer et al,2020). The upper critical zone is 500m in thickness (Maier et al., 2013). It is primarily composed of norite, pyroxenite, and anorthosite. It has significant PGE mineralization, mainly contained in

the Merensky Reef and the UG2 chromitite layer (Mungall, Kamo and McQuade, 2016; Mukherjee, Latypov and Balakrishna, 2017; Mayer et al,2020). A mottled anorthosite layer above the Merensky Reef is used as a marker to separate the critical zone from the marginal zone (Mayer et al,2020).

The marginal zone is 2-3 km thick and primarily composed of grabbronorite-norite sequences. The boundary between the upper and marginal zones is marked by the first appearance of magnetite layers (Maier et al., 2013; Mukherjee, Latypov and Balakrishna, 2017; Mayer et al,2020).

The upper zone is 1–2 km thick and primarily composed of diorite, gabbronorite, anorthosite, and magnetite (Maier et al., 2013; Mukherjee, Latypov and Balakrishna, 2017; Mayer et al,2020).

2.1.4 The eastern limb of the Bushveld Igneous Complex

The Rooiberg Group, the oldest part of the Bushveld Igneous Complex, is highly developed in the interior plateau of the southern half of the eastern limb (Figure 2.2). The upper section of the Transvaal Supergroup, the Pretoria Group, was intruded by 0nvsthe Rustenburg Layered Suite below the Rooiberg felsites and granophyre (Hall, 1932). A thick succession of metasediments, primarily quartzite, shales, and hornfelds, constitute the majority of the Pretoria Group (Eriksson and Clendenin 1990; Scoon and Viljoen 2019).

The Rustenburg Layered Suite predominantly overlies quartzite from the Magaliesberg and other formations in the northern sector of the eastern limb but gradually ascends into younger strata in the southern sector, including the Dullstroom volcanics. The Lebowa Granite Suite is composed of thick sheets of granite and a granophyre overlay and partially intrudes into the Rustenburg Layered Suite. In the northern sector of the eastern limb, granitic sheets replaced older felsites as the ceiling of the Rustenburg Layered Suite (Scoon and Viljoen 2019).

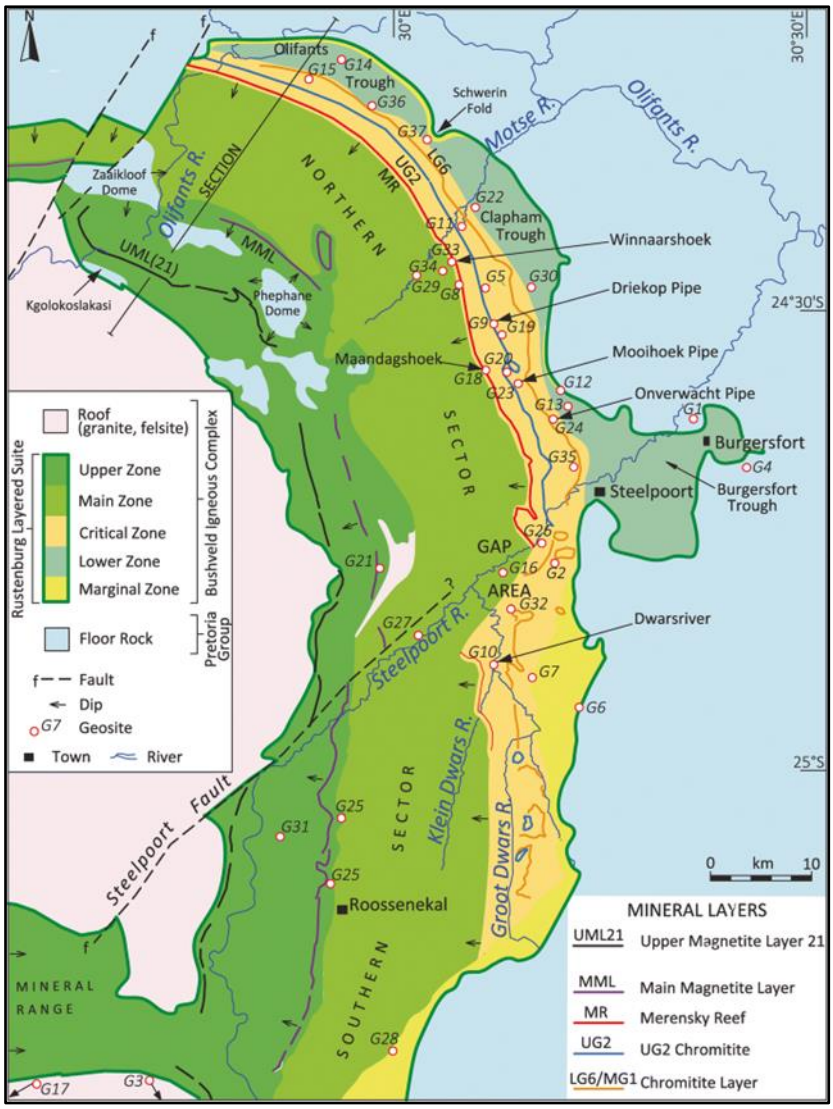

Figure 2. 2 Geological map of the eastern limb of the Bushveld Igneous Complex, modified from the Council for Geoscience (Scoon and Viljoen 2019).

2.1.5 The UG2 chromitite layer

The upper Group 2 chromitite layer (UG2) is located within the upper critical zone in the eastern and western limbs of the Bushveld Igneous Complex. It is a large chromitite seam, varying in thickness from 0.5-1.2 m (Mayer et al,2020). The chromitite seam has similar characteristics along its entire strike length of approximately 280 km (Viljoen, 2016). The UG2 reef is the uppermost layer of the upper critical zone, except for a few places in the eastern limb, south of Burgersfort, where the UG3 layer is present (figure 2.3) (Mungall, Kamo and McQuade, 2016; Langa et al,2021). The

Merensky Reef is located 15-400m above the UG2 Reef (Hutchinson et al. 2015). Langa et al (2021) described the layer as the most PGE-endowed chromitite layer of the Bushveld Igneous Complex, indicating its economic importance.

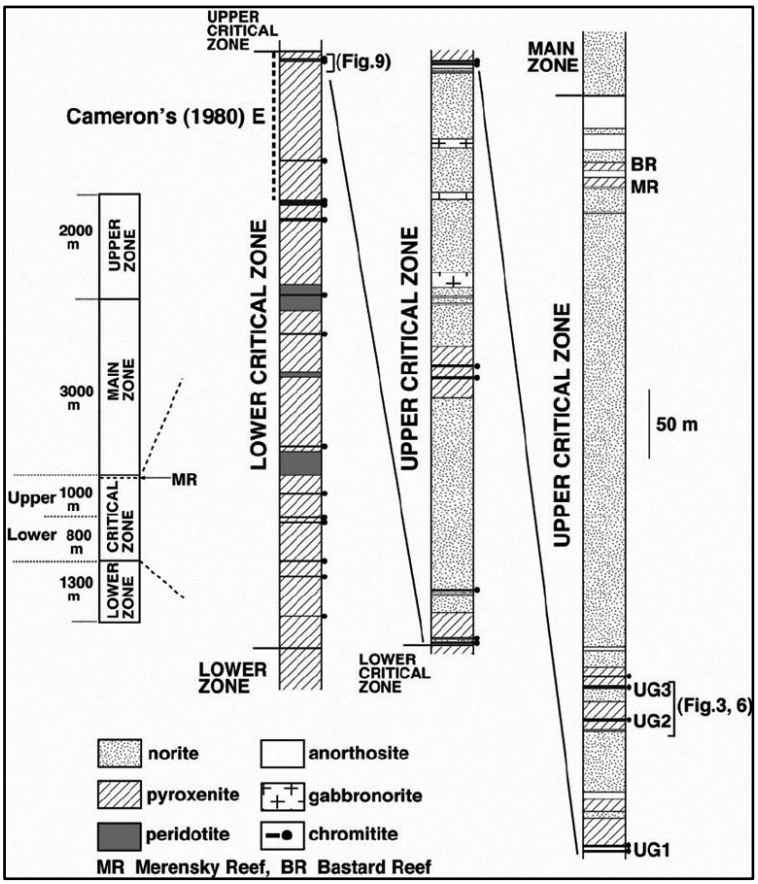

Figure 2. 3 Simplified stratigraphy of the critical zone of the Rustenburg Layered Suite (Mondal and Mathez, 2007).

2.2 Rock Brittle Index

2.2.1 Rock brittleness and the brittleness index

The term “brittle” is defined in the Cambridge dictionary as “delicate and easily broken.” Brittleness is a property of a material that breaks at minimal plastic deformation. Rocks that fracture with minimal ductile deformation when subjected to loading conditions are considered brittle (Nouri et al, 2022). Bates and Jackson (1984) quantified the minimal plastic deformation as less than 3%-5%, in the dictionary of geological terms.

Widely varying definitions of brittleness have emerged. Morley (1954) described brittleness as a drop in the ductility of rock materials. “A material property describing the material loss of carrying capacity with a small deformation” is the definition Chen et al (2019) provided for brittleness. Howell (1959) presented that the brittleness of material is the property of failure with extremely low plasticity. Weibull (1939) defined brittleness as the absence of plasticity. Ramsay (1967) indicated that the loss of cohesion results in the brittle failure of rock. It was also proposed by Obert and Duvall (1967) and Carpinteri (1991) that if a rock material fails at the peak strength or slightly exceeds the yielding strength, it is brittle (Xia et al, 2019).” Brittleness refers to deformation that involves hard, strong material that fractures and splits rather than staying whole while pliably deforming’ (Munoz Taheri and Chanda, 2016).

A considerable amount of literature has been published on the brittleness of rocks and on the different methods used to quantify them. However, it is clearly indicated in the existing body of research, that a standardized definition and measurement for brittleness have not yet been established (Meng, Wong, and Zhou, 2020; Zhang et al., 2021; Zhang, Ranjith, and Perera, 2016; Xia et al., 2017; Tao et al., 2020; Kavi, Amer, and Molladavood, 2018; Wang et al., 2020; Xia et al., 2019). Altindag (2009) and Huckaa and Das (1974) point out that different researchers express, mean, and apply it differently for different motives. Brittleness is challenging to define because the existing definitions are industry specific and there is a lack of research and testing to determine their applicability in other fields. This has resulted in uncertainty in the relationship between rock failure and rock brittleness (Xia et al, 2019).

Despite the uncertainty in the methods used to measure the brittleness of rocks, highly brittle rocks have nine common factors: a large tensile-to-compressive strength, ratio, large internal friction angle, fracture failure, failure at a small stress-strain stage, high resistance.

Brittleness is quantified using a brittleness index (Zhang et al., 2016). There is a consensus among researchers that there is no standardized method of measuring the brittleness index (Meng, Wong and Zhou, 2020; Zhang et al, 2021; Zhang, Ranjith and Perera, 2016; Wang, 2019; Wang et al,2019; Wang et al,2020). Several attempts have been made to quantify the brittleness of materials. After studying ceramic materials,

Quinn and Quinn (1977) proposed the index of brittleness $B \equiv \frac{HE}{K_{ic}^{\ 2}}$, where H denotes the hardness, E Young's modulus and Kic the fracture toughness. Lawn and Marshall (1979) proposed a ratio $\frac{H}{K_c}$, where H denotes the resistance to deformation (hardness), and K_c denotes the resistance to fracture (toughness) as an index of brittleness (Altindag, 2009).

2.2.2 Factors influencing rock brittleness

Different researchers have different understandings of rock brittleness and its influencing factors. Some researchers have argued that brittleness is strictly an intrinsic quality of materials; thus, factors such as the external environment and the stress-strain state should not be considered when quantifying brittleness. However, a link between various external factors, the rock brittle state, and failure patterns has been established. Petrographic parameters play a crucial role in rock brittleness and are influenced by the external environment (Xia et al, 2019).

2.2.2.1 Intrinsic factors influencing rock brittleness

The macroscopic failure of rocks is the result of gradual microscopic failure. Different intrinsic rock properties influence the propagation of cracks at the microscopic level, thereby influencing the brittleness of the rock material, some of which are listed below.

I. Rock type

Lawn and Marshall (1973) defined brittleness as the ease of fracture propagation. Fracture propagation is influenced by the type of mineral and interaction of the grains in a rock. The heterogeneity and grain boundary characteristics of the different rock types (igneous, metamorphic, and sedimentary) vary. Mineral–grain interactions resulting from heterogeneity can result in early fracture initiation. welded grains in meta-clastic or igneous rocks allow for cross-boundary fracture propagation. The formation of a preferred orientation of mineral grains during the process of metamorphism (fabric generation) reinforces the role of inter- and intra-slip and thus reduces the role of fracture propagation in metamorphic rocks. Clastic, cross-contact, and intra-granular fracture propagation are not common in sedimentary rocks (Diederichs, Kaiser and Eberhardt, 2004).

II. Mineralogical composition

The mechanical parameters of rocks are strongly dependent on their mineralogical compositions (Wang et.al, 2017). Chi et al (2016) indicated that there is a direct correlation between rock brittleness and mineralogical composition. Mineralogical composition plays a critical role in determining the ability of rocks to fail, as determined by Young's modulus (Zhang, Ranjith and Perera, 2016). Rocks that contain a high content of brittle minerals have a low Poisson's ratio and a high Young's modulus. (Li, 2022). Minerals, such as quartz and clay, can be classified as brittle or ductile (Xia et al., 2019; Hasson et al., 2022). Rocks with a high content of brittle minerals are considered highly brittle (Liu and Sun, 2015). According to Wang et al (2015), these rocks have low clay content and high quartz and carbonate content. Tapponier and Bruce (1976) indicated that the brittleness and strength of a brittle rock may be restricted by the presence of ductile minerals, that have a different elastic modulus relative to other minerals.

Brittle minerals are an important factor that influence the creation and propagation of rock fractures, which affects the ductility and brittleness of rocks. However, it should be noted that the classification of minerals into brittle and ductile rocks remains subjective, for example, the classification of carbonates is a matter of debate. Gholami et al. (2016) developed a logging correlation study between dynamic elastic parameters and mineral components, and they discovered that the association between Young's modulus and Poisson's ratio and changes in the quality of carbonate minerals is dispersed and not significant (figure 2.4)

One of the parameters that influences brittleness is the elastic modulus, which measures the stiffness of minerals. Different minerals also have different elastic moduli (Table 2.1), resulting in rocks with different failure qualities (Xia et al, 2019). The mechanical parameters of the different mineral components of rocks also affect the rock's homogeneity, which has a direct impact on brittleness because there is an inverse relationship between the homogeneity coefficient and the resistance to failure that results from stress (Tullis & Yund, 1977).

Figure 2.4: Variations in carbonates versus Young's modulus (a) and Poisson's ratio (b) for Carynginia shale from the North Perth Basin, Australia (Gholami et al., 2016).

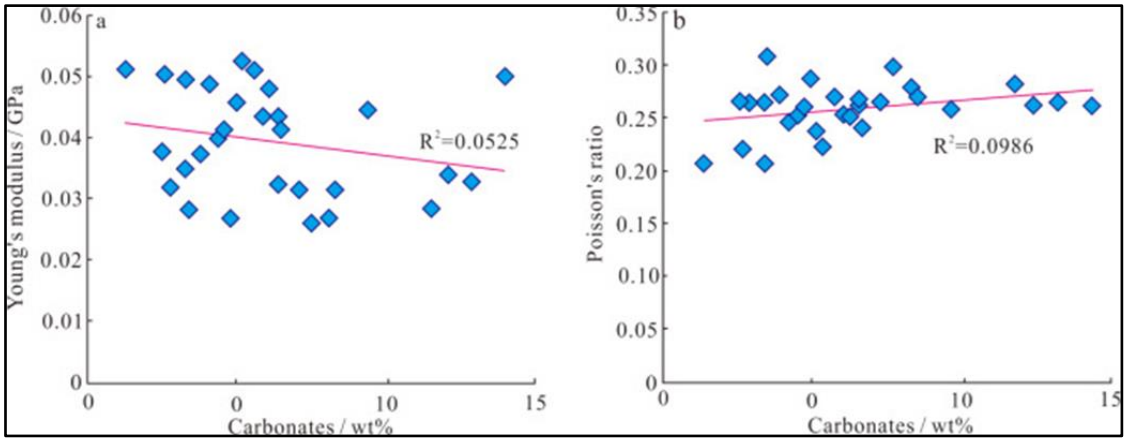

Figure 2. 4 Variations in carbonates versus Young's modulus (a) and Poisson's ratio (b) of Carynginia shale from the North Perth Basin, Australia (Gholami et al., 2016).

Table 2. 1 Elastic modulus of various mineral components for granitic gneiss (Jay, 1995).

Mineral component	Quartz	Amphibole feldspar	K-feldspar	Biotite	Chlorite	Plagioclase
Elastic modulus (Gpa)	114	95	75	67	46	75

III. Grain size

Grain size is one of the most important microstructural parameters that influences the mechanical parameters of rocks (Fredrich and Evans, 1990; Nauri et al, 2021). The strength of brittle rocks with similar lithologies decreases with grain size, making coarse-grained materials weaker than fine-grained materials with the same mineralogical composition. (Fahy and Guccione, 1979; Jiao, 2004; Heidari et at, 2013). After determining the Brazilian tensile strength on layers of sandstones, Tavallali and Vervoort (2010) observed a good correlation between tensile strength and grain size. They observed that the grain size and tensile strength were directly proportional. The

same relationship has been observed for dolomite (Olsson, 1974; Hatzor and Palchik, 1997) and granites (Přikryl, 2001). Grain size has also been observed to have a significant influence on fracture propagation; however, its effect on the stress level during crack initiation is negligible. Eberhardt et al (1999) observed an inversely proportional relationship between grain size, peak stress, and crack damage stress.

IV. The grain shape (and ψp)

Mineral grains of makeup rocks have varying geometries, deformation characteristics, and strengths. The shapes of mineralogical grains are often irregular and diverse. This is because they are a product of a diagenetic environment and influence the mechanical characteristics of the rocks (Han, Zhang and Zhou, 2019). Roundness (ρ) and sphericity (ψp) are factors associated with grain shape (Nauri et al, 2022). Wadel (1932) defined roundness as the ratio of the curvature of the edge of a grain to the overall grain shape. Krumbein (1941) defined sphericity as the ratio of the grain volume to the smallest circumscribing sphere. An inversely proportional relationship exists between porosity, elastic modulus, and peak strength (Han, Zhang and Zhou, 2019; Nauri et al, 2022). Finer grains are often less angular and have lower porosity than coarser grains.

After studying the effects of grain shape on the strength and fracture behaviour of rock materials, Han, Zhang, and Zhou (2019) concluded that the mineralogical shape affects the peak strength of rocks and the elastic modulus. Using a numerical model, they found that rock strength is increased by flat grains, whereas grains with higher roundness increase the porosity, thus decreasing the rock strength.

V. Porosity

The porosity of rocks is viewed as the presence of pores and microstructures. In the field of rock engineering, it is often quantified using uniaxial compressive strength and tensile strength. Porosity has a significant effect on the mechanical parameters of rocks, including the uniaxial compression strength and tensile strength. It is a governing factor for rock strain and failure (Heidari, 2014). Raijabzabeh et al, 2012) determined that the tensile strength and the uniaxial compression strength have an inversely proportional relationship with the brittleness thus the brittleness index changes as a function of rock porosity. A decrease in rock brittleness can occur

because of an increase in strain at failure as a result of an increase in rock porosity. Heidari (2014) argued that the brittleness index of crystalline metamorphic, igneous, and sedimentary rocks with great mineralogical variations cannot be directly related to their porosity. This is because the mechanical behaviour of crystalline rocks is not directly influenced by their porosity.

2.2.2.2 External factors influencing rock brittleness

External factors also influence the brittleness of rocks. Zhang et al (2021) argued that external factors play a greater role in rock brittleness because the intrinsic factors are constant. Some of these external factors are listed below:

I. Temperature

Temperature is one of the most important factors affecting the mechanical properties of rocks. This primarily affects the strength, failure, and deformation characteristics. Temperature also has a significant effect on rock brittleness (Yang et al, 2021; Yin et al, 2022). The physical and mechanical parameters of rocks are weakened by changes in mineral composition and microstructures, which are influenced by temperature changes (Yin et al, 2022). The activation of fluid media brought about by the action of heating results in changes in the fracture mechanisms and rock deformation. The material properties of rocks are affected by the temperature. The type of rock and loading conditions affect how the rock brittleness index behaves microscopically (Yang et al, 2021). According to Kang et al (2020), the porosity, tensile strength, and elastic modulus are all temperature dependent. These factors affect the brittleness of rocks. There is a significant variation between the brittleness of rocks at high temperatures and room temperature. In rocks, an increase in temperature results in a brittle-ductile transition (Sha et al, 2022). Heat at high temperatures influences the composition of minerals and causes damage to the microstructures of rocks, which has an impact on rock behaviour. Heat can generate great thermal stresses between mineral grains, which affects the mechanical properties of the rock, thus encouraging the development and fusion of microcracks inside the rock (Yang et al, 2017). Temperature has an inversely proportional relationship with the elastic modulus and uniaxial compression strength. It has a directly proportional relationship with the permeability, ultimate compression strain, and porosity (Pan and Shao 2022).

II. Confining pressure

The confining pressure is the pressure applied to the rock by the overlying material. It compacts and compresses the rock uniformly in all the directions. According to Lockner and Beeler (2002), confining pressure suppresses the growth of microcracks and thus affects the brittle failure strength. Pincus (2002) described a directly proportional relationship between the rock strength and confining pressure. An experiment conducted on marble by Passchler (1958) found that when the confining pressure exceeded 20 MPa, the peak strain of marble increased significantly and the mechanical properties of rocks shifted from brittle to ductile as the confining pressure increased (Yin et al,2022).

III. Burial depth

The brittleness of rock is related to its burial depth. The failure process of a rock can differs depending on its location relative to the surface of the earth. Rocks tend to be ductile in the deeper parts of the ground and brittle on the surface (Clearly, 1989; Yin et al, 2022). Young et al (2017) indicated that a rock can transform from ductile to semi-brittle or brittle during the process of uplifting from deep burial to shallow subsurface as a result of erosion or tectonic uplifting. With burial depth, brittle to ductile properties of rocks can transform (Yuang et al, 2017).

2.2.2.3 Effect of water content on rock brittleness

In addition to the intrinsic and external factors that influence rock brittleness, water content also affects the brittleness of hard rock (Wang et al, 2016; Xia, Conil and Zha, 2018; Xia et al, 2019). Changes in mechanical properties such as the modulus, peak strength, and brittleness were listed by Wong et al (2016) as one of the effects of water content on rocks. This was after they studied the influence of water on varying rock strengths, specifically focusing on the Young's modulus and uniaxial compressive strength. The influence of water on the mechanical parameters of rocks has been extensively studied (Hawkins and McConnell, 1992; Erguler and Ulusay, 2009; Pettel et al, 2003; Verstrynge et al, 2014). It can be said that the strength of hard rock decreases in the presence of water (Chen et al, 2019). The water content has an inversely proportional relationship with the variations in brittleness; thus, the more moisture present, the less brittle is the rock. This conclusion was reached by Liu and

Shao (2016), who studied the failure modes of four claystone samples under different moisture levels: dry, 79.85%, 85 %, and 98%, at a confining pressure of 12.4 MPa (figure 5).

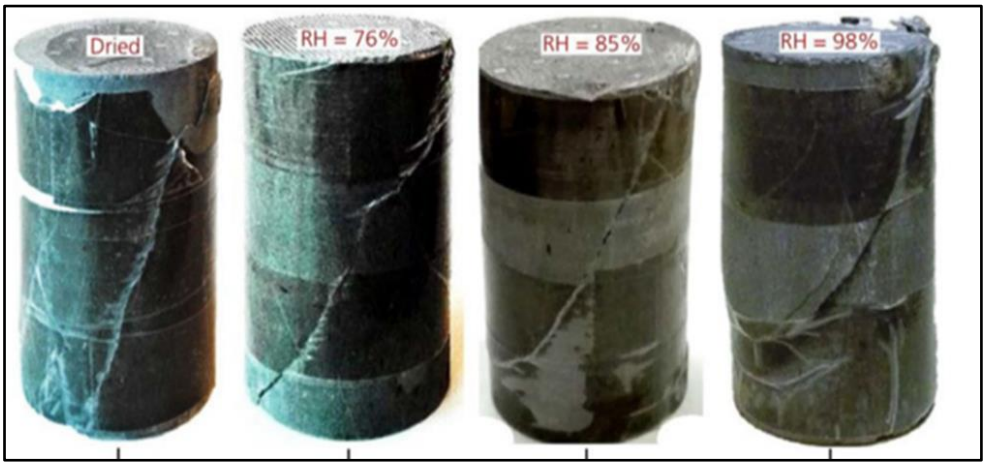

Figure 2. 5 The fracture pattern of specimens under the conditions of different moisture levels (Liu & Shao, 2016).

2.2.3 Applications of rock brittleness estimations

Brittleness is an important characteristic of hard rocks. It is especially essential in the fields of rock engineering and rock mechanics (Meng, Wong, and Zhou, 2020; Zhang et al., 2021; Zhang, Ranjith, and Perera, 2016; Xia et al., 2017; Tao et al., 2020; Kavi, Amer, and Molladavood, 2018; Wang et al., 2020; Xia et al., 2019). This is because they play a critical role in the intended and unintended failure processes associated with drilling operations, tunnelling, and mining (Meng et al., 2020). Correct analysis of the brittleness index is essential in many related operations, some of which are listed below.

2.2.3.1 Assessment of rock-cutting efficiency and drillability.

According to Altindag (2010), the prediction of rock drillability is based on many factors, including the apparent porosity, tensile strength, p-wave velocity, porosity, and quartz content (Akcin et al. 1994; Kahraman 1999; Howarth 1987). The drilling and cutting efficiencies of rocks are determined based on their brittleness. This results in brittleness, which directly affects the costs of engineering projects (Altindag, 2009; 2010). However, there is no universally accepted brittleness concept that is used to measure cutting efficiency, resulting in an uncertainty of the relationship between the

two (Xia et al, 2019; Altindag, 2003). In addition, no single index or test can be used to determine the drillability of rocks (Altindag, 2010). Rocks with high strength are generally more brittle (Xia et al, 2019). Consequently, cutting and drilling efficiencies are evaluated using the ratios corresponding to the tensile strength and compressive strength (Altindag 2010; Xia et al, 2019). This is applicable in the mining industry, where, according to Zhang et al (2021), production efficiency is increased by highly brittle minerals, because they are easier to cut.

It was theoretically proven by Evans and Pomeroy (1966) that there is an inversely proportional relationship between the impact energy of a cutter pick and the brittleness of the rock mass. The cuttability and drillability of coal were shown by Singh (1986) to be strongly dependent on the brittleness of coal. Singh (1987) showed that the brittleness B_2 (see equation 2) and in-situ specific energy of three coals in Utah (USA) have a directly proportional relationship. Kahraman (2002) conducted a study that used raw experimental data from various workers to investigate the relationship between drillability and borability and three different definitions of brittleness. (Xia et al, 2019).

2.2.3.2 Prediction and Mitigation of rock bursts

Rock bursts are sudden and violent failure events that involve the dislocation of rock slabs around an excavation (Lee, Park, and Lee, 2004; Liet et al.,2017; Wang, Huang, and Li, 2020). Initially, the rock masses in the subsurface were in an equilibrium state of energy. The presence of overlying rock masses results in the accumulation of the stored strain energy in the rock mass. Energy equilibrium is disturbed when there is a disturbance in the rock mass as a result of mining or tunnelling. This transforms the areas around the excavation (surrounding rocks) into high-energy regions. Energy cannot be created or destroyed and can only be transferred. If the rocks surrounding the excavation are brittle, very little energy will deform them, as is the case with ductile rocks. The remaining energy is transformed into the kinetic energy of rock blocks, which is discharged as a rock burst. Therefore, it is essential to determine the brittleness index of rocks before mining or tunnelling (Singh, 1986; Lee, Park and Lee, 2004; Xia et al., 2019; Wang, Huang, and Li, 2020). The mean size of rock fragments created in rock bursts is inversely proportional to brittleness. This suggests that the more brittle the rock mass, the more intense the rock burst (Wang, Huang, and Li,

2020). Rock bursts pose a serious threat to underground mining operations and personnel (Singh, 1987); therefore, the correct determination of the brittleness indices of rock masses is crucial in predicting and implementing mitigation measures to prevent rock bursts.

2.2.3.3 Exploitation of unconventional hydrocarbon resources

Geological, natural, and exploitation procedures are used to classify hydrocarbons into conventional and unconventional methods. The depletion of conventional hydrocarbons has resulted in unconventional hydrocarbons being a major candidate for future hydrocarbon production (Muther et al.,2022). Rock brittleness is an important factor in the development of unconventional reservoirs. This is because during the exploitation of unconventional hydrocarbon resources, it plays a role in the design of hydraulic fractures, which are employed to increase the connectivity and permeability and to determine the perfect spot for fracture initiation and perforation (Mews et al.,2019; Meng et al.,2020). Therefore, the correct determination of the brittleness index of rocks is essential for profitable exploitation of unconventional hydrocarbons.

2.3 Rock Brittle index methodologies

Accurate determination of the brittleness indices of rocks plays a critical role in the intended or unintended failure processes associated with excavations. Therefore, it is crucial in geological engineering, rock engineering, and rock mechanics. Many researchers have proposed different definitions of brittleness across different fields; however, their applicability is a topic of debate because of the anisotropic and inhomogeneous nature of rocks. Seventy-five indices are reviewed as follows:

2.3.1 Brittleness indices based on strength parameters (B_1 – B_{13})

The mechanical parameters of rocks are typically determined using laboratory tests. These include the uniaxial compressive strength (UCS) and tensile strength (TS), commonly known as the Brazilian tensile strength (BTS) (figure). The maximum tensile strength that a material can withstand is measured by TS, whereas the UCS is used to assess the ability of a structure to compress under loads. B_1 – B_4 are measured using the relationship between UCS and TS (Gholani and Fakhari, 2017; Xia et al.,2019; Fangdi 2020). However, according to Zhang et al. (2021) and Cai (2010), TS

and UCS are similar, which results in the same TS and UCS relationship in different rocks, making the differentiation of the brittleness of different rocks challenging. A directly proportional relationship exists between the values of B_1 and B_2 and the brittleness of the rock mass (Gong and Zhao, 2007; Zhang and Fu, 2008; Meng et al.,2020). After using experimental data to study the relationship between the UCS and TS, Hucka and Das (1974) proposed the brittleness index B_1. They suggested that brittle failure was more likely to occur with a high ratio between the TS and UCS (Ai et al., 2016).

Brittle indices B_1 (Equation 2.1) and B_2 (Equation 2.2) are less effective in examining the relationship between the brittleness index and drilling efficiency compared to the brittleness indices B_3 (Xia et al.,2019). However, they can be used to determine the brittleness of soft rocks and are typically used to determine the brittleness of coal. Brittleness indices B_1 and B_2 are used in the prediction of rock burst probability, the two brittleness indices are also used to evaluate the drilling efficiency of percussive and rotary drilling (Munoz, Taheri and Chanda, 2016; Meng et al.,2020; Fangdi 2020). The brittleness index B_2 was shown by Singh (1987) to be directly proportional to the in situ specific energy of the three coals in Utah (Altindag, 2009).

The energy per unit mass required to cut the rock is termed specific energy (SE). Brittle rocks generally have a lower SE than ductile rocks (Fangdi, 2020). After studying the relationship between B_1 and SE, Goktan and Yilmaz (2005) could not establish a relationship; however, normalizing SE with uniaxial compressive strength and categorizing the test data for a specific rock group strengthened the link between brittleness B_1 and specific energy (Altindag, 2010).

$$B_1 = \frac{\sigma_c}{\sigma_t} \tag{2.1}$$

$$B_2 = \frac{(\sigma_c - \sigma_t)}{(\sigma_c + \sigma_t)} \tag{2.2}$$

Where σ_c and σ_t are the uniaxial compressive strength (UCS) and Brazilian tensile strength, respectively.

Meng et al. (2020) indicated that brittleness indices B_3 (Equation 2.3), B_4 (Equation 2.4), and B_5 (Equation 2.5) influence rock drillability, drilling rate, and sawability (Altindag 2002, 2003, 2010; Dursun and Gokay, 2016). By studying the relationship between the compressive strength and brittleness indices B_4 and B_5, Xia et al. (2016) discovered that a linear correlation exists with B_5, and a secondary correlation exists with B_4. A clear relationship was established between seismic energy, point load index, density, penetration rate, brittleness index, and B_4 (Fangdi 2020). A high B_4 value has also been shown by Altindag (2002, 2003) that correlate with low rock brittleness. More energy is required to bore or drill rocks with a high B_4. It should be noted, however, that these brittleness indices share similar characteristics with B_1 and B_2 and thus share the same limitations (Meng et al., 2020; Zhang et al., 2021).

$$B_3 = \frac{(\sigma_c + \sigma_t)}{2} \tag{2.3}$$

$$B_4 = \frac{\sigma_c \sigma_t}{2} \tag{2.4}$$

$$B_5 = \sqrt{\frac{\sigma_c \sigma_t}{2}} \tag{2.5}$$

Regression or linear fitting analyses have been used to develop brittleness indices B_6–B_9 (Meng et al., 2020; Fangdi, 2020). Brittleness indices B_6 (Equation 2.6), B_7 (Equation 2.7), B_8 (Equation 2.8) and B_9 (Equation 2.9) were proposed by Yagiz (2009), Yagiz and Gokceoglu (2010), Khandelwal et al. (2017) respectively. Meng et al (2020) indicated that these four indices have no physical meaning and theoretical basis, they were developed for the sole purpose of predicting the brittleness index B_{66} (Equation 2.69). They depend on the assumption that the brittleness index, B_{66},

provides an accurate representation of brittleness. However, this is disputable because rock strength and not brittleness is represented by B_{66}. Therefore, the applicability of these indices remains questionable.

$$B_6 = 0.198\sigma_c - 2.174\sigma_t + 0.913\rho - 3.807 \quad (2.6)$$

$$B_7 = 0.00\gamma^{2.72} + 0.61\sigma_c^{0.81} - 1.37\sigma_t^{1.13} + 5.45 \quad (2.7)$$

$$B_8 = 0.59\sigma_c^{0.769} - 5.085\sigma_t^{0.531} + 0.009\gamma^{2.332} \quad (2.8)$$

$$B_9 = \left\{\ln\left[\tan(10.9 + \rho) + {}^{53.27}/_{\sigma_c} + \tan\sigma_c + \sigma_c + 6.65\right]\right\}^2 + \left[(6.65 - \sigma_t + \tan\sigma_t + \sigma_t/_{4.17\sigma_t}\sqrt[3]{\frac{\gamma^2}{\sigma_2 - 4.17}}\right]^2 \quad (2.9)$$

Where ρ and γ are the density and unit weight of the rock, respectively.

Nejari and Moosavi (2017) proposed the brittleness index, B_{10} (Equation 2.10). According to Fangdi (2020) and Meng et al. (2020), can be used to determine the fracture toughness of modes I and II because a positive linear relationship exists between the two. This index has no physical meaning, despite its established linear relationship with fracture toughness. This is because this relationship is not related to the established definitions of brittleness. The brittleness index B_{10} shares the same shortcomings as B_4 in that it represents rock strength as opposed to brittleness (Meng et al., 2019).

$$B_{10} = {\sigma_t^{0.51} E^{0.51}}\Big/{\sigma_c^{0.21}} \quad (2.10)$$

Where E is the elastic modulus of rock.

Dursun and Gokay (2016) proposed the brittleness index B_{11} (Equation 2.11). A strong correlation exists between the specific energy during rock cutting and B_{11} (Equation 2.11) (Fangdi, 2020; Meng et al., 2020). B_{11} and B_{74} (Equation 2.77) showed a positive linear relationship. It has been determined that neither is a proper representation of rock brittleness (Meng et al. 2020).

$$B_{11} = 0.22\sigma_c - 0.49\sigma_t - 4.939PLS + 91.179 \quad (2.11)$$

Where PLS is the point load strength of rock.

Two tests were used by Tarokh et al. (2016), who treated brittleness not as a property of a material, but as a structural response to determine brittleness. B_{12} (Equation 2.12) was developed from surface instability studies (cubic specimens subjected to a single-axis compression test with one side exposed and the other two restrained), which investigated a rock's tendency to fail along a free surface in an unstable manner. Ductile rocks have B_{12} values close to zero, whereas highly brittle rocks have a value close to one. B_{13} (Equation 2.13) was acquired from a size effect analysis of the three-point bending tests in mode I fractures. By considering the size parameter, B_{13} reflects how geometry and size interact. The value of B_{13} approaches one for highly brittle rock and is close to zero for ductile rock because the surface instability peak stress (SIPS) is only marginally higher than that of the UCS (Fangdi 2020; Meng et al., 2020).

$$B_{12} = {}^{\sigma_C}/_{SIPS} \quad (2.12)$$

$$B_{13} = D\left({}^{\sigma_t}/_{k_{IC}}\right)^2 \quad (2.13)$$

Where SIPS and D are the surface instability peak stress (i.e., the axial stress when the first sign of surface spalling occurs), and structure size parameter (e.g., beam height), respectively.

Brittleness indices based on strength parameters generally have no notable physical meaning, and there is no clear relationship between these indices and rock fractures. Most of these indices indicate rock strength rather than brittleness and cannot be used to account for the effect of the stress state (Meng et al., 2020).

2.3.2 Brittleness indices based on compression stress-strain curves (B_{14} – B_{40})

Stress–strain curves are frequently applied in rock mechanics and engineering to calculate rock strength and quantify rock mass brittleness (Hucka and Das, 1974; Altindag, 2010; Xia et al., 2017). Ductile rocks experience significant inelastic strain

without fracturing, whereas brittle rocks generally fail at moderate strain (Fangdi, 2020). The rock properties are most intuitively reflected by the stress-strain curves obtained by loading the rocks. The behaviour of rocks during post-peak strength loss, stable propagation of microcracks, accelerated extension of cracks, and loss of residual shear stages can be reflected by the stress-strain curve (Zhang et al., 2021). The shapes of the uniaxial and triaxial compressive stress-strain curves were used to obtain the brittleness indices B_{14} (Equation 2.14)–B_{40} (Equation 2.43). Under triaxial or uniaxial compressive stress conditions, the deformation, energy, and stress selected or estimated from pre-or post-peak stress-strain curves are frequently employed to indicate rock brittleness (Meng et al., 2020). Adopting the stress-strain approach to analyse the brittleness of rock masses has the advantages of simplicity, intuition, and avoidance of repeated tests (Zhang et al., 2021).

Liang et al. (2017) utilized B_{14} to obtain the brittleness of shale and classified brittleness into five grades: extremely brittle ($B_{14} > 40$), high brittleness ($30 < B_{14} < 40$), brittle ($20 < B_{14} < 30$), middle brittleness ($10 < B_{14} < 20$), and low brittleness ($B_{14} < 10$). The effects of the elastic strain before the peak strength on rock brittleness are highlighted by the brittleness indices B_{15} (Equation 2.15), B_{16} (Equation 2.16), and B_{17} (Equation 2.17) (Meng et al., 2017). According to Andreev (1995), the role of the elastic strain before the peak strength in determining rock brittleness is highlighted by B_{15} and B_{16}. The results of B_{15} are classified as follows: B_{15} <3% is brittle, 3%<B_{15}<5% is brittle-ductile, and B_{15}>5% is ductile (Fangdi, 2020; Meng et al, 2020). Because the majority of the strain may be reversed for brittle rock, whereas a large amount of inelastic deformation occurs for ductile rocks, the ratio of reversible or elastic strain to total strain at fracture is applied to quantify the brittleness index B_{16} (Hucka and Das, 1974). The brittleness index B_{17} was developed from an inversely proportional relationship between elastic strain and brittleness (Gong and Sun, 2015). However, Meng et al. (2020) stated that B_{17} cannot accurately reflect rock brittleness because the small elastic strain may be accompanied by a very large amount of irreversible strain, which indicates a highly ductile characteristic of rock.

$$B_{14} = {}^{\sigma_c}/_{\varepsilon_p} \tag{2.14}$$

$$B_{15} = \varepsilon_{1i} \times 100\% \tag{2.15}$$

$$B_{16} = {}^{\varepsilon_e}/_{\varepsilon_p} \tag{2.16}$$

$$B_{17} = {}^{1}/_{\varepsilon_e} \tag{2.17}$$

Where where ε_p and ε_e are the peak strain and elastic strain at peak strength, respectively; and ε_{1i} is the absolute irreversible longitudinal (parallel to s1) strain until failure (see Figure 2.6).

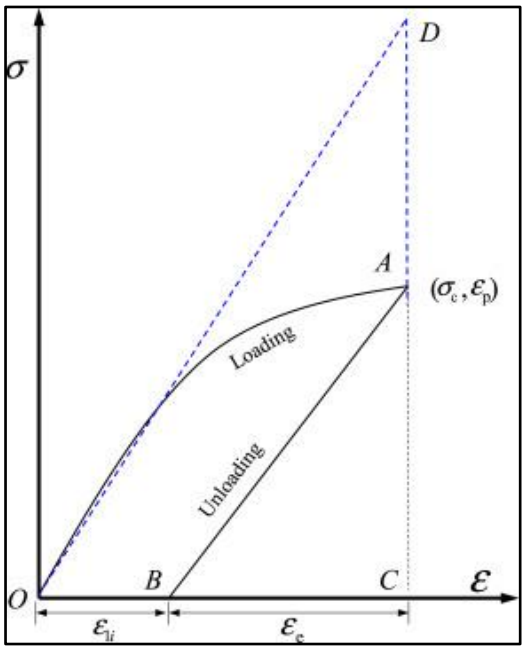

Figure 2. 6 Demonstration of generating B_{17} (After Zhang et al., 2021)

Hajiabdolmajid and Kaiser (2003) proposed a strain-dependent brittleness index B_{18} (Equation 2.18). They considered the mobilization of frictional strength and cohesive components during the rock failure process (Rahimzadeh, Ameri and Molladavoodi, 2018). The breakout zone shape and the long- and short-term stability of underground excavations were evaluated using this index (Hajiabdolmajid and Kaiser, 2003). Meng et al. (2020), however, did not account for the reason why the difference between the two plastic strains can represent rock brittleness.

$$B_{18} = \left(\varepsilon_f^p - \varepsilon_c^p\right) \Big/ \varepsilon_c^p \tag{2.18}$$

Where whereε_c^p and ε_f^p p are the permanent (plastic) volumetric strains necessary for cohesion loss and frictional strengthening, respectively, which can be determined by laboratory cyclic load-unload test (Martin and Chandler, 1994).

After finding a discrete link between the brittleness indices in the uniaxial compression test and crack initiation stress level, Wang et al. (2014) proposed the brittleness index B_{18}. The grain size and mineralogical composition of the rock define the B_{19} (Equation 2.19). B_{19} is between 0.6 to 0.7 for fine-grained rocks such as diorite, limestone, and sandstone and between 0.2 to 0.25 for coarse-grained granite. In conclusion, the smaller the value of B_{19}, the more brittle and heterogeneous the rock (Fangdi, 2020). A strong correlation between B_{19} and B_1 and B_2 was discovered; thus, it shares the same limitations, as previously stated, B_1 and B_2 do not reflect rock brittleness and B_{19} (Meng et al., 2020).

$$B_{19} = \sigma_{ci} \big/ \sigma_c \tag{2.19}$$

Where σ_{ci} is the crack initiation stress (i.e. the stress when the lateral strain curve starts to deviate from linear trend).

Bishop (1967) proposed the brittleness index, B_{20} (Equation 2.20) (Wang et al, 2017; Zhang et al, 2019). They used it to characterize the vulnerability of the soil to progressive flow or failure. However, it is limited because it only considers the magnitude of the stress drop, while disregarding the rate at which the strength decreases from the peak of the residual strength. Brittleness indices B_{21} (Equation 2.21) to B_{24} (Equation 2.24) were created based on B_{19} as it paved the way for quantitative evaluation of rock brittleness in the compression test because the post-peak stress-strain curve was taken into consideration (Meng et al., 2020; Zhang et al., 2021).

$$B_{20} = \left(\tau_p - \tau_r\right) \Big/ \tau_p \tag{2.20}$$

Where τ_p and τ_r are the peak and residual strengths, respectively, in the compression test (see Figure 2.7).

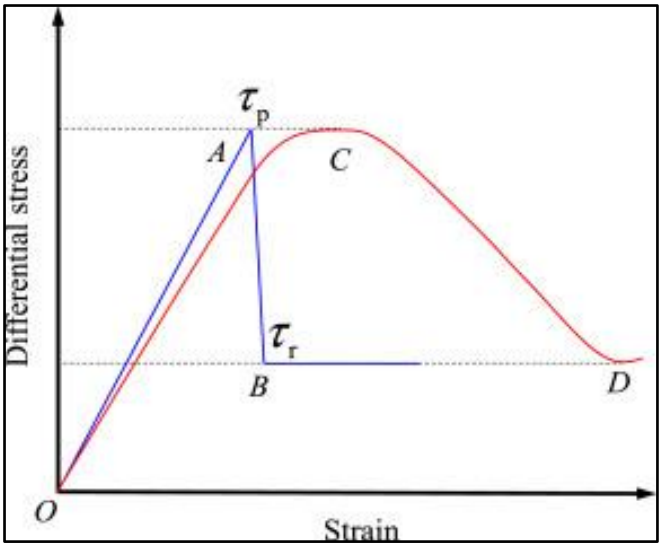

Figure 2. 7 Illustration of B20 index (After Wang et al, 2017; Zhang et al, 2019)

Brittleness index B_{21} (Equation 2.21) is made up of two parts, Li et al (2012) proposed brittleness index B_{21} indicated that the effect of pre-peak deformation is represented by B_a (Equation 2.22) whereas the influence of post-peak response to the rock brittleness is represented by B_b (Equation 2.23). This index was utilised to estimate the brittleness index of shale. It is limited however, because the calculation formula indicates that both B_a and B_{21} have a directly proportional relationship with the peak strain,

However, a higher brittleness is not always indicated by a larger peak strain (Meng et al, 2020).

$$B_{21} = B_a + B_b \tag{2.21}$$

$$B_a = {}^{\varepsilon_p - \varepsilon_n}/_{\varepsilon_m - \varepsilon_n} \tag{2.22}$$

$$B_b = \propto cs + \beta\beta cs + \eta, cs = {\varepsilon_p(\sigma_p - \sigma_r)}\Big/{\varepsilon_p(\varepsilon_r - \varepsilon_p)} \quad (2.23)$$

where $\varepsilon_m$and ε_n are respectively the maximum and minimum peak strains of all the tested rock specimens statistically; and $\propto$, β and η are the coefficients; andσ_p , σ_r and ε_r are the peak stress, residual stress and residual strain, respectively (see Figure 2.8).

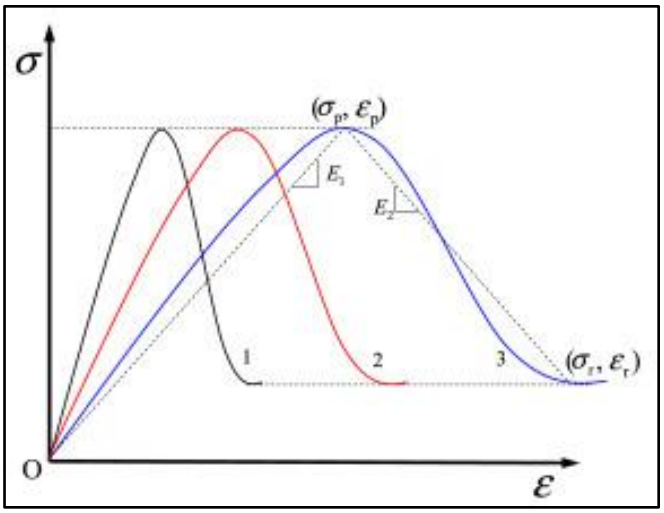

Figure 2. 8 Graphical explanation of B21 (After Li et al., 2012)

Xia et al (2017) proposed brittleness index B_{22} (Equation 2.24) as a result of combining the proportion of elastic energy released when fracture to the total energy stored before to the post peak strength and post-peak modulus. It was utilised to characterise the brittleness of oil reserve specimen. The energy is defined as the area below the stress-strain curve, while the post-peak modulus quantifies the stress drop rate during the post-peak stage. Rock brittleness is frequently assessed quantitatively using the post-peak stage characteristics This index is limited in that obtaining the numerical value requires the addition of two part that have different units (Fungdi, 2020; Meng et al, 2020).

$$B_{22} = B_{POST} + B_E = \frac{\sigma_p - \sigma_r}{\varepsilon_r - \varepsilon_p} + \frac{(\sigma_p - \sigma_r)(\varepsilon_r - \varepsilon_p)}{\sigma_P \varepsilon_P} \quad (2.24)$$

B_{post} represents the stress decrease after peak stress and B_E is the ratio of elastic energy released (S_{AED}, which corresponds to the area of AED in Figure 2.9) during failure to the total energy stored (S_{OAC}) before the peak strength.

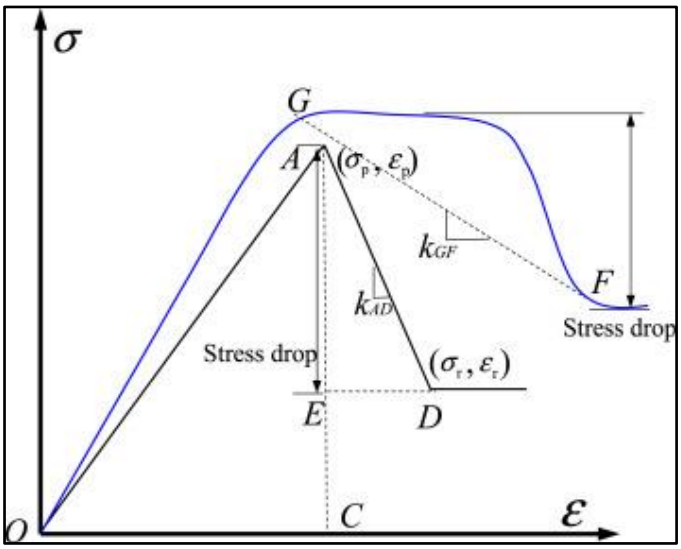

Figure 2. 9 Graphical explanation of B22 (After Xia et al., 2017)

Two brittleness indices B_{23} (Equation 2.25) and B_{24} (Equation 2.26) based on the rate of the post-peak stress drop were proposed by Meng et al. (2015). They can be estimated using the common uniaxial or triaxial compression tests. Rocks are considered to have a high B_{23} and B_{24} if the ratio of the stress drop is high and reflects the potency or intensity of the brittle failure. The effect of confining pressure on brittleness is also depicted by the two brittleness indices (Fungdi, 2020). They are utilised to predict and mitigate dynamic rock burst proneness (Meng et al, 2020).

$K_{AD(GF)}$ is the stress decrease rate after peak strength. The slope of the post-peak stress-strain curve is used to calculate $K_{AD(GF)}$ (Meng et al, 2020).

$$B_{23} = \frac{\sigma_p - \sigma_r}{\sigma_p} \frac{\log_{10}\left|k_{AD(GF)}\right|}{10} \tag{2.25}$$

$$B_{24} = \left(\sigma_p - \sigma_r\right)\frac{\log_{10}\left|k_{AD(GF)}\right|}{10} \tag{2.26}$$

Brittleness index B_{25} (Equation 2.27) is a homogeneity parameter (m) and was proposed by Wang et al (2016) a rock is considered more brittle if it has a higher m and it is considered a brittleness index of shale (Meng et al, 2020).

$$B_{25} = m \tag{2.27}$$

$$m = {}^{1}\!/_{\left(\log_{10} E - \log_{10} E_s\right)} = {}^{1}\!/_{\left[\log_{10} E - \log_{10}\left({}^{\sigma_c}\!/_{\varepsilon_p}\right)\right]} \tag{2.28}$$

where Es is the secant modulus. The uniaxial compressive stress strain curve of the rock specimen associated with a higher m has a sharper post-peak shape, thus the rock is considered more brittle and is more likely to fracture fully.

Brittleness index B_{26} (Equation 2.29) was proposed by Rybacki et al. (2016) to contrast the brittleness of shale samples, and it is based on the deformation characteristics of ductile and brittle rocks. B_{26} =1 represents brittle deformation whereas B_{26} =0 corresponds to elastoplastic behaviour. It is however limited in that different amounts of plastic deformation may characterize rocks with the identical E and H and thus have differing brittleness values (Meng et al, 2020).

$$B_{26} = {}^{H}\!/_{E} = {}^{\frac{\sigma_p - \sigma_e}{\varepsilon_p - \varepsilon_e}}\!/_{E} \tag{2.29}$$

where σ_e is the elastic stress.

Brittleness indices B_{27} (Equation 2.30) to B_{39} (Equation 2.42) are based on energy balance and in the pre-and post-peak stress-strain curves (Meng et al, 2020; Fungdi, 2020; Zhang et al,2021). According to Zhang et al (2021) rock brittleness failure

characteristics are highly related to the energy conversion mechanism thus a common method of evaluating rock brittleness is the energy method.

Brittleness indices B_{27} (Equation 2.30), B_{28} (Equation 2.31) and B_{29} (Equation 2.32) were proposed by (Hucka and Das, 1974), Aubertin et al. (1994) and Li et al. (2017) respectively. They only account for the pre-peak energy characteristics of rocks and do not consider the post-peak energy characteristics (Fungdi, 2020; Zhang et al, 2021). B_{27} can be described as the ratio of the total reserve energy to the total energy at failure (Fungdi, 2020). They are used to evaluate rock proneness to rock burst. The complicated nature and high valuables needed to calculate the brittleness index B_{29} make it hard to use (Meng et al, 2020).

$$B_{27} = {W_r}/{W_t} \tag{2.30}$$

$$B_{28} = {S_2}/{S_1} = {W_t}/{W_r} \tag{2.31}$$

$$B_{29} = \frac{dW_s}{dW_e} = \frac{2\left(1 - D_f\right)}{\left[1 - \emptyset\left(\frac{\varepsilon_f - \varepsilon_0}{S_0}\right)\right]\varepsilon_f^2} \int_0^{\varepsilon f} \left[1 - \emptyset\left(\frac{\varepsilon_f - \varepsilon_0}{S_0}\right)\right] \varepsilon d\varepsilon \tag{2.32}$$

where dW_s and dW_e are the stored energy (the area enclosed by the stress curves OA and AC in Figure 2.9) and elastic energy of deformation, respectively; F½ðεf ε0Þ=S0 is a normal distribution function; Df is the damage variable when the dependent variable is the peak strain εf; and S0 is the distribution parameter of Weibull distribution.

Brittleness indices B30 (Equation 2.33) and B31 (Equation 2.34) were proposed by Tarasov and Potvin (2013) and they considered brittleness as the capacity for self-sustaining macroscopic failure in the post-peak region as a result of the accumulated

elastic energy within the loaded material. B and B range from (+∞, 0) and (-∞ , 1) respectively and brittleness constantly increases from left to right boundary of the two ranges (Meng et al, 2020).

$$B_{30} = {dW_r}/{dW_e} = \frac{(M - E)}{M} \tag{2.33}$$

$$B_{31} = {dW_a}/{dW_e} = \frac{E}{M} \tag{2.34}$$

Where dW_r, dW_e and dW_a are the rupture energy, elastic energy and additional energy (or released energy), respectively.

Brittleness index B_{32} (Equation 2.35) was proposed by Andreev (1995) as the product of the post-peak modulus (M) and the elastic modulus (E) it is not normally used however because it does not have a significant physical basis (Meng et al, 2020).

$$B_{32} = \frac{E}{M} \tag{2.35}$$

Brittleness indicies B_{33} (Equation 2.36) and B_{34} (Equation 2.37) were proposed by Ai et al. (2016) and they defined brittleness as “the ability of rock to accumulate elastic energy during the pre-peak stage and to self-sustain fracture propagation in the post-peak stage”. The brittleness indices are very similar to brittleness indices B_{30} and B_{31} with the exception of taking the pre-peak dissipation energy into account (Meng et al., 2020).

$$B_{33} = \frac{dW_r + dW_d}{dW_e + dW_d} \tag{2.36}$$

$$B_{34} = \frac{dW_a}{dW_e + dW_d} \tag{2.37}$$

Where dW_d is the dissipated energy.

Brittleness indices B_{35} (Equation 2.38), B_{36} (Equation 2.39) and B_{37} (Equation 2.40) were proposed by Munoz et al (2016) and are defined as the proportion of total energy or rupture energy to the elastic energy held at peak strength. They were utilized to evaluate the drilling and rock-cutting performance of varying drilling and cutting tools. B_{30} is inversely proportional to B_{36}. The crack damage stress, UCS and tangent Young's modulus have a directly proportional relationship with B_{35}, B_{36} and B_{37} which illustrates that the strength characteristics of rock are reflected by the indices (Meng et al, 2020).

$$B_{35} = \frac{U_e}{U_{total}} = \frac{dW_{te}}{(dW_d + dW_r)} \tag{2.38}$$

$$B_{36} = \frac{U_e}{U_{post}} = \frac{dW_{te}}{dW_r} \tag{2.39}$$

$$B_{37} = \frac{U_{peak}}{U_{total}} = \frac{dW_{te} + dW_d}{(dW_d + dW_r)} \tag{2.40}$$

where U_e and dW_{te} are the stored elastic energy at peak strength, U_{total} and dW_d, dW_r are the total energy at failure, U_{post} and dW_r are the rupture energy, and U_{peak} and dW_{te} dW_d are the sum of energy at peak strength.

Brittleness indices B38 (Equation 2.41) and B39 (Equation 2.42) were proposed by Kivi et al. (2018) and Li et al. (2019) respectively. They are composed of two parts namely, the ratio of the total elastic energy to the rapture energy at failure and the total elastic energy to the total energy at peak stress and they were utilized to determine the brittleness indices of shale (Meng et al, 2020).

$$B_{38} = \frac{1}{2}\left(\frac{dW_e}{dW_r} + \frac{dW_e}{dW_{te} + dW_d}\right) \tag{2.41}$$

$$B_{39} = B_{pre}B_{post} = \frac{dW_{te}}{dW_{te} + dW_d}\frac{dW_{te}}{dW_r} \tag{2.42}$$

Brittleness index B40 (Equation 2.43) was proposed by Chen et al. (2017), and it was utilized to determine the brittleness indices of granite, sandstone and shale at varying confining pressure. It is not favourable to use, however, because many parameters are involved in this index (Meng et al, 2020).

$$B_{40} = \frac{R_0}{R_u^f} \tag{2.43}$$

2.3.3 Brittleness indices based on elastic parameters (B_{41} – B_{47})

Brittleness indices B41 (Equation 2.44) to B47 (Equation 2.45) are based on elastic parameters. The brittle parameters of rocks are determined using the relationship between the elastic parameters of the rock. They are limited however, in that many samples are required for statistical analysis and testing in order to accurately determine brittleness, which is not cost-effective. The effect of rock mechanic behaviour at post-peak on brittleness and the stress state are not taken into account when this method is used (Zheng et al, 2021). The relationship between stress and strain can be defined by the relationship between Poisson's ratio and the g's modulus it is, therefore, more accurate to predict brittleness than the traditional stress and strain analysis methods (fungdi, 2020; Meng et al, 2020).

According to Meng et al (2020) one of the most used brittleness indices in gas and shale exploration is $B_{41.}$ This index was proposed by Rickman et al. (2008). They considered both Poisson's ratio and Young's modulus, which are estimated from the

dynamic values obtained from the shear and compressive slowness (Mullen et al., 2007; Meng et al., 2020).

$$R_{41} = \frac{1}{2}\left(\frac{E - E_{min}}{E_{max} - E_{min}} + \frac{v_{max} - v}{v_{max} - v_{min}}\right) \quad (2.44)$$

Where E_{max} and E_{min} are the maximum and minimum static Young's moduli, respectively

Brittleness index B42 (Equation 2.45) was proposed by Guo et al. (2015) and is a modification of B which considers the domination of tensile mechanisms in the complex brittle failure of shale. The two brittleness indices, however, have no physical meaning (Meng et al, 2020).

$$R_{42} = \left(\propto \frac{E - E_{min}}{E_{max} - E_{min}} + \beta \frac{v_{max} - v}{v_{max} - v_{min}}\right) \quad (2.45)$$

Brittleness indices B43 (Equation 2.46) and B44 (Equation 2.47) were proposed by Luan et al. (2014) and Sun et al. (2013) respectively and they were utilized to estimate the brittleness indices of shale (Meng et al, 2020). The two indices are not mathematically viable however, because the Poisson's ratio and Young's modulus have different units and thus, they have no physical meaning. They also do not reflect the brittle fracture process of rock (Fungdi, 2020; Meng et al., 2020).

$$B_{43} = {}^{E}/_{v} \quad (2.46)$$

$$B_{44} = {}^{E\rho}/_{v} \quad (2.47)$$

Brittleness indices B45 (Equation 2.48) and B46 (Equation 2.49) were proposed by Chen et al. (2014) and Guo et al. (2021), and they are based on Lame's first parameter,

the Young's modulus, Poisson's ratio and shear modulus for shale gas. The Young's modulus is sensitive to porosity and organic matter, it is argued by (Fungdi, 2020) that the indices cannot be properly applied to the determination of shale brittleness.

$$B_{45} = {}^{E}/_{\lambda} \tag{2.48}$$

$$B_{46} = {}^{(\lambda + 2\mu)}/_{\lambda} \tag{2.49}$$

Brittleness index B47 (Equation 2.50) was proposed by Liang et al. (2017) using a series of linear regressions. It was utilized to estimate the brittleness of shale and was found to be related to brittleness index B_{14} (Meng et al, 2020).

$$B_{47} = a\rho + b\phi + cE + d \tag{2.50}$$

2.3.4 Brittleness indices based on mineralogical composition (B_{48} – B_{55})

Brittleness indices based on mineralogical composition uses the amount of brittle minerals in the total mineral content in a rock to evaluate the brittleness of rocks. The mineralogical characteristics cannot sorely account for rock brittleness characteristics, other factors such as the diagenetic environment, the shape of the brittle minerals and the type of rock cementation should also be considered. These brittleness index can be effective in evaluating the brittleness of rocks in the same geological area but cannot reflect the influence of changes in complex stress conditions on the brittle failure of the rock mass (Zhang et al, 2021). According to Fungdi (2020), rock brittleness is lower than the fraction of brittle mineral compositions. Minerals can be classified as either brittle or ductile, with quartz being an example of brittle minerals and carbonate and clay being examples of ductile minerals (Jarvie et al., 2007). These brittleness indices are commonly employed to design and select hydraulic fracturing in shale reservoirs (Meng et al, 2020).

Brittleness indices B_{48}, B_{49} and B_{50} were proposed by Jarvie et al. (2007), Wang and Gale (2009) and Jin et al. (2014) respectively. The types of brittle minerals being considered is what differentiate brittleness indices B_{48} (Equation 2.51), B_{49} (Equation 2.52) and B_{50} (Equation 2.53) for example, mica, feldspar, quartz, calcite, and dolomite are considered in B_{50} whereas quartz is the only mineral considered brittle in B_{48}. These brittleness indices are limited however, because they assume that brittleness is only dependant on the content of brittle minerals and that each mineral has an equal contribution to the brittleness of rocks, which is not accurate (Meng et al, 2020).

$$B_{48} = \frac{W_{qtz}}{W_{qtz} + W_{carb} + W_{clay}} \tag{2.51}$$

$$B_{49} = \frac{W_{qtz} + W_{dol}}{W_{qtz} + W_{dol} + W_{lm} + W_{clay} + W_{toc}} \tag{2.52}$$

$$B_{50} = \frac{W_{afm} + W_{cal} + W_{dol}}{W_{tot}} \tag{2.53}$$

Brittleness indices B_{51} (Equation 2.54), B_{52} (Equation 2.55), B_{53} (Equation 2.56), and B_{54} (Equation 2.57) were proposed by Shi et al. (2017), Moghadam et al. (2019), Liu and Sun (2015) and Huo et al. (2018) respectively. There is a lack in information as to how to quantify brittleness indices B_{51} and B_{52} and brittleness indices B_{53} and B_{54} are obtained from the ratios of Young's modulus, Poisson's ratio of individual minerals (Meng et al, 2020).

$$B_{51} = \frac{aW_{cal}}{bW_{toc} + cW_{cal} + eW_{fsp}} \tag{2.54}$$

$$B_{52} = \frac{V_{qtz} + V_{fsp} + V_{py} + 0.5V_{carb}}{V_{tot}} \tag{2.55}$$

$$B_{53} = \sum_{i=1}^{n} (\alpha_i f_i) \tag{2.56}$$

$$B_{54} = \frac{\sum_{i=1}^{M} (A_i M_i), A_i = \frac{a_i}{a_{iq'}}\ a_i = E_i}{v_i} \tag{2.57}$$

Also known as the rock tenacity rating index, brittleness index B_{55} (Equation 2.58) was proposed by Suorinent et al. (2009) and it is an index that also considers different contributions of the constituting minerals (Meng et al., 2020).

$$B_{55} = RTRI = S_F G_F F_F \tag{2.58}$$

2.3.5 Brittleness indices based on conventional well digging data (B_{56} – B_{62})

The values of the Young's modulus, neutron porosity, compression and shear wave, neutron porosity and density can be obtained from the analysis of conventional well logs. The velocities of the S and P-wave velocities are used to determine the Poisson's ratio (Lai et al, 2015). Meng et al (2020) indicated that obtaining these indices is not difficult and they can be utilized to screen for favourable hydraulic fracturing options and the characterization of unconventional shale gas reservoirs.

Brittleness indices B_{56} (Equation 2.59) and B_{57} (Equation 2.60) were proposed by Tang et al. (2016) based on the different profile of s- and p-wave velocities around a borehole. During borehole and well drilling, rocks with high brittleness induce more microcracks at the wall of boreholes. It was argued however, by Meng et al (2020) that these indices cannot be used as brittleness indices because they attribute the varying number of microcracks to the different brittleness values of rocks while ignoring the different stress levels along the depth of the borehole (Suorineni et al., 2009).

$$B_{56} = BF_{vp} = \int_{r=R}^{+\infty} \frac{\left(\frac{\Delta v_p(r)}{v_p dr}\right)}{R} (f\ or\ p-wave) \tag{2.59}$$

$$B_{57} = BF_{vs} = \int_{r=R}^{+\infty} \frac{\left(\frac{\Delta v_s(r)}{v_s dr}\right)}{R} (f\ or\ s-wave) \tag{2.60}$$

Brittleness indices B_{58} (Equation 2.61), B_{59} (Equation 2.62), B_{60} (Equation 2.63) and B_{61} (Equation 2.64) were proposed by Lai et al. (2015), Kivi et al. (2017) and Jin et al. (2014) respectively and are a cost-effective alternative to the mineralogical index B. They, therefore, share the same limitations as the brittleness index B_{50} (Meng et al, 2020).

$$B_{58} = 1001.5\left(\frac{GR}{Pe}\right)^{-0.7734} \tag{2.61}$$

$$B_{59} = \varpi_1(p_1 DTC + q_1\phi + r_1) + \varpi_2(p_2 DTC + q_2\phi + r_2 \tag{2.62}$$

$$B_{60} = -1.8748\phi + 0.9679 \tag{2.63}$$

$$B_{61} = aDTC + b \tag{2.64}$$

Artificial neural networks (ANN) were utilized by Kaunda and Asbury (2016) to combine the database on s- and p-wave velocities, rock density and elastic characteristics. It has been found to be more accurate at predicting rock brittleness in comparison to the traditional stress-strain method and multiple regression techniques (Fungdi,2020).

$$B_{62} = 2.02\gamma + 0.008p - 61.12v - 2.60R - 21.76 \quad (2.65)$$

2.3.6 Brittleness indices based on the angle of internal friction (B_{63} – B_{65})

Brittleness indices B_{63} (Equation 2.66), B_{64} (Equation 2.67) and B_{65} (Equation 2.68) were proposed by Hucka and Das (1974) and Zhou et al. (2018) respectively and they are a function of the internal friction angle. The angle in B_{63} is obtained from the slope of Mohr's envelope, it is obtained from the measure of the fracture angle in B_{64} (Fungdi, 2020; Meng et al, 2020). It is generally accepted that the internal friction angle has a directly proportional relationship with brittleness (Hucka and Das, 1974; Zhang et al., 2016). Brittleness index B_{65} combines the internal friction angle and the pre-and post-peak modulus (Fungdi,2020).

$$B_{63} = \sin\varphi \quad (2.66)$$

$$B_{64} = \varphi = 45° - 2 \propto f \quad (2.67)$$

$$B_{65} = \frac{(\sigma_p - \sigma_r)}{\sigma_p e^{E/M} \sin\varphi} \quad (2.68)$$

2.3.7 Brittleness indices based on the force-penetration graph (B66 – B68)

Brittleness indices B_{66} (Equation 2.69), B_{67} (Equation 2.70) and B_{68} (Equation 2.51) were proposed by Yagiz et al. (2009), Copur et al. (2003) and Liu et al. (2016) respectively and they are based on the penetration test. These indices are often employed to assess the fragmentation efficiency of disc cutters (Meng et al, 2020).

Brittleness index B_{66} is a commonly used index in underground tunnelling and was a basis of other indices namely B_6 to B_9 and B_{62}. Yagiz (2009) utilized graphs from the punch penetration test to evaluate rock brittleness by evaluating the ratio between the penetration depth and the maximum force applied. For very high brittle rock, $B_{66} \geq 40$, for ductile rock, $B_{66} \leq 19$ (Fungdi, 2020). it was noted, however, that the index is a more accurate representation of rock compressive strength as opposed to brittleness (Meng et al, 2020).

$$B_{66} = {F_{max}}/{p} \tag{2.69}$$

B_{67} (Equation 2.70) is the ratio of force decrement period to increment period and B_{68} (Equation 2.71) is defined as s the ratio of cumulative decrease force to increase force. Brittle materials are more likely to violently and frequently after plastic or elastic deformation, and a brittle material's increment time is shorter than that of a ductile material thus B and B are larger for brittle rocks as compared to ductile rocks (Fungdi, 2020).

$$B_{67} = {p_{dec}}/{p_{inc}} = \frac{\frac{1}{s}\sum_{i=1}^{s} p_{deci_i}}{\frac{1}{n}\sum_{j=1}^{n} p_{inc_j}} \tag{2.70}$$

$$B_{68} = {p_{down}}/{p_{up}} = \frac{\sum_{i=1}^{s} F_{down_i}}{\sum_{j=1}^{n} F_{up_j}} \tag{2.71}$$

2.3.8 Brittleness indices based measured from indentation test (B_{69} – B_{73})

According to Meng et al (2020) indentation tests are usually utilised to evaluate the hardness of materials, as a result, there have been brittleness indices proposed based on them.

Brittleness index B_{68} (Equation 2.72) was proposed by and is quantified by the difference between the micro- and macro-indentation hardness values. It has however been stated that further research is needed in the application of this index to assess brittleness because the difference between micro and macro indentation hardness values is vague thus the index has an unclear physical meaning (Meng et al, 2020).

$$B_{69} = \frac{\left(H_{\mu} - H\right)}{K} \tag{2.72}$$

Brittleness indices B_{70} (Equation 2.73) and B_{71} (Equation 2.74) were proposed by Lawn and Marshall (1979). They defined brittleness as the ratio of hardness to toughness. These indices are based on fracture mechanics and were propose for ceramic materials. The inhomogeneous and anisotropic nature of rocks make them different from ceramic hence making the application of these indices to rock brittleness evaluation inaccurate (Fungdi, 2020; Meng et al, 2020).

$$B_{70} = \frac{H}{K_{IC}} \tag{2.73}$$

$$B_{71} = \frac{HE}{K_{Ic}^2} \propto \frac{deformation\ energy\ per\ unit\ volume}{fracture\ surface\ energy\ per\ unit\ area} \tag{2.74}$$

Brittleness index B_{72} (Equation 2.75) was proposed by Sehgal et al. (1995) and was used to denote the brittleness index of glass. It can be concluded because of this that the index is not suitable for rock brittleness evaluation because of the differences between glass and rocks (Meng et al, 2020).

$$B_{72} = \frac{C}{a} \tag{2.75}$$

Brittleness index B_{73} (Equation 2.76) was proposed by Fan et al. (2019), and it was used to denote shale. This index was found to have limitations, however, because the deformation volume brought about by crack propagation and initiation is hard to measure (Meng et al, 2020).

$$B_{73} = \frac{v_c}{v_I} = \frac{v_c}{v_c + v_v} \tag{2.76}$$

2.3.9 Brittleness indices based on contents of fines after impact (B74 – B75)

Brittleness indices B_{74} (Equation 2.77) and B_{75} (Equation 2.78) were proposed by Dahl (2003) and Hucka and Das (1974) respectively the bases of the dependence of the formation of fines on material strength and the loss of cohesion strength under impact from a particular height. They deduced that brittleness can be determined by the number of fines formed under the impact test (Fundhdi, 2020). These indices are limited however because they do not consider the effect of the stress state on brittleness (Meng et al, 2020).

$$B_{74} = S_{20} \tag{2.77}$$

$$B_{75} = q\sigma c \tag{2.78}$$

2.3.10 Brittleness indices based on over-consolidation characteristics (B_{76} to B_{77})

The consolidation state of sedimentary rocks has been determined to have an effect on their brittleness, it is on this basis that brittleness indices B_{76} (Equation 2.79) and B_{77} (Equation 2.80) were proposed by Ingram and Urai (1999) and Nygard et al. (2006) respectively. These indices are limited in that they were developed using soil

mechanics properties and they can only be applied to sedimentary rocks and are not applicable to igneous and metamorphic rocks (Meng et al, 2020).

$$B_{76} = \frac{UCS_{OC}}{UCS_{NC}} \tag{2.79}$$

$$B_{77} = OCR^{b} = \left(\frac{\sigma'_{vmax}}{\sigma_{v}}\right)^{b} \tag{2.80}$$

2.4 Summery of the Chapter

It can be concluded that despite various scholars striving to solve the problem associated with the development accurate brittleness index. The developed methods appear to suffer various challenges, for example, most mechanical methods do not consider the impact of mineralogical composition on the brittleness of the rock units. Therefore, there is a need to develop brittleness methods that integrate both mechanical methods with rock unit mineralogical composition among others.

CHAPTER THREE

RESEARCH DESIGN AND METHODOLOGY

3.1. Preliminary Work

This is the first step in the study's approach, complete to gain a general understanding of the currently available literature in the study area. It is subdivided into a desktop study, that includes the literature review and reconnaissance.

3.1.1. Desktop Study

This constitutes a fundamental phase in the research process. This method entails a systematic collection of relevant data from diverse sources, including but not limited to journals, articles, books, and reports. The main aim of a desktop study is a critical evaluation of the current body of literature to gain an in-depth understanding of the research topic before engaging in primary research methodologies such as experiments.

Key components of a desktop study include the identification of relevant literature sources through thorough investigations across academic databases that provide scientifically viable, peer-reviewed information on the research field. This investigation provides a clear representation of the current body of literature and is essential in identifying the gap in literature. This, in turn, guides the formulation of the research questions and hypothesis.

Moreover, the identification of the gap in the literature is essential in the formulation of the research aims and objectives. This ensures that the study to be conducted contributes meaningfully to the research field.

3.1.2. Reconnaissance survey

This marks the subsequent phase of the study, which aims to reconcile the literature with the physical conditions on the field. This was undertaken to gain a broad understanding of the mineralogical and geological features of the platinum-bearing reefs on the eastern limb of the Bushveld Igneous Complex. Several locations on the

UG2 platinum reef were explored to attain foundational data before a more detailed investigation of the mineralogical composition was conducted.

3.2. Petrographic Analysis

3.2.1. Sample Collection and Analysis

A sample of chromite from the platinum-bearing reefs (UG2) was obtained from a borehole (see Figure 3.1) from the eastern limb of the Bushveld Igneous Complex. Samples were bagged and labelled properly. Fifty polished sections (see Figure 3.2) were prepared from the collected sample to be used in petrographic studies. A digital microscope (see Figure 3.3) was utilised to produce digital images. The sample was evaluated for rock properties including the degree of sorting, packing properties of grains, nature of grain contact and degree of textural interlocking.

The petrographic microscope was used to perform a consolidation factor Modal analysis, using the point counting technique proposed by Gezi-Dickenson (Ingersoll et al. 1984). The method proposed by Hutchison (1974) was used to determine mean grain size. The method proposed by Kahn (1956) was used to quantify the packing density and packing proximity. Comprehensive charts developed by Powers (1953) and Rittenhouse (1943) were used to evaluate the roundness (ρ) and sphericity (Ψp) parameters, respectively (these constitute the grain shape). The degree of grain sorting was determined using the classification chart developed by Beard and Weyl (1973).

Figure 3. 1 UG2 samples used for the study.

Figure 3. 2 Some of the prepared polish sections of UG2.

Figure 3. 3 Microscope used for petrographic analysis.

3.2.2. Textural Studies

In examining the texture of the thin sections, various aspects were considered, including mean grain size, grain shape (roundness and sphericity), sorting, textural interlocking, grain contact nature, packing properties (density and proximity), and consolidation factor.

- Mean grain size was determined by studying 100 randomly chosen grains from multiple fields of view per thin section, following Hutchinson's method (1974), which measured the average length of two perpendicular axes crossing each grain's centre.
- Grain roundness (ρ) and sphericity (Ψp) were assessed using Powers' comparative chart (1953) for roundness and Rittenhouse's chart (1943) for maximum projection sphericity, based on visual analysis of 50 randomly selected particles in each polish section (Figure 3.2).

- The degree of sorting was determined using Beard and Weyl's classification chart (1973), with five random fields of view per polish section being evaluated (Figure 3.2).
- Packing density and packing proximity are two important parameters used to describe the arrangement and distribution of grains within a sedimentary rock, particularly in sandstones. They indicate how closely packed the grains are and can influence properties such as porosity and permeability. Packing density refers to the volume fraction of solid grains within a rock sample. Packing proximity refers to the spatial arrangement of grains within a rock sample, particularly the distance between neighbouring grains. Kahn (1956) method was used to determine the packing density and packing proximity (Figures 3.6 3.7 and 3.8). The packing density was calculated by dividing the total length of grains intercepted by an imaginary line by the length of the entire imaginary line.

$$P_d = \frac{Total\ length\ of\ grains\ along\ the\ traverse\ imaginary\ line}{length\ of\ traverse\ imaginary\ line} \times 100\ (\%) \qquad (3.1)$$

Packing proximity was determined by comparing the quantity of grain-to-grain contacts along an imaginary line to the overall number of contacts between particles along the imaginary line (Equation 3.2).

$$P_p = \frac{Total\ number\ of\ grain\ to\ grain\ contact\ along\ the\ imaginary\ traverse\ line}{Total\ number\ of\ contacts\ along\ the\ imaginary\ traverse\ line} \times 100(\%) \qquad (3.2)$$

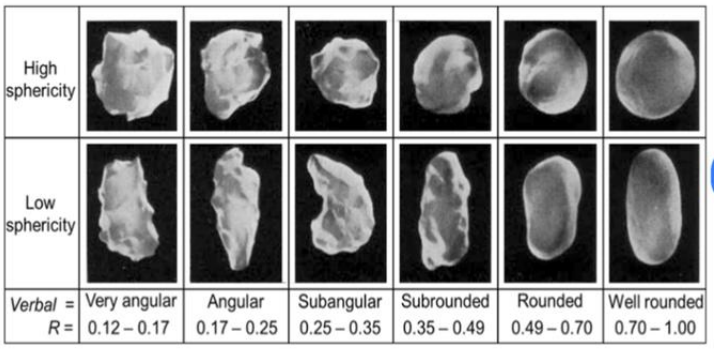

Figure 3. 4 Roundness and sphericity comparative (Powers, 1953).

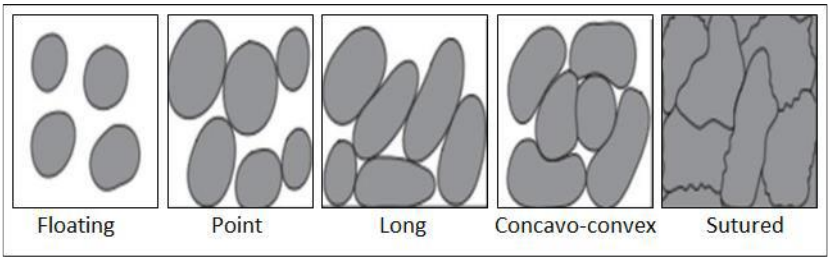

Figure 3. 5 Grain to grain contact types (Chima et al., 2014).

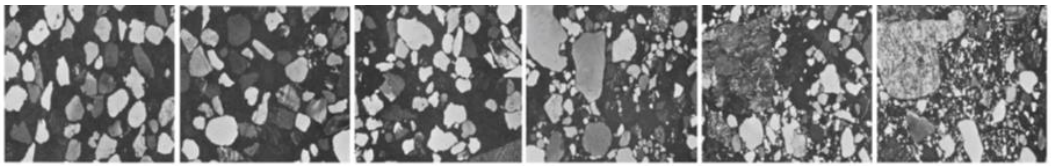

Figure 3. 6 Sorting groups comparative thin section (Beard and Weyl, 1973).

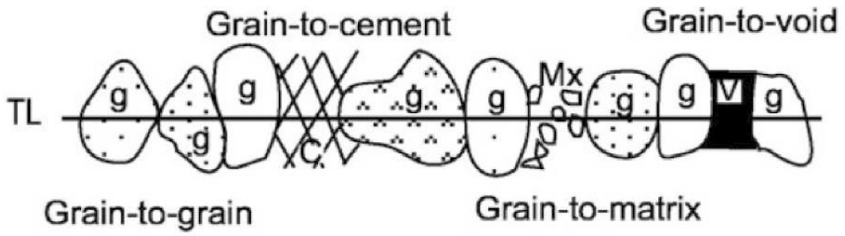

Figure 3. 7 Contact nature (Tamrakar et al., 2007).

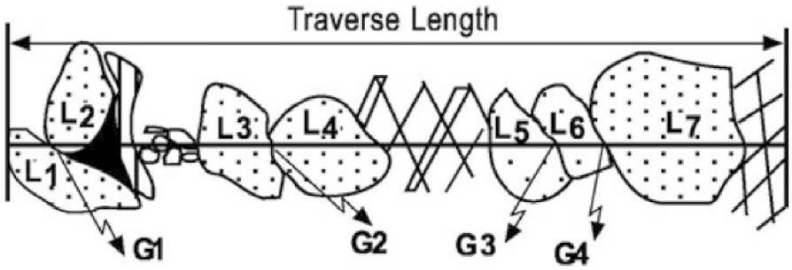

Figure 3. 8 Methods for determining packing density and packing proximity (Tamrakar et al 2007).

3.3 Rock Unit Properties

3.3.1 Uniaxial Compressive Test

The uniaxial compressive test was performed using a standardized procedure to assess the compressive strength of rock samples. Initially, rock specimens were

prepared by cutting them into cylindrical shapes with precise dimensions, typically measuring 50 mm in diameter and 100 mm in height. The specimens were then carefully examined to ensure they were free of visible defects and irregularities.

The samples were placed in a uniaxial compressive testing machine, which was equipped with two rigid plates that applied a unidirectional compressive load. The specimen was aligned between the plates to ensure even distribution of the load. The load was applied gradually at a constant rate until the sample failed. Throughout the test, the load and corresponding deformation of the specimen were continuously recorded by the testing machine.

Upon failure, the maximum load sustained by the specimen was noted. The compressive strength of the rock was calculated by dividing the maximum load by the cross-sectional area of the specimen. The test was repeated on multiple samples to obtain a consistent set of data. The results were analysed to determine the rock's compressive strength and were documented along with any observations regarding the failure mode, such as whether the failure was brittle or ductile. The findings were used to assess and describe the mechanical properties (Strength) with reference to standardized values (Table 3.1).

Table 3. 1 Standardized UCS description (ISRM, 1981).

Description	Uniaxial Compressive Strength (MPa)
Very weak	Less than equal 10
Weak	10 - 50
Medium	50 - 100
Strong	100 - 250
Very Strong	>250

3.3.2 Numerical Simulation

Some of the rock unit parameters could not be identified using UCS therefore further predictions using RocData were utilised. The model was able to provide other parameters such as shear stress, and normal stresses among others as shown in

Figure 3. 11. The simulated rock properties were there used to develop models using statistical analysis as denoted below.

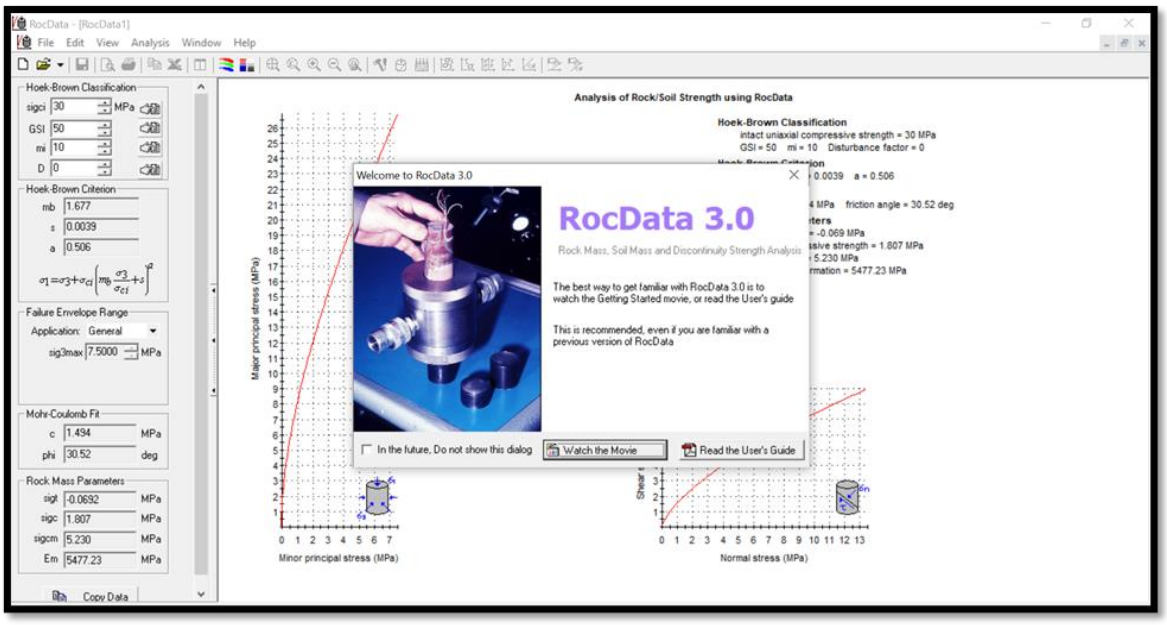

Figure 3. 9 Example of RocData model simulating rock unit parameters

3.4 Statistical analysis.

Statistical analysis was utilized to investigate the relationship between the brittleness index and petrographic characteristics. Overall, the statistical data analysis performed in the study aimed to identify the petrographic variables that have a significant impact on brittleness indices and develop predictive models to estimate brittleness based on these variables.

3.3.1 Regression analysis

By employing simple and multivariate linear regression techniques, the researchers aimed to develop predictive models to estimate the brittleness of different sandstone types based on their petrographic properties and evaluate the performance of these models using rigorous statistical analysis.

3.3.2 Simple Linear Regression

The researchers initially used simple linear regression to establish a simple predictive relationship between the petrographic characteristics of the studied sandstones and their brittleness indices. This involved conducting bivariate correlation analysis and

calculating Pearson's correlation coefficients to identify statistically significant correlations at the 95% confidence level.

3.3.3 Multivariate Linear Regression

The study employed multivariate linear regression, specifically the backward multiple linear regression analysis (BMLR) technique, to determine the relationships among the dependent variables (brittleness indices) and petrographic parameters as independent variables. The BMLR involved the simultaneous inclusion of all independent variables in the model, followed by the elimination of unimportant variables step by step based on their coefficient of multiple determination and significance level.

3.3.4 Evaluation of Regression Models

The regression models were evaluated using various statistical measures, including the coefficient of determination (R-squared), the adjusted coefficient of determination, the standard error of estimate (SEE), standardized beta weights, t-test statistics, and F-test statistics. These measures were used to assess the capacity performance of the obtained predictive equations an

3.3.5 Model development

By following these steps and utilizing rigorous statistical analysis, the researchers developed predictive models to estimate the brittleness of different sandstone types based on their petrographic properties, aiming to provide cost-effective and meaningful relationships between petrographic variables and brittleness indices.

Model Selection: The backward multiple linear regression analysis (BMLR) technique was utilized to select the most important independent variables and develop predictive models that can explain the dependent variables adequately.

Evaluation of Models: The developed regression models were evaluated using statistical measures such as the coefficient of determination (R-squared), the adjusted coefficient of determination, the standard error of estimate (SEE), standardized beta weights, t-test statistics, and F-test statistics to assess their predictive capability and overall validity.

Model Refinement: The BMLR technique involved the elimination of unimportant variables step by step based on their coefficient of multiple determination and significance level, leading to the development of optimal predictive models with fewer independent variables.

CHAPTER FOUR

DETERMINATION OF THE BRITTLENESS OF UG2REEF BASED ON EMPIRICAL FORMULAS

4.1 Introduction

Brittleness is a fundamental mechanical property of rock that is widely studied in the field of rock mechanics. Commonly used parameters such as Brazilian tensile strength and uniaxial compressive strength are often used to evaluate brittleness due to their relative ease of measurement (Bilen et al., 2021). However, research on the mechanical properties of the Eastern Limb of the UG2 platinum reef, part of the Bushveld Igneous Complex, has been limited due to challenges associated with its beneficiation. Nonetheless, several authors have conducted studies that have addressed these challenges, and the UG2 reef has been identified as the most PGE-endowed chromitite layer, highlighting its economic significance (Langa et al., 2021). Therefore, there is a need to develop methods to easily determine the brittleness of the Eastern limb of the UG2 reef to facilitate exploration of PGEs.

This study focused on filling this knowledge gap by investigating the mechanical properties of the UG2 reef and examining the impact of various mechanical parameters, beyond traditional stress and strain measures, on its brittleness. To achieve this, a series of tests were conducted to determine key mechanical properties of the UG2 reef. While some properties were obtained directly from these tests, others required the use of numerical simulations.

The collected mechanical parameters were then used to calculate the brittleness indices of the UG2 reef, employing traditional brittleness indexes B1-B6 as benchmarks. These benchmarks provided a basis for evaluating and contrasting newly developed brittleness indices derived from multivariate linear models. Through this approach, the study focused on indicating the significance of different mechanical parameters in determining the brittleness of the UG2 reef.

4.2 Results and Discussions

The analysis commences with a discussion of the mechanical properties of the UG2 platinum reef, followed by the estimation of brittleness indices using empirical methods. This is succeeded by the development of modified brittleness indices based on stress-strain relationship indices, and a subsequent discussion of the outcomes.

4.2.1 Mechanical Prosperities of UG2 Reef

The present section focuses on the mechanical properties of the UG2 reefs, which encompasses the outcomes of the uniaxial compressive strength, Young's modulus (E), Poisson's ratio (υ), Peak Strain (ep), tensile strength (σt), and compressive strength (σc). As depicted in Table 4.1, these are the crucial mechanical properties of the UG2 reef.

Research conducted by Watson et al (2021) on pillars situated on the limb disclosed a laboratory test average UCS of 81 MPa. This study discloses that the uniaxial compressive strength (UCS) of the UG2 reef showcases a broad range, from 30 MPa to 60 MPa, with an average of 55Mpa, which signifies the samples' heterogeneous nature. The work carried out by Oates and Malan (2023) revealed that the UCS ranges from 136.8 Mpa to 152.6 Mpa, with an average UCS of 144.7Mpa. The testing results from this study indicate that the samples are relatively weaker than those obtained by other researchers. The Young's modulus (E) demonstrates a range of 80 GPa to 95 GPa, with an average of 92.82 GPa, indicating the variable structural integrity within the samples. As per Watson et al (2021), the average Youngs modulus is 184 Gpa. The results obtained suggest that the Young's modulus is relatively lower than that obtained by other authors.

Additionally, the Poisson's ratio (υ) spans from 0.25 to 0.35, with an average of 0.30 emphasizing the variation in the materials responses to external stressors. Work conducted by Watson et al (2021) indicated an average Poisson’s ratio of 0.33. The results obtained indicate that the Poisson’s ratio is relatively equivalent to that obtained from work conducted by other authors.

The stress levels across the samples vary from 0.219 to 0.583 MPa, exhibiting the differences in their responses to pressure. The range of tensile stress and

compressive stress is from -0.0067 to -0.178 MPa. Finally, the peak strain (εp) ranges from 0.000375 to 0.000727 MPa, capturing the strain thresholds characteristic of the UG2 specimens under test conditions.

Table 4. 1 Mechanical properties of UG2 reef.

UG2 Reef		Mechanical Properties					
		UCS (MPa)	Young modulus (GPa) (E)	Poisson's ratio (υ)	Peak Strain (eP)	Compressive strength (σc)	Tensional strength (σt)
Normal reef	Sample 1	30	80	0.25	0.000375	0.219	-0.0067
	Sample 2	35	82	0.26	0.000426	0.255	-0.0078
	Sample 3	40	85	0.27	0.000470	0.292	-0.0089
	Sample 4	45	86	0.28	0.000523	0.328	-0.0100
	Sample 5	50	90	0.29	0.000555	0.365	-0.0111
	Sample 6	55	92	0.30	0.000597	0.401	-0.0122
	Sample 7	60	95	0.31	0.000631	0.438	-0.0134
	Sample 8	65	96	0.32	0.000677	0.474	-0.0145
	Sample 9	70	100	0.33	0.000700	0.511	-0.0156
	Sample 10	75	105	0.34	0.000714	0.547	-0.0167
	Sample 11	80	110	0.35	0.000727	0.583	-0.0178

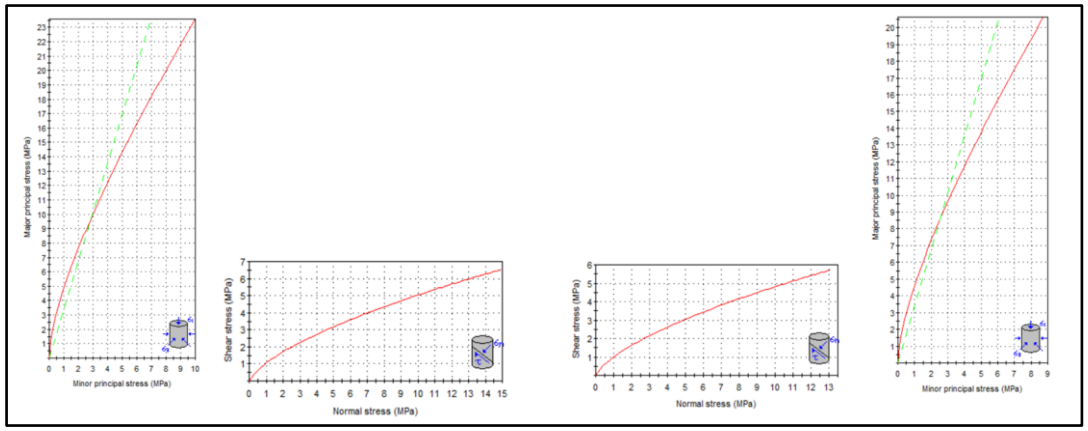

Figure 4. 1 Simulated mechanical properties of UG2 sample 3

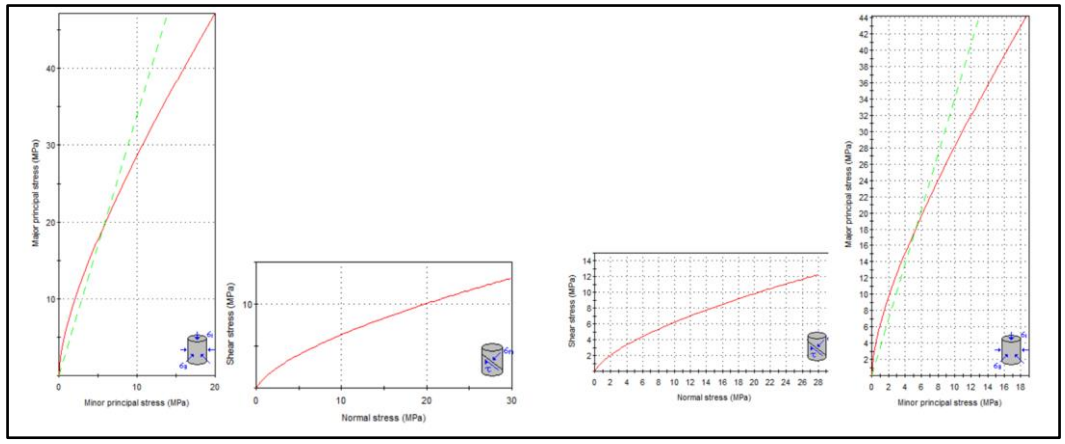

Figure 4. 2 Simulated mechanical properties of UG2 sample 4

The Figures 4.1 to 4.4 above provide insights into the mechanical properties and failure criteria of a material under different stress conditions. The left and right graphs plot the major principal stress (σ1) against the minor principal stress (σ3). In both graphs, the red solid line represents the linear relationship between these principal stresses, indicating a directly proportional relationship between the major and minor principal stresses. The green dashed line represents the Hoek-brown failure criterion, and it represents the combinations of principal stresses at which the material fails. The consistent presence of these lines in both graphs reinforce the material's predictable behaviour under varying principal stress conditions, even with different stress ranges.

The middle graphs depict a non-linear relationship between the normal stress (σ) and shear stress (τ). The shear stress increases steeply at lower normal stresses and then starts to level off at higher normal stresses. Understanding the material's yield and failure behaviour under combined stress circumstances requires an understanding of this graph. The curve provides insights into the material's shear strength, cohesion (c), and the angle of internal friction (φ). The maximum shear stresses the material can endure, indicated by the peak of the curve, defines its shear strength, while the initial steep rise corresponds to the material's inherent resistance to shear deformation.

The graphs collectively represent the mechanical behaviour of the material under different loading situations. The left and right graphs emphasize the material's response to principal stresses, essential for understanding its performance under complex loading states, such as in three-dimensional stress conditions. In contrast, the middle graph focuses on the shear stress response under normal stress, a critical factor for assessing shear failure. Together, these graphs provide a comprehensive view of the material's strength and failure characteristics and in combination with the results obtained from the laboratory tests outlined in chapter three (03) provide a comprehensive analysis of the mechanical characteristics of the UG2 reef, depicted in Table 4.1.

4.2.2 Estimation of brittleness of UG2 using empirical methods

The analysis of the brittleness indices, depicted in Table 4.2, for the UG2 Reef samples reveals distinct trends in numerous parameters. B_1 and B_2 ratios remain relatively constant across all samples, indicating the UG2's consistent basic mechanical properties. However, B_3, B_4 and B_5 exhibit a clear increasing trend from Sample 1 to Sample 11, suggesting an overall intensification of the material's combined strength attributes. In contrast, B_6 shows a trend of increasing values, indicating a reduction in brittleness as the sample number increases. This indicates that later samples demonstrate improved resistance to fracturing, which could be attributed to variations in the material composition.

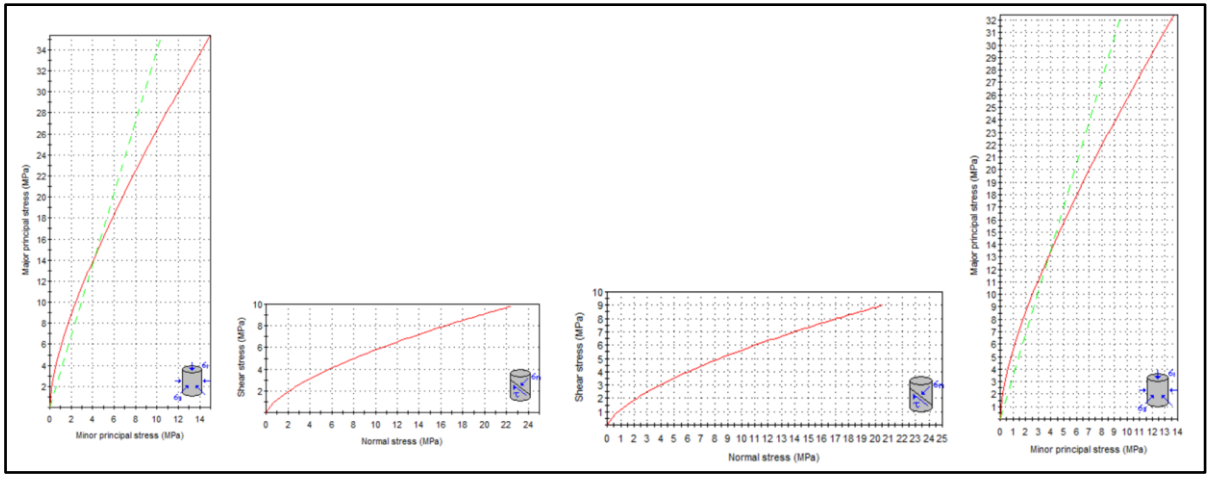

Figure 4. 3 Simulated mechanical properties of UG2 sample 1

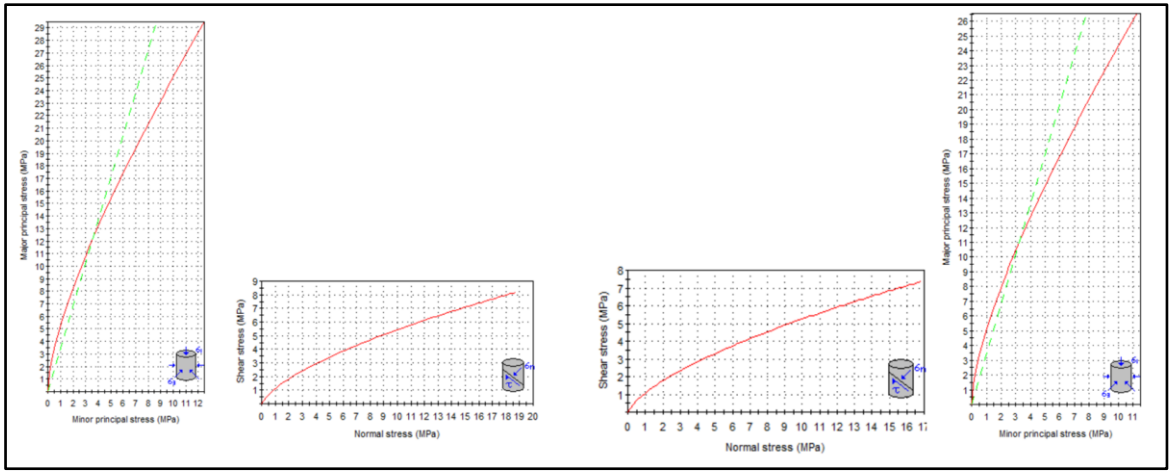

Figure 4. 4 Simulated mechanical properties of UG2 sample 2

Table 4. 2 Estimated brittleness of UG2 based on empirical methods

UG2 Reef		**Brittleness**					
		$B_1 = \frac{\sigma_c}{\sigma_t}$	$B_2 = \frac{(\sigma_c - \sigma_t)}{(\sigma_c + \sigma_t)}$	$B_3 = \frac{(\sigma_c + \sigma_t)}{2}$	$B_4 = \frac{\sigma_c \sigma_t}{2}$	$B_5 = \sqrt{\frac{\sigma_c \sigma_t}{2}}$	$B_6 = 0.198\sigma_c - 2.174\sigma_t + 0.913\rho - 3.807$
Normal reef	Sample 1	32.68	0.9406	0.11285	0.000733	0.0270	-0.1900
	Sample 2	32.69	0.9406	0.1314	0.000994	0.0313	-0.1853
	Sample 3	32.80	0.9408	0.15045	0.000129	0.0113	-0.1804
	Sample 4	32.8	0.9408	0.169	0.00164	0.1280	-0.1756
	Sample 5	32.88	0.9409	0.3761	0.002007	0.0447	-0.1707
	Sample 6	32.86	0.9409	0.2066	0.002446	0.0494	-0.1659
	Sample 7	32.68	0.9406	0.2257	0.005869	0.0766	-0.1612
	Sample 8	32.68	0.9406	0.24425	0.003436	0.0586	-0.1565
	Sample 9	32.75	0.9407	0.2633	0.003985	0.0631	-0.1515
	Sample 10	32.75	0.9407	0.28185	0.004567	0.0675	-0.1468
	Sample 11	32.75	0.9407	0.3004	0.0051887	0.0720	-0.1421

Table 4. 3 Developed model from empirical analysis on brittleness of UG2 using mechanical properties

Index	*Model no.*	*Independent variables*	*R*	R^2	R^2_a	*SE*	*Sig.F*
B1	1	UCS, E ,υ,e_p, σ_c, σ_t	0.993	0.987	0.775	0.011	0.000
	2	UCS, σ_c, σ_t	0.987	0.974	0.963	0.013	0.000
	3	σ_c, σ_t	0.986	0.973	0.966	0.013	0.000
B2	1	UCS, E ,υ,e_p, σ_c, σ_t	0.990	0.981	0.762	0.000	0.000
	2	σ_c, σ_t	0.979	0.959	0.948	0.000	0.000
B3	1	UCS,E ,υ,ep, σc, σt	0.845	0.714	0.229	0.060	0.196
B4	1	UCS,E ,υ,ep, σc, σt	0.944	0.891	0.583	0.000	0.030
	2	σt	0.875	0.766	0.740	0.000	0.000
B5	1	UCS,E ,υ,ep, σc, σt	0.599	0.359	-0.481	0.035	0.749
B6	1	UCS,E ,υ,ep, σc, σt	0.999	0.999	0.799	0.000	0.000
	2	σ_c, σ_t	0.999	0.999	0.999	0.000	0.000

4.2.3 Developing Multivariant Linear Models

New brittleness, based on mechanical properties and pre-existing brittleness indexes were successfully developed based on the analysis. These indexes were developed using various variables, which are detailed in Table 4.3. The two B3 and B5 indices could not be used further for the construction of new brittleness indexes because the models have demonstrated that neither of them has any correlation with any variables. The findings show that the four brittleness indices that were generated can be used to explain or identify the UG2 reef's brittleness indexes.

$$B_1 = 32.72 + 88.6\sigma_C - 2900.53\sigma_t$$

$$B2 = 0.940 + 0.142\ \sigma_C - 4.66\sigma_t$$

$$B4 = -0.00275 - 0.45.48\sigma_t$$

$$B6 = 0.218 - 0.197\sigma_C + 2.168\sigma_t$$

4.3 Discussion of the results

4.3.1 The effect of the Young's modulus (E) and the Poisson's ratio (ʋ) on brittleness

Young's modulus and Poisson's ratio depict the reciprocal effect of stress acting on a material and the strain produced. In this study, the analysis of the effect of Young's modulus was investigated using multivariate linear models. Brittleness index 1, model 1 includes Young's modulus (E) along with other variables and shows a high R (0.993) and R^2 (0.987), but a much lower adjusted R^2 (0.775). This inconsistency indicates overfitting when all independent variables are included. Similar patterns are observed in models B2 model 1, B3 model 1, B4 model 1, B5 model 1, and B6 model 1, with high R and R^2 values but significantly lower adjusted R^2 values, suggesting that including Young's modulus contributes to overfitting without improving model relevance. Specifically, the adjusted R^2 values for these models are 0.762, 0.229, 0.583, -0.481, and 0.799, respectively. Therefore, the inclusion of Young's modulus does not consistently contribute to an accurate prediction of the brittleness index for the UG2 reef.

Similar to Young's modulus, Poisson's ratio (υ) is included in models B1 model 1, B2 model 1, B3 model 1, B4 model 1, B5 model 1, and B6 model 1. These models also show high R and R^2 values but much lower adjusted R^2 values, indicating overfitting. The adjusted R^2 values for these models suggest that Poisson's ratio does not significantly enhance the predictive power of the brittleness index models and instead contributes to overfitting.

The analysis presents that both Young's modulus and Poisson's ratio are not significant in quantifying the brittleness index of the UG2 reef, contrary to the literature. According to Zhang et al (2016) these parameters are more accurate in quantifying brittleness compared to the individual use of stresses and strain. Grieser and Bray (2007) indicated that a low Poisson's ratio and a high Young's modulus are preferable for brittle failure, this is indicated in the data for this study. Additionally, a close relationship between both Young's modulus and Poisson's ratio to the brittleness index was established by Rickman et al (2008) who utilized the parameters to quantify brittleness (equation). The brittleness index based on elastic parameters by Rickman et al. (2008) is also a commonly used index to evaluate rock brittleness. The author reported that the brittleness was generally determined by elastic modulus and Poisson's ratio, and found that the greater these two parameters got, the greater the brittleness. The insignificance of Young's modulus and Poisson's ratio is unexpected and can possibly be attributed to brittleness.

4.3.2 The effect of Peak Strain (ep) on brittleness

The peak strain is the maximum deformation a material can withstand before it fails. In this study, the analysis of the effect of the peak strain was investigated using multivariate linear models. Brittleness Models B1 model 1, B2 model 1, B3 model 1, B4 model 1, B5 model 1, and B6 model 1 include peak strain (ep) as an independent variable. Like Young's modulus and Poisson's ratio, the inclusion of peak strain results in high R and R^2 values but lower adjusted R^2 values, indicating overfitting. The adjusted R^2 values are notably low, with model B3 model 1 showing an adjusted R^2 of only 0.229, which highlights the weak contribution of peak strain to the predictive accuracy of the brittleness index models.

It was expected that an inverse Relationship would be obtained between the peak strain and brittleness, because brittle materials tend to have low peak strain values

because they fail suddenly with minimal plastic deformation. In contrast, ductile materials tend to undergo significant plastic deformation before failure, resulting in higher peak strain values.

Very little was found in the literature on the question of the effect of the peak strain on rock brittleness. However, a study conducted by Yuwei et al (2017) on the Evaluation method of rock brittleness based on statistical constitutive relations for rock damage concluded that the brittleness of rock in coal, shale, and tight sand decreases as the damage variable of peak strain increases. This supports the expected relationship.

4.3.3 The effect of tensile strength (σ_t) and compressive strength (σ_c) on brittleness

As outlined in chapter 2, many researchers and engineers prefer brittleness indexes based on tensile and compressive strengths because they are fundamental mechanical parameters that are easily obtained in routine laboratory loading tests.

In this study, the analysis of the effect of the Young's modulus was investigated using multivariate linear models. Tensile strength (σt) is identified as a significant predictor for the brittleness index. In models B1 model 3, B2 model 2, B4 model 2, and B6 model 2, which focus on fewer variables (including σt), there are high R and R^2 values along with improved adjusted R^2 values. For example, model B1.3 shows an R of 0.986, R^2 of 0.973, and an adjusted R^2 of 0.966. Similarly, B2 model 2 and B6 model 2 have very high R and R^2 values with adjusted R^2 values of 0.948 and 0.999, respectively. These results indicate that σt is a strong predictor of the brittleness index.

Similarly, the compressive strength (σc) also emerges as a significant predictor for the brittleness index. Models B1 model 3, B2 model 2, and B6 model 2, which include σc, maintain high R and R^2 values along with significantly improved adjusted R^2 values, suggesting a strong model fit. For instance, model B1 model 3 has an adjusted R^2 of 0.966, while B6 model 2 shows an adjusted R^2 of 0.999.

These findings highlight that σ_c, along with σ_t, provides a more accurate and less overfitted model for predicting brittleness. The effect of the compressive and tensile strength on brittleness have been well established in the literature. (Altindag, 2010), Özfırat et al. (2016), Altindag (2003) and Altindag (2010) developed brittleness

indexes based on these parameters and the significance of these parameters was expected and thus aligns with the available literature. Khandelwal et al. (2017) using two modelling techniques estimated rock brittleness which is combination of rock properties rather than only one parameter, results showed that the uniaxial compressive strength is the most influential factor on brittleness index.

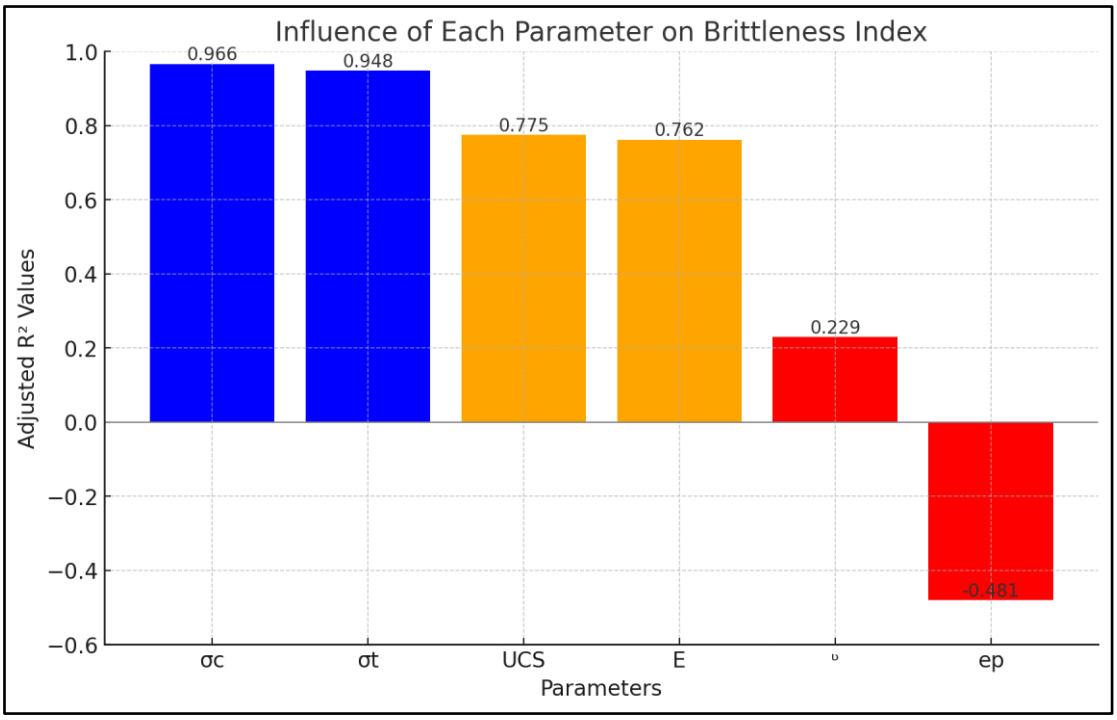

Figure 4. 5 Rock parameters and their influence on the brittleness of UG2 reef.

4.4 Summary of the chapter

The analysis shows that compressive strength (σc) and tensile strength (σt) are the most consistent and significant predictors of the brittleness index. Models that include these variables, especially without additional variables that contribute to overfitting, provide high R, R^2, and adjusted R^2 values. Other variables like UCS, E, and ep appear to contribute less consistently to the predictive power of the models and often lead to overfitting when included. Therefore, focusing on σc and σt offers a more accurate prediction of the brittleness index. The influence of each parameter is illustrated in figure 4.5 above. The brittleness indexes developed thus focused on the compressive and tensile strength.

The significance (Sig.F) and standard error (SE) of these models was utilized to evaluate their reliability and precision. The findings reveal that most models exhibit highly significant relationships between the independent variables and brittleness, as indicated by Sig.F values of 0.000. This high level of statistical significance underscores the validity of these models in predicting brittleness. Exceptionally, models B2 and B6 are exceptional, demonstrating near-perfect prediction accuracy with SE values of 0.000, making them exceptionally reliable predictors of brittleness.

In contrast, model B3, with a Sig.F value of 0.196 and an SE of 0.060, shows a lack of statistical significance and lower prediction precision, indicating it is not a dependable model for brittleness prediction. Moderately accurate models such as B1 and B4, with SE values ranging from 0.011 to 0.035, still offer reasonable reliability and can be useful for practical applications, though they are less precise compared to the best-performing models.

The combination of statistical significance and prediction accuracy provided by the Sig.F and SE values is crucial in assessing the overall quality of the models. Models B2 and B6, which display both low SE and significant Sig.F values, emerge as the most effective models for predicting the brittleness of the UG2 reef.

CHAPTER FIVE

DETERMINATION OF THE BRITTLENESS OF UG2 REEF BASED ON MINERALOGICAL CHARACTERISTICS

5.1 Introduction

The mechanical approach is a widely employed and clear method for quantifying brittleness. Previous studies, such as those conducted by Wang et al (2015) and Yongshang et al (2020), have shown that the mechanical properties of rock masses are significantly influenced by their mineralogical composition. Minerals can be classified as either brittle or ductile, like quartz and clay (Xia et al., 2019; Hasson et al., 2022). The traditional approach to quantifying brittleness using mineralogy focused on determining the weight fraction of quartz (Jarvie et al., 2007), and the weight fraction of quartz, feldspar, mica, and carbonate minerals by Jin et al. (2015). Despite the existence of established brittleness indices based on mineralogical composition, the selection of brittle components in rocks remains subjective, leading to conflicting results.

There is a scarcity of literature on the brittleness of minerals not typically classified as "brittle/ductile," including chromite, which makes up 60-90% of minerals in the Eastern limb of the UG2 reef. Existing brittleness indices do not consider the effects of essential internal parameters and external mechanical conditions (Meng et al., 2019; Xia et al., 2019). Additionally, conventional methods fail to account for the complex nature of rock formation, which involves multi-stage tectonic movement and geological evolution over millions of years (Meng et al., 2019).

To address this knowledge gap, this study aimed to investigate the mechanical properties of the UG2 reef and assess the influence of various mineralogical parameters, extending beyond the traditional classification of brittle to ductile minerals, on its brittleness. The study used microscopic examination of UG2 reef samples to gather different mineralogical characteristics of the reef. These characteristics were then used to develop new brittleness indices, based on multivariable linear models, that take into account additional factors such as textural variables, contact type, contact nature, and packing density.

5.2 Results and Discussions

The analysis commences with a discussion of the mineralogical properties of the UG2 platinum reef, followed by a discussion of the textural studies. This is succeeded by the development of modified brittleness indices based on the mineralogical characteristics, and a subsequent discussion of the outcomes.

5.2.1 Mineralogical studies

The UG2 chromitite layer is predominantly composed of chromite, constituting a substantial 60-90% of its volume (Rose et al., 2008). This is imitated in the analysed samples. Silicate minerals (quartz) fill the space between chromite minerals. Base-metal sulphide (BMS) minerals, predominantly pentlandite and to a lesser amount chalcopyrite are present as major constituents, albeit in trace amounts at boundaries between chromite and silicate minerals. The chromitite layer appears to maintain its integrity with limited signs of alteration, deformation, or mineral replacement.

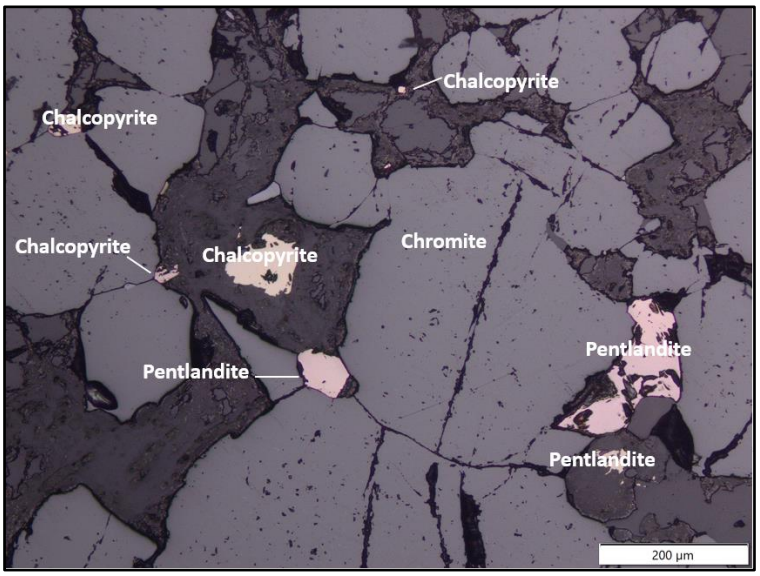

Figure 5. 1Mineralogical composition of UG2 reef

5.2.2 Textural studies

The samples reveal a variable distribution of grain sizes. Predominantly, the samples exhibit a prevalence of coarse grains, comprising approximately 5% to 90% of the total composition. Alongside these coarse grains, a significant presence of medium-sized

grains is noted, ranging from 7% to 50%. Furthermore, a distinguishable proportion of fine grains is evident, with concentrations ranging between 3% to 29%. Type of grain-to-grain contacts includes tangential (Ta), long (Lo), concavo-convex (Cc), and sutured (Su) contacts. Concavo-concave grain contacts are the most abundant type of grain contact, followed by sutured, tangential, longitudinal and floating grains respectively.

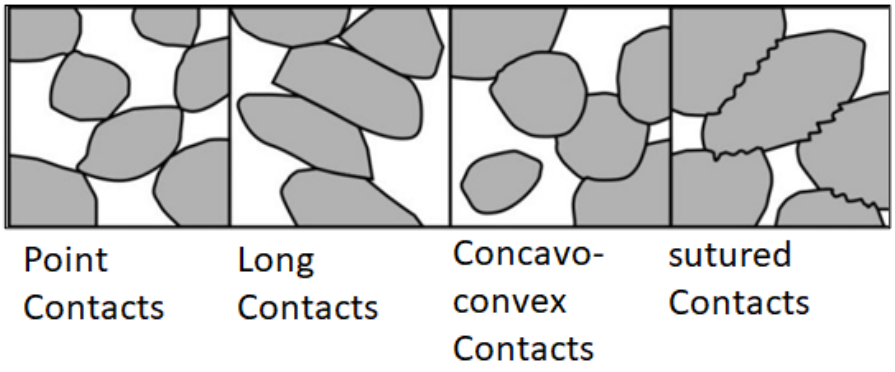

Figure 5. 2 Types of grain contacts observed

The contact nature includes single contact (GG), double contact (GD) and triple contact (GT). The most abundant contact nature is single contact, followed by double contacts and triple contacts respectively. However, samples from the UG2 split reef have a visually distinct arrangement of grains that appear to be a result of the process of sintering chromite, where chromite grains undergo enlargement until they are in close proximity, eliminating interstitial silicates.

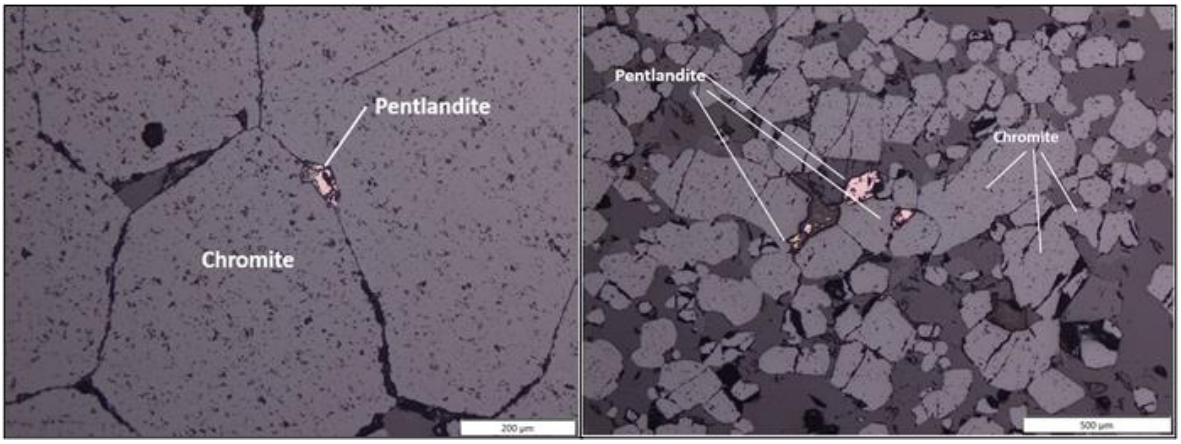

Figure 5. 3 Grain contacts observed from UG2 reef

Table 5. 1 Developed models (B1) from mineralogical characteristics of UG2

	Model no.	*Independent variables*	*R*	R^2	R^2_a	*SE*	*Sig.F*
All Parameters	1	FG,MG,CG,SU,CC,LO,TA,FI,GG,GD,GT,GA,PD,PP, P_{CC}					
Textural Variables	1	FG,MG,CG	0.3025	0.0915	-0.2605	0.0767	0.755
Type contact	1	SU,CC,LO,TA,FI	0.882	0.778	0.556	0.047	0.097
Contact nature	1	GG,GD,GT,GA	0.852	0.727	0.545	0.048	0.064
Packing	1	PD,PP, P_{CC}	0.688	0.473	0.248	0.062	0.188

Table 5. 2 Developed models (B2) from mineralogical characteristics of UG2

	Model no.	*Independent variables*	*R*	R^2	R^2_a	*SE*	*Sig.F*
All Parameters	1	FG,MG,CG,SU,CC,LO,TA,FI,GG,GD,GT,GA,PD,PP, P_{CC}					
Textural Variables	1	FG,MG,CG	0.3025	0.0915	-0.2605	0.0767	0.755
Type contact	1	SU,CC,LO,TA,FI	0.882	0.778	0.556	0.047	0.097
Contact nature	1	GG,GD,GT,GA	0.852	0.727	0.545	0.048	0.064
Packing	1	PD,PP, P_{CC}	0.688	0.473	0.248	0.062	0.188

Table 5. 3 Mineralogical properties of UG2 samples

	Textural Parameters %			Microfabric									PD%	PP%	PCC%
				Contact type %					Contact nature %						
	FG	MG	CG	SU	CC	LO	TA	FI	GG	GD	GT	GA			
Sample 01	50%	45%	5%	29.73	40.54	8.12	10.81	8.12	72.97	16.22	8.11	8.12	64%	91.89%	0.73%
Sample 02	10%	20%	70%	13.33	40.00	6.67	40.00	0	40	40	26.67	0	83%	100%	0.65%
Sample 03	5%	35%	60%	21.05	26.32	15.80	10.53	26.32	82.61	8.70	8.70	26.32	81%	73.68%	0.61%
Sample 04	29%	50%	21%	0	11.11	22.22	11.11	55.56	55.56	11.11	0	55.56	22%	44.44%	0.38%
Sample 05	10%	20%	70%	33.33	33.33	0	11.11	22.22	77.78	11.11	11.11	22.22	5%	77.78%	0.69%
Sample 06	65%	35%	0%	25	22.22	13.89	13.89	25	75	12.50	12.50	25	67%	75%	0.62%
Sample 07	5%	25%	70%	21.43	28.57	7.14	42.86	0	72.73	9.09	18.18	0	97%	100%	0.66%
Sample 08	3%	32%	65%	71.43	0	28.57	0	0	71.43	0	28.57	0	53%	100%	0.89%
Sample 09	10%	45%	45%	19.05	38.10	23.81	14.29	4.76	80	15	5	4.76	77%	95.24%	0.70%
Sample 10	15%	15%	70%	25	25	25	25	0	58.33	16.67	25	0	68%	100%	0.70%
Sample 11	3%	7%	90%	71.43	0	0	28.57	0	0	25	75	0	93%	100%	0.83%

The mineralogical characteristics of the UG2 sample were analysed using the mineralogical properties of the sample refer to Tables 5.2 and 5.3 and Appendix B. in contrast to the mechanical properties, the mineralogical properties showed that the contact type and nature of chromitite grains played a significant role in developing a model. However, model B_6 was not found to correlate with the data; thus, the model was successfully developed. The developed models are as follows:

B1= 32.034 + 0.0065GG + 0.0056GD + 0.0075GT + 0.0062GA (Contact type)

B1= 27.1172 + 0.0571SU + 0.0585CC + 0.0533LO + 0.0538TA + 0.0588FI (Contact nature)

B2= 0.932 + (8.57SU + 8.77CC + 8.01Lo + 8.06TA + 8.88FI) X 10—5 (Contact type)

B2= 0.939 + (1.05GG + 1.21GT + 1.02GA) X 10-5 + 8.71 X 10-6GD (Contact nature)

B3= -6.682 + 0.0707SU + 0.0707CC + 0.0667Lo + 0.0670TA + 0.0686FI (Contact type)

B4= 0.0035 – 5X10-5GA

B5= 0.300 – 0.00257GG – 0.00281GD – 0.0020GT

5.3 Discussion of the Results

As outlined in chapter 2, the quantification of brittleness based on mineralogical characteristics has mostly been focused on the amount of brittle minerals vs ductile minerals. Very was found in the literature on the subject of the effects of texture, type of contact, contact nature and packing. In this study, the analysis of these parameters was investigated using multivariate linear models.

5.3.1 The Effect of Texture on Brittleness

The model focusing on textural variables (FG, MG, CG) indicates that these variables have a restricted effect on predicting the brittleness of the UG2 reef. With an R^2 value of 0.0915, only 9.15% of the variability in brittleness can be explained by fine-grained, medium-grained, and coarse-grained textures. The negative adjusted R^2 (-0.2605) indicates that the model does not fit well when considering the number of predictors, indicating that texture alone is not a significant contributor to brittleness prediction.

5.3.2 The Effect of Type of Contact on Brittleness

The model incorporating type of contact variables (SU, CC, LO, TA, FI) significantly influences brittleness prediction. With an R^2 value of 0.778, this model explains 77.8% of the variability in brittleness, indicating that the nature of the contact between particles is a crucial factor in determining brittleness. The high R^2 and adjusted R^2 (0.556) values suggest that sutured, concavo-convex, longitudinal, floating and point contacts collectively provide a strong predictive capability. Thus, the type of contact among particles is a major determinant of brittleness in the material.

5.3.3 The Effect of Contact Nature on Brittleness

The contact nature model (GG, GD, GT, GA) also plays a significant role in predicting brittleness. With an R^2 value of 0.727, this model accounts for 72.7% of the variability in brittleness. The adjusted R^2 value of 0.545 further confirms a good fit for the model, highlighting that GG-Single contact, GD- Double contact, GT- triple contact, GA-abundant grain contacts are important variables. These results indicate that the specific nature of how particles interact within the material greatly impacts its brittleness, making contact nature a major determinant of brittleness in the material.

5.3.4 The Effect of Packing on Brittleness

The model focusing on packing variables (PD, PP, PCC) shows a moderate effect on brittleness prediction. With an R^2 value of 0.473, this model explains 47.3% of the variability in brittleness. The adjusted R^2 of 0.248 indicates a moderate fit, suggesting that the packing density, packing proximity and the consolidation factor contribute to brittleness, but to a lesser extent compared to type of contact and contact nature. This moderate R^2 value implies that while packing variables do influence brittleness, they are not as dominant as other factors like the type of contact and contact nature in predicting brittleness in the material.

The effects of the different parameters are visualized in Figures 5.4 and 5.5. This visualization illustrates that the type of contact and contact nature models significantly contribute to describing the variability in brittleness, with type contact being the highest at 77.8%, followed by contact nature at 72.7%. The packing model accounts for a

moderate portion at 47.3%, whereas the textural variables model has a minimal contribution of 9.15%.

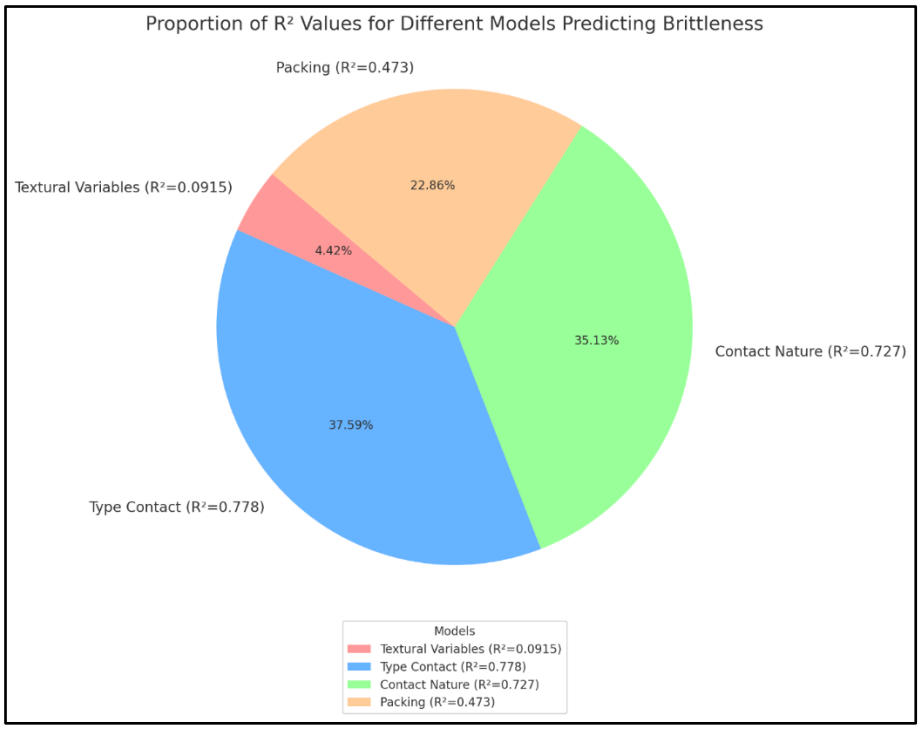

Figure 5. 4 Proportion of R^2 values for different models predicting brittleness

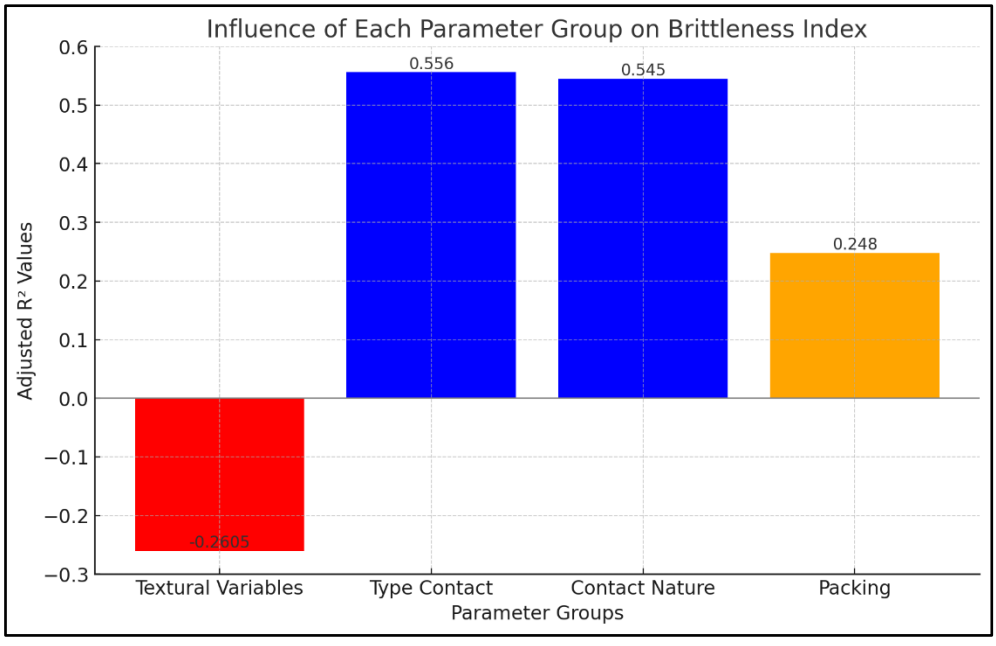

Figure 5. 5 Effect of Mineralogical parameters on brittleness

5.5 Summary of the chapter

The analysis shows that the type of contact variables (SU, CC, LO, TA, and FI) and contact nature variables (GG, GD, GT, and GA) are the most significant predictors of the brittleness index. These models displayed strong correlations and as indicated by their high R and R^2 values. Even though some models failed to achieve statistical significance, their relatively low standard error (SE) values suggest a high degree of prediction precision. In contrast, the textural variables model (FG, MG, CG) indicated a weak correlation with a poor fit, as indicated by its reduced R and R^2 values, negative adjusted R^2, and higher SE. The packing variables model (PD, PP, and PCC) showed a moderate correlation and explanatory power but did not attain statistical significance.

The significance (Sig.F) and standard error (SE) of these models were utilized to evaluate their reliability and precision. The significance (Sig.F) values indicate the probability that the observed relationships between the independent variables and brittleness are not due to random chance. Across most models, Sig.F values are consistently at 0.000, suggesting highly significant relationships. This high level of statistical significance indicates that the chosen independent variables are strong predictors of brittleness, thereby enhancing the models' reliability.

The standard error (SE) measures the accuracy of the predictions made by the models. Models such as B2 and B6 exhibit an SE of 0.000, reflecting perfect prediction accuracy for brittleness. These models are considered highly reliable, demonstrating minimal prediction error. In contrast, model B3 shows an SE of 0.060, indicating less precision and greater variability in predictions. Higher SE values suggest that the model's predictions deviate more from the actual values, which is shown in models B1, B4, and B5, where SE values are 0.011, 0.013, and 0.035, respectively.

The combination of statistical significance and prediction accuracy provided by the Sig.F and SE values is crucial in assessing the overall quality of the models. Models B2 and B6, Models B2 and B6, which display perfect SE and significant Sig.F emerge as the most effective models for predicting the brittleness of the UG2 reef.

CHAPTER SIX

CONCLUSIONS AND RECOMMENDATIONS

6.1 Summary of the study

The research project aims to characterize the brittleness indices of platinum-bearing reefs (UG2), located on the eastern limb of the Bushveld Igneous Complex, using mechanical and mineralogical studies. A summary of the dissertation's results coupled with suggestions for additional research is presented in this chapter.

Brittleness is an important characteristic of hard rocks. The correct analysis of brittleness is essential in, amongst other things, the safe selection and design of excavation and mining machinery. The brittleness of rock masses contributes to many essential rock behaviours, some of which directly impact human life, such as slope instability and production in mining. This research therefore contributes to the safety of mine workers, as the brittleness indexes determined will provide essential information that can be used to put safety measures in place as needed and can help engineers in the design and usage of suitable mining machinery for better safer production.

Various strategies were employed to attain specific objectives that were established. The primary goal was to establish predictive models that can be utilised to quantify the brittleness of the UG2 cromotite layer. To this aim, laboratory analysis of UG2 samples was performed to obtain the mechanical parameters, additional some of the parameters were obtained from numerical simulations. Predictive models were established from those parameters. Similarly, an analysis of the mineralogical characteristics of the reef was performed and predictive models were developed. Finally, the validity of these models was analysed using statistical methods.

6.1.1 Summary of findings on mechanical analysis

This study investigates the mechanical properties and brittleness of the UG2 platinum reef in the Eastern Limb of the Bushveld Igneous Complex, an area rich in Platinum Group Elements (PGEs) but challenging to explore due to beneficiation difficulties. Due to the existence of many different brittleness indices, it is very important to understand the characteristics of the rock mass to apply the correct brittleness index and obtain an accurate representation of the rock mass. An analysis of the mechanical properties such as uniaxial compressive strength (UCS), Young's modulus, Poisson's ratio, peak strain, tensile strength, and compressive strength through both direct tests and numerical simulations was thus performed. A broad range of UCS values, indicating heterogeneity within the samples, and identifies significant differences in Young's modulus compared to other workers, highlighting the variable structural integrity of the UG2 reef samples.

The study estimates brittleness indices using traditional empirical methods (B1-B6) and develops new indices through multivariate linear models. The results show that while some indices like B3 and B5 do not correlate well with mechanical parameters, indices such as B1, B2, B4, and B6 are effective in predicting brittleness. The analysis reveals that compressive strength (σc) and tensile strength (σt) are the most significant predictors of brittleness, providing high R, R^2, and adjusted R^2 values, suggesting strong model fit. Other variables like Young's modulus, Poisson's ratio, and peak strain contribute less consistently and often lead to overfitting when included.

The findings emphasise the significance of using compressive and tensile strengths as primary predictors for brittleness in the UG2 reef. The study concludes that models focusing on σc and σt are more accurate and reliable for predicting brittleness compared to those including additional variables that may cause overfitting. The statistical significance and precision of the models were evaluated using significance (Sig.F) and standard error (SE) values, with models B2 and B6 emerging as exceptionally reliable. This research provides a strong framework for understanding the mechanical behavior and brittleness of the UG2 reef, facilitating more efficient exploration and extraction of PGEs on the reef.

6.1.2 Summary of findings on mineralogical analysis

Traditional methods for quantifying brittleness have focused on the weight fractions of specific minerals, such as quartz and feldspar. However, these methods can be subjective, leading to conflicting results. Notably, there is limited literature on the brittleness of minerals not typically classified as brittle or ductile, like chromite, which dominates the UG2 reef's mineral composition. Traditional brittleness indices often overlook critical internal parameters and external mechanical conditions, failing to account for the complex geological processes that shape rock formations.

This study addresses these gaps by investigating the mechanical properties of the UG2 reef and examining how various mineralogical parameters affect its brittleness. Through microscopic examination, the study identified different mineralogical characteristics, such as the type and nature of grain contacts, and used these to develop new brittleness indices utilizing multivariable linear models. The findings revealed that traditional texture-based variables had a limited effect on brittleness prediction, while the type of grain contacts and their nature were significant predictors. Sutured, concavo-convex, longitudinal, floating, and point contacts emerged as crucial factors in determining brittleness, indicating that how particles interact within the material significantly impacts its brittleness.

The study concluded that the type of contact and contact nature models were the most reliable predictors of the UG2 reef's brittleness, showing high correlation and explanatory power. Models focusing on these parameters demonstrated strong predictive capabilities, as indicated by their high R^2 and adjusted R^2 values, and low standard error (SE), suggesting high precision. In contrast, models based on textural variables and packing showed weaker correlations and moderate explanatory power. The statistical significance and accuracy of these models, particularly B2 and B6, underscored their effectiveness in predicting brittleness.

6.2 Summary of the study

Based on the findings from the study, several conclusions were drawn. In terms of mechanical analysis on the estimation of the brittleness of UG2, four brittleness indices were successfully developed (B1, B2, B4 and B6) from the previously established empirical methods. However, new modifications or developments from B3 and B5 were not possible due to a lack of correlation with variables.

Owing to the previous conclusions, the effect of parameters such as Young's Modulus (E) and Poisson's Ratio (υ) on the estimation of brittleness of UG2 reef was looked into. it was concluded that the inclusion of Young's modulus and Poisson's ratio in models resulted in overfitting and did not improve model relevance. Contrary to literature, these parameters were not significant in quantifying the brittleness index of the UG2 reef.

Similarly, the effect of Peak Strain (ep) was also assessed, the results showed a weak contribution to the predictive accuracy of brittleness index models. An inverse relationship was expected between peak strain and brittleness was supported by limited literature. Lastly, the effect of Tensile Strength (σt) and Compressive Strength (σc) was also looked into. It was denoted that both σt and σc were identified as significant predictors for the brittleness index. Models focusing on fewer variables, including σt and σc, showed high R, R^2, and adjusted R^2 values. Compressive and tensile strengths provide a more accurate prediction of brittleness, aligning with literature.

In terms of model evaluation, models B2 and B6 demonstrated near-perfect prediction accuracy and reliability with SE values of 0.000. B1 and B4 models offered reasonable reliability but were less precise compared to B2 and B6. Model B3 lacked statistical significance and precision, making it less reliable for brittleness prediction.

On the other part of mineralogical analysis, multiple models were developed to predict brittleness based on mineralogical and textural characteristics as shown in Chapter 5. However, the most key contributing factors include:

- The type of contact and contact nature are the most significant predictors of brittleness in the UG2 reef, as indicated by their high R and R^2 values and low SE.
- Texture alone is not a significant contributor to brittleness quantification, as shown by the weak correlation and poor fit of the textural variables model.
- Packing variables contribute to brittleness but are not as dominant as the type of contact and contact nature.

Lastly in terms of their model evaluation, the following were denoted:

- The models that include type of contact and contact nature variables showed strong predictive capabilities, with high R^2 values (0.778 and 0.727, respectively).
- Textural variables (FG, MG, CG) alone had a minimal effect on brittleness prediction, with a low R^2 value (0.0915).
- Packing variables (PD, PP, PCC) had a moderate effect on brittleness prediction, with an R^2 value of 0.473.

Statistical Significance and Precision:

- The significance (Sig.F) values for most models were 0.000, indicating highly significant relationships between the independent variables and brittleness.
- Models B2 and B6 showed perfect prediction accuracy with a standard error (SE) of 0.000, making them the most reliable for predicting the brittleness of the UG2 reef.
- Other models, such as B1, B4, and B5, had higher SE values, indicating less precision and greater variability in predictions.

6.4 Recommendations of the study

A number of possible areas of research were identified based on the scope of the study. These include:

Future Studies:

- Expanding Mineralogical Focus- Investigate the brittleness of other minerals not typically classified as brittle or ductile, similar to the study of chromite in this research. Understanding the brittleness of a wider range of minerals can refine brittleness models further.
- Advanced Modeling Techniques- Develop and test more sophisticated modeling techniques, such as machine learning and artificial intelligence, to predict brittleness. These techniques can handle large datasets and complex interactions more efficiently.
- Field Validation- Conduct field validation of the developed models in different geological settings to test their applicability and accuracy. Field studies will help in refining the models based on real-world data and conditions.

REFERENCES

Ai, C., Zhang, J., Li, Y.W., Zeng, J., Yang, X.L. and Wang, J.G., 2016. Estimation criteria for rock brittleness based on energy analysis during the rupturing process. Rock Mechanics and Rock Engineering, 49(12), pp.4681-4698.

Akcin, N.A., Muftuoglu, Y.V. and Bas, N., 1994. Prediction of drilling performance for electro-hydraulic percussive drills. In: Mine Planning and Equipment Selection (Eds. Pasamehmetoglu et al.), pp.483-488.

Altindag, R., 2002. The evaluation of rock brittleness concept on rotary blast hole drills. Journal of the Southern African Institute of Mining and Metallurgy, 102, pp.61–66.

Altindag, R., 2003. Correlation of specific energy with rock brittleness concepts on rock cutting. Journal of the Southern African Institute of Mining and Metallurgy, 103, pp.163–171.

Altindag, R., 2009. Assessment of some brittleness indexes in rock-drilling efficiency. Rock Mechanics and Rock Engineering, 43, pp.361-370. DOI: 10.1007/s00603-009-0057-x.

Altindag, R., 2010. Assessment of some brittleness indices in rock-drilling efficiency. Rock Mechanics and Rock Engineering, 43(3), pp.361–370. Available at: https://doi.org/10.1007/s00603-009-0057-x.

Andreev, G.E., 1995. Brittle failure of rock materials: test results and constitutive models. A.A. Balkema.

Aubertin, M., Gill, D.E. and Simon, R., 1994. On the use of the brittleness index modified (BIM) to estimate the post-peak behavior of rocks. In: Proceedings of the 1st North American rock mechanics symposium. A.A. Balkema, pp.945-952.

Backers, T., Dresen, G., Rybacki, E. and Stephansson, O., 2004. New data on mode II fracture toughness of rock from the punchthrough shear test. International Journal

of Rock Mechanics and Mining Sciences, 41, pp.2–7. doi: 10.1016/j.ijrmms.2004.03.010.

Bates, R.L. and Jackson, J.A., 1984. Dictionary of geological terms. 3rd ed. The American Geological Institute.

Beard, D.C. and Weyl, P.K., 1973. Influence of texture on porosity and permeability of unconsolidated sand. AAPG Bulletin, 57(2), pp.349–369.

Bieniawski, Z.T. and Hawkes, I., 1978. Suggested methods for determining tensile strength of rock materials. International Journal of Rock Mechanics and Mining Sciences & Geomechanics Abstracts, 15, pp.99–103.

Bieniawski, Z.T., 1967. Mechanism of brittle fracture of rock: Part I—Theory of the fracture process. International Journal of Rock Mechanics and Mining Sciences & Geomechanics Abstracts, 4, pp.395–406. doi:10.1016/0148-9062(67)90030-7.

Bilen, C., Er, S., Tuğrul, A. and Yılmaz, M., 2021. A new approach for the prediction of brittleness index based on chemical properties of basaltic rocks. Acta Geodyn. Geomater., 18(3), pp.285-299. DOI: 10.13168/AGG.2021.0020.

Bishop, A.W., 1967. Progressive failure with special reference to the mechanism causing it. In: Proceedings of the geotechnical conference, Oslo, pp.142-150.

Bourdeau, J.E., Zhang, S.E., Hayes, B., Logue, A. and Bybee, G.M., 2023. Evidence for the incremental assembly of the Pyroxenite Marker, Bushveld Complex, by the emplacement of crystal slurries. LITHOS, 438-439, 107007.

Brace, W.F., Paulding, B.W. and Scholz, C., 1966. Dilatancy in the fracture of crystalline rocks. Journal of Geophysical Research, 71(16), pp.3939–3953. doi:10.1029/JZ071i016p03939.

Cai, M., 2010. Practical estimates of tensile strength and Hoek–Brown strength parameter mi of brittle rocks. Rock Mechanics and Rock Engineering, 43(2), pp.167–184. Available at: https://doi.org/10.1007/s00603-009-0053-1.

Carpinteri, A., 1991. Size-scale transition from ductile to brittle failure: Structural response vs. crack growth resistance curve. International Journal of Fracture, 51, pp.175–186.

Cawthorn, R.G. and Webb, S.J., 2001. Connectivity between the western and eastern limbs of the Bushveld Complex. Tectonophysics, 330, pp.195–209.

Chen, G., Jiang, W., Sun, X., Zhao, C. and Qin, C., 2019. Quantitative evaluation of rock brittleness based on crack initiation stress and complete stress–strain curves. Bulletin of Engineering Geology and the Environment, 78, pp.5919–5936.

Chen, G., Jiang, W., Sun, X., Zhao, C. and Qin, C., 2019. Quantitative evaluation of rock brittleness based on crack initiation stress and complete stress–strain curves. Bulletin of Engineering Geology and the Environment.

Chen, G., Li, T., Wang, W., Zhu, Z., Chen, Z. and Tang, Q., 2019. Weakening effects of the presence of water on the brittleness of hard sandstone. Bulletin of Engineering Geology and the Environment, 78, pp.1471-1483..

Chen, J.J., Zhang, G.Z., Chen, H.Z. and Yin, X.Y., 2014. The construction of shale rock physics effective model and prediction of rock brittleness. In: Proceedings of the 2014 SEG annual meeting. Society of Exploration Geophysicists (SEG), pp.2861-2865.

Chen, Y., Jin, Y., Chen, M., Yi, Z.C. and Zheng, X.J., 2017. Quantitative evaluation of rock brittleness based on the energy dissipation principle: an application to type II mode crack. Journal of Natural Gas Science and Engineering, 45, pp.527-536.

Cherepanov, G.P., 1979. Mechanics of brittle fracture. New York, USA: McGraw-Hill.

Chi, A., Li, Y.W., Zeng, J., Yang, Z.L. and Wang, J.G., 2016. Estimation criteria for rock brittleness based on energy analysis during the fracturing process. Rock Engineering and Rock Mechanics, 49, pp.6481–6498.

Cleary, M.P., 1989. Lecture: effects of depth on rock fracture. OnePetro. Available at: https://doi.org/10.1190/1.1585507.

Comakli, R., Kahraman, S., Balci, C. and Tumac, D., 2016. Estimating specific energy from the brittleness indexes in cutting metallic ores. The Journal of the Southern African Institute of Mining and Metallurgy, 116, pp.763-768..

Cook, N.G.W., 1965. The failure of rock. International Journal of Rock Mechanics and Mining Sciences & Geomechanics Abstracts, 2, pp.389–403. doi:10.1016/0148-9062(65)90004-5.

Copur, H., Bilgin, N., Tuncdemir, H. and Balci, C., 2003. A set of indices based on indentation tests for assessment of rock cutting performance and rock properties. Journal of the Southern African Institute of Mining and Metallurgy, 103(9), pp.589-599.

Dahl, F., 2003. DRI, B.W.I. CLI standards. Trondheim, Norway: Norwegian University of Science and Technology (NTNU).

Diederichs, M.S., Kaiser, P.K. and Eberhardt, E., 2004. Damage initiation and propagation in hard rock during tunnelling and influence of near-face stress rotation. International Journal of Rock Mechanics and Mining Sciences, 41(5), pp.785–812. DOI: 10.1016/j.ijrmms.2004.02.003.

Dursun, A.E. and Gokay, M.K., 2016. Cuttability assessment of selected rocks through different brittleness values. Rock Mechanics and Rock Engineering, 49(4), pp.1173-1190.

Eales, H.V. and Cawthorn, R.G., 1996. The Bushveld Complex. In: Cawthorn, R.G. (ed.) Layered Intrusions. Oxford: Elsevier, pp.181-229.

Eberhardt, E., Stimpson, B. and Stead, D., 1999. Effects of grain size on the initiation and propagation thresholds of stress-induced brittle fractures. Rock Mechanics and Rock Engineering, 32(2), pp.81–99.

Erguler, Z.A. and Ulusay, R., 2009. Water-induced variations in mechanical properties of clay-bearing rocks. International Journal of Rock Mechanics & Mining Sciences, 46, pp.355–370.

Eriksson, P.G. and Clendenin, C.W., 1990. A review of the Transvaal sequence. Journal of African Earth Sciences, 10, pp.101–116.

Evans, I. and Pomeroy, C.D., 1966. The Strength, Fracture, and Workability of Coal. Oxford: Pergamon Press.

Fahy, M.P. and Guccione, M.J., 1979. Estimating strength of sandstones using petrographic thin-section data. Bulletin of the International Association of Engineering Geology, 16(4), pp.467–485.

Fairhurst, C.E. and Hudson, J.A., 1999. Draft ISRM suggested method for the complete stress-strain curve for intact rock in uniaxial compression. International Journal of Rock Mechanics and Mining Sciences & Geomechanics Abstracts, 36, pp.281–289.

Fan, M., Jin, Y., Chen, M. and Geng, Z., 2019. Mechanical characterization of shale through instrumented indentation test. Journal of Petroleum Science and Engineering, 174, pp.607-616.

Farhadian, H., 2021. A new empirical chart for rockburst analysis in tunnelling: Tunnel rockburst classification (TRC). International Journal of Mining Science and Technology, 31(4), pp.603–610.

Fernandes, N., Kekana, W.O., Mahlangu, M.P., Betz, G. and Carpede, A., 2021. UG2 pillar strength: Verification of the PlatMine formula. Journal of the Southern Africa Institute of Mining and Metallurgy, 121(8), pp.449-456. DOI: http://dx.doi.org/10.17159/2411-9717/1491/2021.

Finn, C.A., Bedrosian, P.A., Cole, J.C., Khoza, T.D. and Webb, S.J., 2015. Mapping the 3D extent of the Northern Lobe of the Bushveld layered mafic intrusion from geophysical data. Precambrian Research, 268, pp.279–294.

Fredrich, J.T., Evans, B. and Wong, T.F., 1990. Effect of grain size on brittle and semibrittle strength: Implications for micromechanical modelling of failure in compression. Journal of Geophysical Research, 95(B7), pp.10907–10920. DOI: 10.1029/JB095iB07p10907

Gawherjee, R., Latypov, R. and Balakrishna, A., 2017. An intrusive origin of some UG-1 chromitite layers in the Bushveld Igneous Complex, South Africa: Insights from field relationships. Ore Geology Reviews, 90, pp.94-109.

Gholami, R., Rasouli, V., Sarmadivaleh, M., Minaeian, V. and Fakhari, N., 2016. Brittleness of gas shale reservoirs: A case study from the north Perth basin, Australia. Journal of Natural Gas Science and Engineering, 33, pp.1244–1259.

Gong, Q.M. and Zhao, J., 2007. Influence of rock brittleness on TBM penetration rate in Singapore granite. Tunnelling and Underground Space Technology, 22(3), pp.317–324. Available at: https://doi.org/10.1016/j.tust.2006.07.004.

Gong, X. and Sun, C.C., 2015. A new tablet brittleness index. European Journal of Pharmaceutics and Biopharmaceutics, 93, pp.260-266.

Grieser, B. and Bray, J., 2007. Identification of production potential in unconventional reservoirs. In: Proceedings of the Production and Operations Symposium, Oklahoma City, USA: Society of Petroleum Engineers (SPE).

Guo, J.C., Zhao, Z.H., He, S.G., Liang, H. and Liu, Y.X., 2015. A new method for shale brittleness evaluation. Environmental Earth Sciences, 73(10), pp.5855-5865.

Guo, Z., Chapman, M. and Li, X., 2012. Exploring the effect of fractures and microstructure on brittleness index in the Barnett Shale. In: Proceedings of the 2014 SEG Annual Meeting, Society of Exploration Geophysicists (SEG), pp.4609–4613.

Hajiabdolmajid, V. and Kaiser, P., 2003. Brittleness of rock and stability assessment in hard rock tunnelling. Tunnelling and Underground Space Technology, 18, pp.35-48.

Hall, A.L., 1932. The Bushveld Igneous Complex in the central Transvaal. Geological Society of South Africa Memoir, 28.

Hallbauer, D.K., Wagner, H. and Cook, N.G.W., 1973. Some observations concerning the microscopic and mechanical behaviour of quartzite specimens in stiff, triaxial compression tests. International Journal of Rock Mechanics and Mining Sciences & Geomechanics Abstracts, 10, pp.713–726. doi:10.1016/0148-9062(73)90015-6.

Han, S., Gao, Q., Cheng, Y., Yan, C. and Shi, X., 2020. Experimental study on brittle response of shale to cryogenic fluid nitrogen treatment. Journal of Petroleum Science and Engineering. Available at: https://doi.org/10.1016/j.petrol.2020.107463.

Han, Z., Zhang, L. and Zhou, J., 2019. Numerical investigation of mineral grain shape effects on strength and fracture behaviors of rock material. Applied Sciences, 9, p.2855. DOI: 10.3390/app9142855.

Hassan, A., Chan, S., Mahmoud, M., Aljawad, M.S., Humphrey, J. and Abdulraheem, A., 2022. Artificial Intelligence-Based Model of Mineralogical Brittleness Index Based

on Rock Elemental Compositions. Arabian Journal for Science and Engineering, 47, pp.11745–11761. Available at:

Hatzor, Y.H. and Palchik, V., 1997. The influence of grain size and porosity on crack initiation stress and critical flaw length in dolomites. International Journal of Rock Mechanics and Mining Sciences, 34(5), pp.805–816.

Hawkins, A.B. and McConnell, B.J., 1992. Sensitivity of sandstone strength and deformability to changes in moisture content. Quarterly Journal of Engineering Geology, 25, pp.115–123.

Heidari, M., Khanlari, G.R., Torabi-Kaveh, M., Kargarian, S. and Saneie, S., 2013. Effect of porosity on rock brittleness. Rock Mechanics and Rock Engineering, 47, pp.785-790. DOI: 10.1007/s00603-013-0400-0.

Hernandez-Uribe, L.A., Aman, M. and Espinoza, D.N., 2017. Assessment of mudrock brittleness with micro-scratch testing. Rock Mechanics and Rock Engineering, 50, pp.2849-2860.

Howarth, D.F., 1987. The effect of pre-existing microcavities on mechanical rock performance in sedimentary and crystalline rocks. International Journal of Rock Mechanics and Mining Sciences & Geomechanics Abstracts, 24, pp.223–233.

Howell, J.V., 1959. Glossary of geology and related sciences. Isis, 50(3), pp.269–270.

Hucka, V. and Das, B., 1974. Brittleness determination of rocks by different methods. International Journal of Rock Mechanics and Mining Sciences & Geomechanics Abstracts, 11(10), pp.389-392.

Hudson, J.A., Crouch, S.L. and Fairhurst, C., 1972. Soft, stiff and servo-controlled testing machines: A review with reference to rock failure. Engineering Geology, 6(3), pp.155–189. doi:10.1016/0013-7952(72)90001-4.

Hughes, A.E., Haque, N., Northey, S.A., and Giddey, S., 2021. Platinum Group Metals: A Review of Resources, Production and Usage with a Focus on Catalysts. Resources, 10(9), p.93. doi:10.3390/resources10090093.

Huo, Z., Zhang, J., Li, P., Tang, X., Yang, X., Qiu, Q., Dong, Z. and Li, Z., 2018. An improved evaluation method for the brittleness index of shale and its application – A

case study from the southern north China basin. Journal of Natural Gas Science and Engineering, 59(June), pp.47-55.

Hutchinson, C.S., 1974. Laboratory handbook of petrography techniques. New York: Wiley, p.527.

Hutchinson, D., Foster, J., Prichard, H. and Gilbert, S., 2015. Concentration of particulate platinum-group minerals during magma emplacement: a case study from the Merensky Reef, Bushveld Complex. Journal of Petrology, 56(1), pp.113–159. DOI: 10.1093/petrology/egu073.

Huthmann, F.M., Yudovskaya, M.A., Frei, D. and Kinnaird, J.A., 2016. Geochronological evidence for an extension of the Northern Lobe of the Bushveld Complex, Limpopo Province, South Africa. Precambrian Research, 280, pp.61-75.

Ingersoll, R.V., Bullard, T.F., Ford, R.L., Grimm, J.P., Pickle, J.D. and Sars, S.W., 1984. The effect of grain size on detrital modes: a test of the Gazzi-Dickinson point-counting method. Journal of Sedimentary Petrology, 54(1), pp.103–116.

Ingram, G.M. and Urai, J.L., 1999. Top-seal leakage through faults and fractures: the role of mudrock properties. Geological Society London Special Publications, 158(1), pp.125-135.

Jarvie, D.M., Hill, R.J., Ruble, T.E. and Pollastro, R.M., 2007. Unconventional shale-gas systems: the Mississippian Barnett Shale of north-central Texas as one model for thermogenic shale-gas assessment.

Jin, X.C., Shah, S.N., Roegiers, J.C. and Zhang, B., 2014b. Fracability evaluation in shale reservoirs – an integrated petrophysics and geomechanics approach. In: Proceedings of the SPE Hydraulic Fracturing Technology Conference. Society of Petroleum Engineers (SPE).

Jin, X.C., Shah, S.N., Truax, J.A. and Roegiers, J., 2014a. A practical petrophysical approach for brittleness prediction from porosity and sonic logging in shale reservoirs. In: Proceedings of the SPE Annual Technical Conference and Exhibition. Society of Petroleum Engineers (SPE).

Johnson, J.W. and Holloway, D.G., 1966. On the shape and size of the fracture zones on glass fracture surfaces. The Philosophical Magazine: A Journal of Theoretical Experimental and Applied Physics, 14(130), pp.731–743. doi:10.1080/14786436608211968.

Kahn, J.S., 1956. The analysis and distribution of the properties of packing in sand-size sediments. 1. On the measurement of packing in sandstone. Journal of Geology, 64, pp.385–395.

Kahraman, S., 1999. Rotary and percussive drilling prediction using regression analysis. International Journal of Rock Mechanics and Mining Sciences, 36, pp.981–989.

Kahraman, S., 2002. Correlation of TBM and drilling machine performance with rock brittleness. Engineering Geology, 65, pp.269–283.

Kang, P., Hong, L., Fazhi, Y., Quanle, Z., Xiao, S. and Zhaopeng, L., 2020. Effects of temperature on mechanical properties of granite under different fracture modes. Engineering Fracture Mechanics, 226, p.106838. Available at:

Kang, Y., Shang, C., Zhou, H., Huang, Y., Zhao, Q., Dengg, Z., Wang, H. and Ma, Y.Z., 2020. Mineralogical brittleness index as a function of weighting brittle minerals—from laboratory tests to case study. Journal of Natural Gas Science and Engineering, 77, p.103278.

Kaunda, R.B. and Asbury, B., 2016. Prediction of rock brittleness using nondestructive methods for hard rock tunneling. Journal of Rock Mechanics and Geotechnical Engineering, 8(4), pp.533-540.

Khan, K.N., Ma, L., Emad, M.Z., Feroze, T., Gao, Q., Alarifi, S.S., Sun, L., Hussain, S. and Wang, H., 2024. Predicting Sandstone Brittleness under Varying Water Conditions Using Infrared Radiation and Computational Techniques. Water, 16, p.143. https://doi.org/10.3390/w16010143.

Khandelwal, M., Faradonbeh, R.S., Monjezi, M., Armaghani, D.J. and Majid, M.Z., 2017. Function development for appraising the brittleness of intact rocks using genetic programming and non-linear multiple regression models. Engineering with Computers, 33(1), pp.13–21.

Kivi, I.R., Ameri, M. and Molladavoodi, H., 2018. Shale brittleness evaluation based on energy balance analysis of stress-strain curves. Journal of Petroleum Science and Engineering, 167, pp.1-19.

Kivi, I.R., Zare-Reisabadi, M., Saemi, M. and Zamani, Z., 2017. An intelligent approach to brittleness index estimation in gas shale reservoirs: A case study from a western Iranian basin. Journal of Natural Gas Science and Engineering, 44, pp.177-190.

Kivi, I.R., Zare-Reisabadi, M., Saemi, M. and Zamani, Z., 2017. An intelligent approach to brittleness index estimation in gas shale reservoirs: A case study from a western Iranian basin. Journal of Natural Gas Science and Engineering, 44, pp.177–190.

Kivi, R.I., Ameri, M. and Molladavoodi, H., 2018. Shale brittleness evaluation based on energy balance analysis of stress-strain curves. Journal of Petroleum Science and Engineering. doi: 10.1016/j.petrol.2018.03.061.

Kolbadinejad, S. and Ghaemi, A., 2023. Recovery and extraction of platinum from spent catalysts: A review. Case Studies in Chemical and Environmental Engineering, 7.

Kotze, E., Roelofse, F., Grobler, D., Gauert, C. and Purchase, M., 2022. Geological setting and concentration of scandium in the Flatreef and eastern limb chromitites of the Bushveld Complex. Journal of the Southern African Institute of Mining and Metallurgy, 122(9), pp.517–526. doi:10.17159/2411-9717/1987/2022.

Kruger, F.J., 2005. Filling the Bushveld Complex magma chamber: lateral expansion, roof and floor interaction, magmatic unconformities, and the formation of giant chromitite, PGE and Ti-V-magnetite deposits. Mineral Deposita, 40, pp.451–472.

Krumbein, W.C., 1941. Measurement and geological significance of shape and roundness of sedimentary particles. Journal of Sedimentary Petrology, 11(2), pp.64–72.

Lai, J., Wang, G., Huang, L., Li, W., Ran, Y., Wang, D., Zhou, Z. and Chen, J., 2015. Brittleness index estimation in a tight shaly sandstone reservoir using well logs. Journal of Natural Gas Science and Engineering, 27, pp.1536-1545.

Langa, M.M., Jugo, P.J., Leybourne, M.I. and Grobler, D.F., 2023. Stratigraphic variations in chromite chemistry through the UG-2 and UG-2E chromitites, Bushveld Igneous Complex: Implications for chromitite petrogenesis. International Geology Review. doi:10.1080/00206814.2023.2169961.

Langa, M.M., Jugo, P.J., Leybourne, M.I., Grobler, D.F., Adetunji, J. and Skogby, H., 2021. Chromite chemistry of a massive chromitite seam in the northern limb of the Bushveld Igneous Complex, South Africa: Correlation with the UG-2 in the eastern and western limbs and evidence of variable assimilation of footwall rocks. Mineralium Deposita, 56, pp.31–44. doi:10.1007/s00126-020-00964-y.

Latypov, R., Chistyakova, S., Page, R. and Hornsey, R., 2015. Field evidence for the in situ crystallization of the Merensky Reef. Journal of Petrology, [online] 0(0), pp.1-32. doi:10.1093/petrology/egv023.

Lawn, B.R. and Marshall, D.B., 1979. Hardness, toughness, and brittleness: an indentation analysis. Journal of the American Ceramic Society, 62(7-8), pp.347-350.

Li, H., 2022. Research progress on evaluation methods and factors influencing shale brittleness: A review. Energy Reports, 8, pp.4344–4358.

Li, P., Liu, Q., Zhou, P. and Li, Y., 2023. Mapping global platinum supply chain and assessing potential supply risks. Sustainable Energy Systems, 11. doi:10.3389/fenrg.2023.1033220.

Li, Q.H., Chen, M., Jin, Y., Wang, F.P. and Zhang, B.W., 2012. Indoor evaluation method for shale brittleness and improvement. Chinese Journal of Rock Mechanics and Engineering, 31(8), pp.1680-1685.

Li, Y., Jia, D., Rui, Z., Peng, J., Fu, C. and Zhang, J., 2017. Evaluation method of rock brittleness based on statistical constitutive relations for rock damage. Journal of Petroleum Science and Engineering, 153, pp.123-132.

Li, Y.W., Long, M., Zuo, L.H., Li, W. and Zhao, W.C., 2019. Brittleness evaluation of coal based on statistical damage and energy evolution theory. Journal of Petroleum Science and Engineering, 172, pp.753-763.

Liang, L., Liu, X., Xiong, J., Wu, T. and Ding, Y., 2017. New model to evaluate the Brittleness in shale formation. In: Proceedings of the international geophysical conference, Qingdao, China. Society of Exploration Geophysicists (SEG) and Chinese Petroleum Society, pp.1248-1251.

Liu, Q.S., Liu, J.P., Shi, K., Pan, Y.C., Huang, X., Liu, X.W. and Wei, L., 2016. Evaluation of rock brittleness indexes on rock fragmentation efficiency by disc cutter. Chinese Journal of Rock Mechanics and Engineering, 35(3), pp.498-510. (In Chinese).

Liu, Z. and Sun, Z., 2015. New brittleness indexes and their application in shale/clay gas reservoir prediction. Petroleum Exploration and Development, 42(1), pp.129-137.

Liu, Z.B. and Shao, J.F., 2016. Moisture effects on damage and failure of Bure claystone under compression. Geotechnique Letters, 6(3), pp.182–186. DOI: 10.1680/jgele.16.00054.

Lockner, D.A. and Beeler, N.M., 2002. International Handbook of Earthquake and Engineering Seismology, Part A. International Geophysics. In: The Encyclopaedia of Volcanoes, 2nd edition, 2015.

Luan, X., Di, B., Wei, J., Li, X., Qian, K., Xie, J. and Ding, P., 2014. Laboratory measurements of brittleness anisotropy in synthetic shale with different cementation. In: SEG technical Program expanded abstracts 2014. Society of Exploration Geophysicists (SEG), pp.3005-3009.

Maier, W.D., Barnes, S.J. and Groves, D.I., 2013. The Bushveld Complex, South Africa: Formation of platinum–palladium, chrome- and vanadium-rich layers via hydrodynamic sorting of a mobilized cumulate slurry in a large, relatively slowly cooling, subsiding magma chamber. Mineralium Deposita, 48, pp.1–56. doi:10.1007/s00126-012-0436-1.

Martin, C.D. and Chandler, N.A., 1994. The progressive fracture of Lac du Bonnet granite. International Journal of Rock Mechanics and Mining Sciences & Geomechanics Abstracts, 31(6), pp.643–659.

Mayer, C.C., Jugo, P.J., Leybourne, M.I., Grobler, D.F. and Voinot, A., 2020. Strontium isotope stratigraphy through the Flatreef PGE-Ni-Cu mineralization at Turfspruit, northern limb of the Bushveld Igneous Complex: Evidence of correlation with the

Merensky Unit of the eastern and western limbs. Mineralium Deposita, 56, pp.59–72. doi:10.1007/s00126-020-01006-3.

McDonald, I., Harmer, R.E., Holwell, D.A., Hughes, H.S.R. and Boyce, A.J., 2016. Cu-Ni-PGE mineralisation at the Aurora Project and potential for a new PGE province in the Northern Bushveld Main Zone. Ore Geology Reviews, 80, pp.1135-1159.

Meng, F., Wong, F.L. and Zhou, H., 2020. Rock brittleness indices and their applications to different fields of rock engineering: A review. Journal of Rock Mechanics and Geotechnical Engineering. doi:10.1016/j.jrmge.2020.06.008.

Meng, F.Z., Zhou, H., Wang, Z.Q., Zhang, L.M., Kong, L., Li, S.J. and Zhang, C.Q., 2016. Experimental study on the prediction of rockburst hazards induced by dynamic structural plane shearing in deeply buried hard rock tunnels. International Journal.

Meng, F.Z., Zhou, H., Zhang, C., Xu, R. and Lu, J., 2015. Evaluation methodology of brittleness of rock based on post-peak stress-strain curves. Rock Mechanics and Rock Engineering, 48(5), pp.1787-1805.

Mews, K., Alhubail, M.M. and Barati, R., 2019. A review of brittleness index correlations for unconventional tight and ultra-tight reservoirs. Geosciences, 9(7), p.319. Available at: .

Moghadam, A., Harris, N.B., Ayranci, K., Gomez, J.S., Angulo, N.A. and Chalaturnyk, R., 2019. Brittleness in the Devonian Horn River Shale, British Columbia, Canada. Journal of Natural Gas Science and Engineering, 62, pp.247–258.

Mogi, K., 1964. Deformation and fracture of rocks under confining pressure: Compression tests on dry rock sample. Bulletin of Earthquake Research Institute, University of Tokyo, 42, pp.491–514.

Morley, A., 1954. Strength of materials, 11th edn. Longmans, London.

122. Mukherjee, R., Latypov, R., and Balakrishna, A., 2017. An intrusive origin of some UG-1 chromitite layers in the Bushveld Igneous Complex, South Africa: Insights from field relationships. Ore Geology Reviews, 90, pp.94–109.

Mullen, M., Roundtree, R. and Barree, B., 2007. A composite determination of rock properties for stimulation design (what to do when you don't have a sonic log). In: Proceedings of the Rocky Mountain Oil & Gas Technical Symposium, Denver, USA.

Mungal, J.E., Kamo, S.L. and McQuade, S., 2016. U–Pb geochronology documents out-of-sequence emplacement of ultramafic layers in the Bushveld Igneous Complex of South Africa. Nature Communications. doi:10.1038/ncomms13385.

Munoz, H., Taheri, A. and Chanda, E.K., 2016. Fracture energy-based brittleness index development and brittleness quantification by pre-peak strength parameters in rock uniaxial compression. Rock Mechanics and Rock Engineering, 49, pp.4587-4606.

Munoz, H., Taheri, A. and Chanda, E.K., 2016. Rock drilling performance evaluation by an energy dissipation based rock brittleness index. Rock Mechanics and Rock Engineering, 49(8), pp.3343–3355.

Mutele, L. and Hunt, J.P., 2022. Investigation of hydrothermally altered "Mantos" zones in granites of the southwestern Bushveld Complex, South Africa: Insight into their mode of formation and F-REE mineralisation. Journal of African Earth Sciences, 194, 104629.

Muther, T., Qureshi, H.A., Syed, F.I., Aziz, H., Siyal, A., Dahaghi, A.K. and Negahban, S., 2022. Unconventional hydrocarbon resources: Geological statistics, petrophysical characterization, and field development strategies. Journal of Petroleum Exploration and Production Technology, 12, pp.1463-1488. .

Nauri, M., Khanlari, G., Rafiel, B., Sarfarazi, V. and Zaheri, M., 2022. Estimation of Brittleness Indexes from Petrographic Characteristics of Different Sandstone Types (Cenozoic and Mesozoic Sandstones), Markazi Province, Iran. Rock Mechanics and Rock Engineering, 55, pp.1955–1995. Available at: .

Nejati, H.R. and Moosavi, S.A., 2017. A new brittleness index for estimation of rock fracture toughness. Journal of Mining & Environment, 8(1), pp.83-91.

Nejati, H.R., Ghazvinian, A., Moosavi, S.A. and Sarfarazi, V., 2013. A new brittleness index for estimation of rock fracture toughness. Journal of Mining and Environment, pp. DOI: 10.1007/5I0064-013-0522-3.

Neuendorf, K.K., Mehl, J.P. and Jackson, J.A., 2005. Glossary of geology. 15th ed. American Geological Institute.

Nguuri, T.K., Gore, J., James, D.E., Webb, S.J., Wright, C., Zengeni, T.G., Gwavava, O. and Snoke, J.A., 2001. Crustal signature beneath southern Africa and its implication for the formation and evolution of the Kaapvaal and Zimbabwe cratons. Geophysical Research Letters, 28, pp.2501–2504.

Nouri, M., Khanlari, G., Rafiei, B., Sarfarazi, V. and Zaheri, M., 2022. Estimation of Brittleness Indexes from Petrographic Characteristics of Different Sandstone Types (Cenozoic and Mesozoic Sandstones), Markazi Province, Iran. Rock Mechanics and Rock Engineering, 55, pp.1955-1995. .

Nygard, R., Gutierrez, M., Bratli, R.K. and Høeg, K., 2006. Brittle-ductile transition, shear failure and leakage in shales and mudrocks. Marine and Petroleum Geology, 23, pp.201-212.

Oates, T.E. and Malan, D.F., 2023. A study of UG2 pillar strength using a new pillar database. Journal of the Southern African Institute of Mining and Metallurgy, 123(5), pp.265–274. Available at: http://dx.doi.org/10.17159/2411-9717/2656/2023.

Obert, L. and Duvall, W.I., 1967. Rock mechanics and the design of structures in rock. New York, NY: Wiley. [Accessed 25 August 2024].

Olsson, W.A., 1974. Grain size dependence of yield stress in marble. Journal of Geophysical Research, 79(32), pp.4859–4862.

Ozfirat, M.K., Yenice, H., Simsir, F. and Yarali, O., 2016. A new approach to rock brittleness and its usability at prediction of drillability. Journal of African Earth Sciences, 119, pp.94-101.

Özfırat, M.K., Yenice, H., S¸imşir, F. and Yaralı, O., 2016. A new approach to rock brittleness and its usability at prediction of drillability. Journal of African Earth Sciences, 119, pp.94–101.

Pan, P.Z. and Shao, C.Y., 2022. Experimental studies on the physical and mechanical properties of heated rock by air, water, and high-viscosity fluid cooling. Geomechanics for Energy and the Environment, 31, p.100315. Available at: .

Passchier, C.W., 1958. Experimental deformation and faulting in Wombeyan marble. Geological Society of America Bulletin, 69, pp.465–476.

Pincus, H.J., 2003. IX Future of Rock Mechanics. In: Rock Mechanics: The Encyclopedia of Physical Science and Technology, 3rd edition, 2000.

Powers, M.C., 1953. A new roundness scale for sedimentary particles. Journal of Sedimentary Petrology, 23, pp.117–136.

Přikryl, R., 2001. Some microstructural aspects of strength variation in rocks. International Journal of Rock Mechanics and Mining Sciences, 38(5), pp.671–682.

Quinn, J.B. and Quinn, G.D., 1997. Indentation brittleness of ceramics: a fresh approach. Journal of Materials Science, 32(16), pp.4331-4346.

Rahimzadeh Kivi, I., Ameri, M. and Molladavoodi, H., 2018. Shale brittleness evaluation based on energy balance analysis of stress-strain curves. Journal of Petroleum Science and Engineering, 167, pp.1–19.

Rajabzadeh, M.A., Moosavinasab, Z. and Rakhshandehroo, G., 2012. Effects of rock classes and porosity on the relation between uniaxial compressive strength and some rock properties for carbonate rocks. Rock Mechanics and Rock Engineering, 45(1), pp.113–122.

Ramsay, J.G., 1967. Folding and fracturing of rocks. McGraw-Hill, London. [Accessed 25 August 2024].

Rasmussen, K.D., Wenzel, H., Bangs, C., Petavratzi, E. and Liu, G., 2019. Platinum demand and potential bottlenecks in the global green transition: A dynamic material flow analysis. Environmental Science & Technology, 53(19), pp.11541–11551. doi:10.1021/acs.est.9b01912.

Reichmuth, D.R., 1967. Point load testing of brittle materials to determine tensile strength and relative brittleness. In: Proceedings of the 9th US Symposium on Rock Mechanics (USRMS). American Rock Mechanics Association (ARMA), pp.134-159.

Rickman, R., Mullen, M.J., Petre, J.E., Grieser, W.V. and Kundert, D., 2008. A practical use of shale petrophysics for stimulation design optimization: all shale plays are not

clones of the Barnett Shale. In: SPE annual technical conference and exhibition. Society of Petroleum Engineers (SPE).

Rittenhouse, G., 1943. A visual method of estimating two-dimensional sphericity. Journal of Sedimentary Petrology, 13, pp.79–81.

Rose, D.H., Viljoen, K.S. and Mulaba-Bafubiandi, A., 2018. A mineralogical perspective on the recovery of platinum group elements from Merensky Reef and UG2 at the Two Rivers mine on the Eastern limb of the Bushveld Complex in South Africa. Mineralogy and Petrology, 112, pp.881–902. doi:10.1007/s00710-018-0594-7.

Rybacki, E., Meier, T. and Dresen, G., 2016. What controls the mechanical properties of shale rocks? Part II: Brittleness. Journal of Petroleum Science and Engineering, 144, pp.39-58.

Schmidtke, R.H. and Lajtai, E.Z., 1985. The long-term strength of Lac du Bonnet granite. International Journal of Rock Mechanics and Mining Sciences & Geomechanics Abstracts, 22, pp.461–465. doi:10.1016/0148-9062(85)90010-5.

Scoon, R. and Viljoen, M., 2019. Africa's Top Geological Sites 8. The Eastern Limb of the Bushveld Complex. ResearchGate, pp.55–60.

Scoon, R.N. and Costin, G., 2018. Chemistry, morphology and origin of magmatic-reaction chromite stringers associated with anorthosite in the Upper Critical Zone at Winnaarshoek, Eastern Limb of the Bushveld Complex. Journal of Petrology, 59(8), pp.1551–1578. doi:10.1093/petrology/egy071.

Scoon, R.N. and Viljoen, M., 2016. Africa's Top Geological Sites 8: The Eastern Limb of the Bushveld Complex, South Africa. The Eastern Limb of the Bushveld Complex.

Scoon, R.N. and Viljoen, M.J., 2019. Geoheritage of the Eastern Limb of the Bushveld Igneous Complex, South Africa: A uniquely exposed layered igneous intrusion. Geoheritage, 11, pp.1723–1748. doi:10.1007/s12371-019-00360-7.

Sehgal, J., Nakao, Y., Takahashi, H. and Ito, S., 1995. Brittleness of glasses by indentation. Journal of Materials Science Letters, 14(3), pp.167-169.

Setera, S.B., VanTongeren, J.A., Turrin, B.D. and Swisher, C.C., 2023. A low temperature hydrothermal cutoff: plagioclase 40Ar/39Ar thermochronology of the

Rustenburg Layered Suite, Bushveld Complex. Contributions to Mineralogy and Petrology, 178(2). doi:10.1007/s00410-022-01984-9.

Sha, S., Rong, G., Tan, J., He, R. and Li, B., 2020. Tensile strength and brittleness of sandstone and granite after high-temperature treatment: A review. Arabian Journal of Geosciences, 13, p.598.

Shawaf, A., Rasouli, V. and Dehdouh, A., 2023. Applications of Differential Effective Medium (DEM)-Driven Correlations to Estimate Elastic Properties of Jafurah Tuwaiq Mountain Formation (TMF). Processes, 11, p.1643.

Shi, X., Wang, J., Ge, X., Han, Z., Qu, G. and Jiang, S., 2017. A new method for rock brittleness evaluation in tight oil formation from conventional logs and petrophysical data. Journal of Petroleum Science and Engineering, 151, pp.169–182.

Shi, X., Yang, X., Meng, Y. and Li, G., 2016. An anisotropic strength model for layered rocks considering planes of weakness. Rock Mechanics and Rock Engineering, 49(9), pp.3783–3792.

Singh, S.P., 1986. Brittleness and the mechanical wining of coal. Mining Science and Technology, 3, pp.173–180.

Singh, S.P., 1987. Criterion for the assessment of the cuttability of coal. In: Underground Mining Methods and Technology (Eds. Szwilski, A.B. and Richards, M.J.), Amsterdam: Elsevier, pp.225–239.

Skursch, O., Corfu, F., Tegner, C., Lesher, C.E., Andreasen, R. and Hagen, P.G.A., 2022. Zircon U–Pb chronology and Hf isotopes of the Lebowa Granite Suite and petrogenesis of the Bushveld Complex, South Africa. Contributions to Mineralogy and Petrology, 177, 26. doi:10.1007/s00410-022-01889-7.

Stoch, B., Basson, I.J. and Miller, J.A., 2020. Implicit geomodelling of the Merensky and UG2 Reefs of the Bushveld Complex from open-source data: Implications for the Complex's structural history. Minerals, 10, p.975. doi:10.3390/min10110975.

Sun, S.Z., Wang, K.N., Yang, P., Li, X.G., Sun, J.X., Liu, B.H. and Jin, K., 2013. Integrated prediction of shale oil reservoir using pre-stack algorithms for brittleness

and fracture detection. In: Proceedings of the international petroleum technology conference, pp.1-8.

Suorineni, F.T., Chinnasane, D.R. and Kaiser, P.K., 2009. A procedure for determining rock-type specific Hoek–Brown brittle parameters. Rock Mechanics and Rock Engineering, 42(6), pp.849–881.

Tang, X.M., Xu, S., Zhuang, C., Su, Y.D. and Chen, X.L., 2016. Quantitative evaluation of rock brittleness and fracability based on elastic-wave velocity variation around borehole. Petroleum Exploration & Development, 43(3), pp.457–464.

Tao, W., Tang, H., Wang, Y. and Ma, J., 2020. Evaluation of methods for determining rock brittleness under compression. Journal of Natural Gas Science and Engineering, 78, p.103321.

Tapponier, R. and Brace, W.F., 1976. Development of stress-induced microcracks in Westerly granite. International Journal of Rock Mechanics and Mining Sciences & Geomechanics Abstracts, 13, pp.103–112.

Tarasov, B.G. and Potvin, Y., 2013. Universal criteria for rock brittleness estimation under triaxial compression. International Journal of Rock Mechanics and Mining Sciences, 59, pp.57-69.

Tarokh, A., Peng, J., Fakhimi, A. and Labuz, J.F., 2016. Evaluation of brittleness from spalling and bending test. In: Proceedings of the 50th US rock mechanics/geomechanics symposium. American Rock Mechanics Association (ARMA).

Tavallali, A. and Vervoort, A., 2010. Effect of layer orientation on the failure of layered sandstone under Brazilian test conditions. International Journal of Rock Mechanics and Mining Sciences, 47(2), pp.313–322.

Tullis, J. and Yund, R.A., 1977. Experimental deformation of dry Westerly granite. Journal of Geophysical Research, 82(36), pp.5705–5718. DOI: 10.1029/JB082i036p05705.

Vermaak, C.F., 1976. The Merensky Reef; thoughts on its environment and genesis. Economic Geology, 71, pp.1270-1298.

Verstrynge, E., Pyka, G. and Van Balen, K., 2014. The influence of moisture on the mechanical behaviour of sandstone assessed by means of micro-computed tomography. In: 9th International Masonry Conference, Guimaraes, Portugal.

Viljoen, M., 2016. The Bushveld Complex - Host to the World's Largest Platinum, Chromium and Vanadium Resources. Episodes: Journal of International Geoscience, 39(2), pp.238–268.

Wadell, H., 1932. Volume, shape, and roundness of rock particles. Journal of Geology, 40, pp.443–451.

Wang, D., Ge, H., Wang, X., Wang, J., Meng, F., Suo, Y. and Han, P., 2015. A novel experimental approach for feasibility evaluation in tight-gas reservoirs. Journal of Natural Gas Science and Engineering, 23, pp.239–249.

Wang, M., Li, P., Wu, X. and Chen, H., 2016. A study on the brittleness and progressive failure process of anisotropic shale. Environmental Earth Sciences, 75(10), p.886.

Wang, M., Li, P., Wu, X. and Chen, H., 2016. A study on the brittleness and progressive failure process of anisotropic shale. Environmental Earth Sciences, 75(10), p.886.

Wang, S., Huang, L. and Li, X., 2020. Analysis of rockburst triggered by hard rock fragmentation using a conical pick under high uniaxial stress. Tunnelling and Underground Space Technology, p.103195.

Wang, T., Zhang, H., Gamage, R.P., Zhao, W., Ge, J. and Li, Y., 2020. The evaluation criteria for rock brittleness based on double body analysis under uniaxial compression. Geomechanics and Geophysics for Geo-Energy and Geo-Resources, 6, p.49.

Wang, T., Zhang, T., Ranjith, P.G., Li, Y., Song, Z., Wang, S. and Zhao, W., 2019. A new approach to the evaluation of rock mass rupture and brittleness under triaxial stress condition. Journal of Petroleum Science and Engineering. doi: 10.1016/j.petrol.2019.106482.

Wang, Y., Li, C.H., Hu, Y.Z. and Zhou, X.L., 2017. A new method to evaluate the brittleness for brittle rock using crack initiation stress level from uniaxial stress–strain curves. Environmental Earth Sciences, 76, p.799.

Wang, Y., Li, X., Wu, Y.F., Ben, Y.X., Li, D.S., Hao, J.M. and Zhang, B., 2014. Research on relationship between crack initiation stress level and brittleness indices for brittle rocks. Chinese Journal of Rock Mechanics and Engineering, 33(2), pp.264-275.

Watson, B.P. and Gerber, R., 2018. Determination of stable spans in UG2 excavations. The Southern African Institute of Mining and Metallurgy. doi:10.17159/2411-9717/2018/v118n5a6.

Watson, B.P., Theron, W., Fernandes, N., Kekana, W.O., Mahlangu, M.P., Betz, G. and Carpede, A., 2021. UG2 pillar strength: Verification of the PlatMine formula. Journal of the Southern African Institute of Mining and Metallurgy, 121(8), pp.449–456. Available at: http://dx.doi.org/10.17159/2411-9717/1491/2021.

Webb, S.J., Cawthorn, R.G., Nguuri, T., and James, D., 2003. Gravity modeling of Bushveld Complex connectivity supported by Southern African Seismic experiment results. South African Journal of Geology, 107, pp.207–218.

Weibull, W., 1939. A statistical theory of the strength of materials. Proceedings of the American Mathematical Society, 151, pp.1034–1034.

Wilson, A.H., 2012. A chill sequence to the Bushveld Complex: insight into the first stage of emplacement and implications for the parental magmas. Journal of Petrology, 53, pp.1123–1168.

Wood, D.A., 2022. Predicting brittleness indices of prospective shale formations from sparse well-log suites assisted by derivative and volatility attributes. Advances in Geo-Energy Research, 6(4), pp.334-346.

Xia, Y., Zhou, H., Zhang, C., He, S., Gao, Y. and Wang, P., 2019. The evaluation of rock brittleness and its application: A review study. European Journal of Environmental and Civil Engineering. DOI: 10.1080/19648189.2019.1655485.

Xia, Y., Zhou, H., Zhang, C., He, S., Gao, Y. and Wang, P., 2019. The evaluation of rock brittleness and its application: A review study. European Journal of Environmental and Civil Engineering. doi:10.1080/19648189.2019.1655485.

Xia, Y.J., Li, L.C., Tang, C.A., Li, X.Y., Ma, S. and Li, M., 2017. A new method to evaluate rock mass brittleness based on stress-strain curves of Class I. Rock Mechanics and Rock Engineering. 50(5), pp.1123-1139.doi:10.1007/s00603-017-1174-6.

Yagiz, S. and Gokceoglu, C., 2010. Application of fuzzy inference system and nonlinear regression models for predicting rock brittleness. Expert Systems with Application, 37(3), pp.2265–2272.

Yagiz, S., 2009. Assessment of brittleness using rock strength and density with punch penetration test. Tunnelling and Underground Space Technology, 24(1), pp.66-74.

Yang, D., Wang, G., Kang, Z., Zhao, J. and Lv, Y., 2020. Experimental investigation of anisotropic thermal deformation of oil shale under high temperature and triaxial stress based on mineral and micro-fracture characteristics. Natural Resources Research, 29(6), pp.3987–4002. Available at: https://doi.org/10.1007/s11053-020-09663-x.

Yang, S.Q., Ranjitha, P.G., Jinga, H.W., Tiana, W.L. and Ju, Y., 2017. An experimental investigation on thermal damage and failure mechanical behavior of granite after exposure to different high temperature treatments. Geothermics, 65, pp.180–197.

Yin, T., Ma, J., Wu, Y., Zhuang, D. and Yang, Z., 2022. Effect of high temperature on the brittleness index of granite: an experimental investigation. Bulletin of Engineering Geology and the Environment, 81, p.476.

Yin, T.B., Zhuang, D.D., Li, Q., Tan, X.S. and Wu, Y., 2021. Effect of oxygen on damage mechanism and mechanical properties of sandstone at high temperature. Bulletin of Engineering Geology and the Environment, 80, pp.6047–6064.

Yuan, Y., Jin, Z., Zhou, Y., Liu, J., Li, S. and Liu, Q., 2017. Burial depth interval of the shale brittle–ductile transition zone and its implications in shale gas exploration and production. Petroleum Science, 14, pp.637-647. DOI: 10.1007/s12182-017-0189-7.

Zeh, A., Ovtcharova, M., Wilson, A.H. and Schaltegger, U., 2015. The Bushveld Complex was emplaced and cooled in less than one million years: results of zirconology, and geotectonic implications. Earth and Planetary Science Letters, 418, pp.103–114.

Zhang, D., Ranjith, P.G. and Perera, M.S.A., 2016. The brittleness indices used in rock mechanics and their application in shale hydraulic fracturing: A review. Journal of Petroleum Science and Engineering, 143, pp.158–170. doi:10.1016/j.petrol.2016.02.011.

Zhang, J.H., Chen, Z.Y. and Wang, X.G., 2007. Centrifuge modeling of rock slopes susceptible to block toppling. Rock Mechanics and Rock Engineering, 40(4), pp.363-382. DOI: 10.1007/s00603-006-0112-9.

Zhang, J.J. and Fu, B.J., 2008. Rockburst and its criteria and control. Chinese Journal of Rock Mechanics and Engineering, 27(10), pp.2034–2042.

Zhang, Y., Feng, X., Yang, C., Han, Q., Wang, Z. and Kong, R., 2021. Evaluation method of rock brittleness under true triaxial stress states based on pre-peak deformation characteristic and post-peak energy evolution. Rock Mechanics and Rock Engineering, 54, pp.1277–1291.

Zhou, H., Chen, J., Lu, J.J., Jiang, Y. and Meng, F.Z., 2018. A new rock brittleness evaluation index based on the internal friction angle and class I stress-strain curve. Rock Mechanics and Rock Engineering, 51(7), pp.2309-2316.

Zhou, H., Meng, F.Z., Zhang, C.Q., Hu, D.W., Yang, F.J. and Lu, J.J., 2015. Analysis of rockburst mechanisms induced by structural planes in deep tunnels. Bulletin of Engineering Geology and the Environment, 74(4), pp.1435–1451. doi:10.1007/s10064-014-0696-3.

Zhou, H., Yang, Y.S., Xiao, H.B., Zhang, C.Q. and Fu, Y.P., 2013. Research on loading rate effect of tensile strength property of hard brittle marble-test characteristics and mechanism. Chinese Journal of Rock Mechanics and Engineering, 32, pp.1868–1875.

Appendix

Appendix A

Mechanical Properties

B1

Model 1

0

Regression Statistics	
Multiple R	0.993968
R Square	0.987972
Adjusted R Square	0.775945
Standard Error	0.011169
Observations	11

ANOVA

	df	*SS*	*MS*	*F*	*Significance F*
Regression	6	0.05123086	0.008538477	82.14233639	0.00038472
Residual	5	0.00062368	0.000124737		
Total	11	0.05185455			

	Coefficients	*Standard Error*	*t Stat*	*P-value*	*Lower 95%*	*Upper 95%*	*Lower 95.0%*	*Upper 95.0%*
Intercept	31.49342	0.71993776	43.74463663	1.17829E-07	29.6427567	33.34407455	29.642757	33.34407
UCS (MPa)	0.012973	0.09124745	0.142178816	0.892490248	-0.22158558	0.24753249	-0.2215856	0.247532

Young modulus (GPa) (^{E})	0.01537	0.00945458	1.625712733	0.164939082	-0.00893334	0.03967419	-0.0089333	0.039674
Poisson's ratio (^{υ})	0	0	65535	#NUM!	0	0	0	0
Peak Strain (eP)	1586.249	782.062002	2.028291111	#NUM!	-424.104969	3596.603782	-424.10497	3596.604
Compressive stress (σc)	76.41659	14.7167047	5.192507017	0.003488742	38.5860986	114.2470862	38.586099	114.2471
Tensional stress (σt)	-2650.48	193.094261	-13.72637417	3.68248E-05	-3146.84867	-2154.119471	-3146.8487	-2154.12

Model 2

Regression Statistics	
Multiple R	0.987030198
R Square	0.974228612
Adjusted R Square	0.963183731
Standard Error	0.013816986
Observations	11

ANOVA

	df	*SS*	*MS*	*F*	*Significance F*
Regression	3	0.050518182	0.01683939	88.20634921	6.33E-06
Residual	7	0.001336364	0.00019091		
Total	10	0.051854545			

	Coefficients	*Standard Error*	*t Stat*	*P-value*	*Lower 95%*	*Upper 95%*	*Lower 95.0%*	*Upper 95.0%*

Intercept	32.72590909	0.015410365	2123.62977	1.35588E-21	32.68947	32.76235	32.68947	32.76235
UCS (MPa)	-0.046727273	0.105658048	-0.44225001	0.671649832	-0.29657	0.203114	-0.29657	0.203114
Compressive stress (σc)	95	15.44785952	6.14971931	0.000467668	58.47162	131.5284	58.47162	131.5284
Tensional stress (σt)	-2900	178.376517	-16.2577454	8.1101E-07	-3321.79	-2478.21	-3321.79	-2478.21

Model 3

SUMMARY OUTPUT

Regression Statistics	
Multiple R	0.986665
R Square	0.973509
Adjusted R Square	0.966886
Standard Error	0.013104
Observations	11

ANOVA

	df	*SS*	*MS*	*F*	*Significance F*
Regression	2	0.050481	0.02524	146.9920569	4.93E-07
Residual	8	0.001374	0.000172		
Total	10	0.051855			

	Coefficients	*Standard Error*	*t Stat*	*P-value*	*Lower 95%*	*Upper 95%*	*Lower 95.0%*	*Upper 95.0%*
Intercept	32.72705	0.014408	2271.492	1.58025E-24	32.69383	32.76028	32.69383	32.76028

Compressive stress (σc)	88.60734	5.167935	17.1456	1.36147E-07	76.69006	100.5246	76.69006	100.5246
Tensional stress (σt)	-2900.53	169.1671	-17.146	1.36125E-07	-3290.63	-2510.43	-3290.63	-2510.43

B2

Model 1

Regression Statistics	
Multiple R	0.990630014
R Square	0.981347825
Adjusted R Square	0.762695649
Standard Error	2.25543E-05
Observations	11

ANOVA

	df	*SS*	*MS*	*F*	*Significance F*
Regression	6	1.3382E-07	2.2303E-08	52.613049 3	0.00092378 9
Residual	5	2.54348E-09	5.087E-10		
Total	11	1.36364E-07			

	Coefficients	*Standard Error*	*t Stat*	*P-value*	*Lower 95%*	*Upper 95%*	*Lower 95.0%*	*Upper 95.0%*

Intercept	0.938545017	0.001453874	645.547833	1.693E-13	0.934807715	0.942282318	0.934807715	0.942282318
UCS (MPa)	8.04932E-05	0.000184269	0.43682427	0.68045928	-0.000393186	0.000554172	-0.000393186	0.000554172
Young modulus (GPa) (^{E})	2.61495E-05	1.9093E-05	1.36958617	0.22912328	-2.29306E-05	7.52296E-05	-2.29306E-05	7.52296E-05
Poisson's ratio (^{υ})	0	0	65535	#NUM!	0	0	0	0
Peak Strain (eP)	2.912034295	1.579330106	1.84384144	#NUM!	-1.147762988	6.971831578	-1.147762988	6.971831578
Compressive stress (σc)	0.112783332	0.029719555	3.79491992	0.0126943	0.036386783	0.189179881	0.036386783	0.189179881
Tensional stress (σt)	-4.215497419	0.389942969	-10.8105486	0.0001175	-5.217877733	-3.213117105	-5.217877733	-3.213117105

Model 2

Regression Statistics	
Multiple R	0.979379
R Square	0.959184
Adjusted R Square	0.94898
Standard Error	2.64E-05
Observations	11

ANOVA

	df	*SS*	*MS*	*F*	*Significance F*
Regression	2	1.31E-07	6.54E-08	94.00102	2.78E-06
Residual	8	5.57E-09	6.96E-10		

Total	10	1.36E-07

	Coefficients	*Standard Error*	*t Stat*	*P-value*	*Lower 95%*	*Upper 95%*	*Lower 95.0%*	*Upper 95.0%*
Intercept	0.940681	2.9E-05	32436.13	9.14E-34	0.940614	0.940748	0.940614	0.940748
Compressive stress (σc)	0.142554	0.010402	13.70395	7.75E-07	0.118566	0.166542	0.118566	0.166542
Tensional stress (σt)	-4.66729	0.340513	-13.7066	7.74E-07	-5.45251	-3.88206	-5.45251	-3.88206

B3

Model 1

Regression Statistics	
Multiple R	0.845296
R Square	0.714525
Adjusted R Square	0.22905
Standard Error	0.060421
Observations	11

ANOVA

	df	*SS*	*MS*	*F*	*Significance F*
Regression	6	0.045688	0.007615	2.502931	0.196868
Residual	5	0.018254	0.003651		
Total	11	0.063941			

	Coefficients	*Standard Error*	*t Stat*	*P-value*	*Lower 95%*	*Upper 95%*	*Lower 95.0%*	*Upper 95.0%*

Intercept	-2.23054	3.894827	-0.57269	0.591643	-12.2425	7.781434	-12.2425	7.781434
UCS (MPa)	-0.41233	0.493644	-0.83527	0.441636	-1.68128	0.856625	-1.68128	0.856625
Young modulus (GPa) (^{E})	0.029694	0.051149	0.580535	0.586734	-0.10179	0.161176	-0.10179	0.161176
Poisson's ratio ($^{\upsilon}$)	0	0	65535	#NUM!	0	0	0	0
Peak Strain (eP)	2290.155	4230.916	0.541291	#NUM!	-8585.76	13166.07	-8585.76	13166.07
Compressive stress (σc)	78.94896	79.61664	0.991614	0.366917	-125.712	283.61	-125.712	283.61
Tensional stress (σt)	-867.918	1044.63	-0.83084	0.443916	-3553.23	1817.389	-3553.23	1817.389

B4

Model 1

Regression Statistics	
Multiple R	0.944438
R Square	0.891964
Adjusted R Square	0.583927
Standard Error	0.000892
Observations	11

ANOVA

	df	*SS*	*MS*	*F*	*Significance F*
Regression	6	3.28E-05	5.47E-06	8.256132	0.030251
Residual	5	3.98E-06	7.96E-07		
Total	11	3.68E-05			

	Coefficients	*Standard Error*	*t Stat*	*P-value*	*Lower 95%*	*Upper 95%*	*Lower 95.0%*	*Upper 95.0%*
Intercept	-0.09254	0.057497	-1.60954	0.168412	-0.24034	0.055256	-0.24034	0.055256
UCS (MPa)	-0.00451	0.007287	-0.61889	0.563093	-0.02324	0.014223	-0.02324	0.014223
Young modulus (GPa) (^{E})	0.001175	0.000755	1.555739	0.180494	-0.00077	0.003116	-0.00077	0.003116
Poisson's ratio ($^{\upsilon}$)	0	0	65535	#NUM!	0	0	0	0
Peak Strain (eP)	96.83731	62.458	1.550439	#NUM!	-63.7161	257.3907	-63.7161	257.3907
Compressive stress (σc)	-0.64479	1.175324	-0.5486	0.606875	-3.66605	2.37648	-3.66605	2.37648
Tensional stress (σt)	-35.667	15.42113	-2.31286	0.068662	-75.3083	3.974294	-75.3083	3.974294

Model 2

Regression Statistics	
Multiple R	0.875446
R Square	0.766406
Adjusted R Square	0.740452
Standard Error	0.000978
Observations	11

ANOVA

	df	*SS*	*MS*	*F*	*Significance F*
Regression	1	2.82E-05	2.82E-05	29.52845	0.000414
Residual	9	8.6E-06	9.56E-07		

Total	10	3.68E-05

	Coefficients	*Standard Error*	*t Stat*	*P-value*	*Lower 95%*	*Upper 95%*	*Lower 95.0%*	*Upper 95.0%*
Intercept	-0.00275	0.001066	-2.58016	0.029689	-0.00516	-0.00034	-0.00516	-0.00034
Tensional stress (σt)	-0.4548	0.083696	-5.43401	0.000414	-0.64414	-0.26547	-0.64414	-0.26547

B5

Regression Statistics	
Multiple R	0.599552
R Square	0.359463
Adjusted R Square	-0.48107
Standard Error	0.035174
Observations	11

ANOVA

	df	*SS*	*MS*	*F*	*Significance F*
Regression	6	0.003472	0.000579	0.56119	0.749012
Residual	5	0.006186	0.001237		
Total	11	0.009658			

	Coefficients	*Standard Error*	*t Stat*	*P-value*	*Lower 95%*	*Upper 95%*	*Lower 95.0%*	*Upper 95.0%*
Intercept	-0.12192	2.267359	-0.05377	0.959199	-5.95035	5.706512	-5.95035	5.706512
UCS (MPa)	0.270651	0.287373	0.941809	0.389532	-0.46807	1.009367	-0.46807	1.009367

Young modulus (GPa) (^{E})	0.000237	0.029776	0.007948	0.993966	-0.07631	0.076779	-0.07631	0.076779
Poisson's ratio ($^{\upsilon}$)	0	0	65535	#NUM!	0	0	0	0
Peak Strain (eP)	714.6759	2463.012	0.290163	#NUM!	-5616.7	7046.05	-5616.7	7046.05
Compressive stress (σc)	-40.8302	46.34853	-0.88094	0.418676	-159.973	78.31244	-159.973	78.31244
Tensional stress (σt)	-100.957	608.1276	-0.16601	0.874651	-1664.2	1462.285	-1664.2	1462.285

B6

Model 1

SUMMARY OUTPUT

Regression Statistics	
Multiple R	0.999999
R Square	0.999998
Adjusted R Square	0.799995
Standard Error	3.51E-05
Observations	11

ANOVA

	df	*SS*	*MS*	*F*	*Significance F*
Regression	6	0.002533	0.000422	411072.6	1.58E-11
Residual	5	6.16E-09	1.23E-09		
Total	11	0.002534			

	Coefficients	*Standard Error*	*t Stat*	*P-value*	*Lower 95%*	*Upper 95%*	*Lower 95.0%*	*Upper 95.0%*
Intercept	0.216005	0.002263	95.44434	2.39E-09	0.210187	0.221822	0.210187	0.221822
UCS (MPa)	0.000158	0.000287	0.550935	0.60539	-0.00058	0.000895	-0.00058	0.000895
Young modulus (GPa) (^{E})	3.8E-05	2.97E-05	1.279375	0.256917	-3.8E-05	0.000114	-3.8E-05	0.000114
Poisson's ratio ($^{\upsilon}$)	0	0	65535	#NUM!	0	0	0	0
Peak Strain (eP)	2.723091	2.45844	1.10765	#NUM!	-3.59653	9.042712	-3.59653	9.042712
Compressive stress (σc)	-0.23945	0.046262	-5.17579	0.003538	-0.35837	-0.12052	-0.35837	-0.12052
Tensional stress (σt)	2.6338	0.606999	4.339054	0.007436	1.07346	4.19414	1.07346	4.19414

Model 2

SUMMARY OUTPUT

Regression Statistics	
Multiple R	0.999998
R Square	0.999996
Adjusted R Square	0.999995
Standard Error	3.38E-05
Observations	11

ANOVA

	df	*SS*	*MS*	*F*	*Significance F*
Regression	2	0.002533	0.001267	1108684	1.69E-22
Residual	8	9.14E-09	1.14E-09		
Total	10	0.002534			

	Coefficients	*Standard Error*	*t Stat*	*P-value*	*Lower 95%*	*Upper 95%*	*Lower 95.0%*	*Upper 95.0%*
Intercept	0.218836	3.72E-05	5888.212	7.75E-28	0.21875	0.218922	0.21875	0.218922
Compressive stress (σc)	-0.1979	0.013331	-14.8456	4.18E-07	-0.22864	-0.16716	-0.22864	-0.16716
Tensional stress (σt)	2.168925	0.43637	4.970375	0.001093	1.162653	3.175197	1.162653	3.175197

Appendix B

Mineralogical

B1

All variables

SUMMARY OUTPUT

Regression Statistics	
Multiple R	1
R Square	1
Adjusted R Square	65535

Standard Error	0
Observations	11

ANOVA

	df	*SS*	*MS*	*F*	*Significance F*
Regression	15	0.051855	0.003457	#NUM!	#NUM!
Residual	0	0	65535		
Total	15	0.051855			

	Coefficients	*Standard Error*	*t Stat*	*P-value*	*Lower 95%*	*Upper 95%*	*Lower 95.0%*	*Upper 95.0%*
Intercept	31.2834	0	65535	#NUM!	31.2834	31.2834	31.2834	31.2834
FG	0	0	65535	#NUM!	0	0	0	0
MG	0.01127	0	65535	#NUM!	0.01127	0.01127	0.01127	0.01127
CG	-0.0004	0	65535	#NUM!	-0.0004	-0.0004	-0.0004	-0.0004
SU	-0.0158	0	65535	#NUM!	-0.0158	-0.0158	-0.0158	-0.0158
CC	0	0	65535	#NUM!	0	0	0	0
LO	4.91E-05	0	65535	#NUM!	4.91E-05	4.91E-05	4.91E-05	4.91E-05
TA	-0.00194	0	65535	#NUM!	-0.00194	-0.00194	-0.00194	-0.00194
FI	0	0	65535	#NUM!	0	0	0	0
GG	0.020354	0	65535	#NUM!	0.020354	0.020354	0.020354	0.020354
GD	0.005062	0	65535	#NUM!	0.005062	0.005062	0.005062	0.005062
GT	0.042591	0	65535	#NUM!	0.042591	0.042591	0.042591	0.042591
GA	0	0	65535	#NUM!	0	0	0	0
PD	-0.00578	0	65535	#NUM!	-0.00578	-0.00578	-0.00578	-0.00578
PP	-0.00175	0	65535	#NUM!	-0.00175	-0.00175	-0.00175	-0.00175
pcc	0	0	65535	#NUM!	0	0	0	0

Textural

SUMMARY OUTPUT

Regression Statistics	
Multiple R	0.302584
R Square	0.091557
Adjusted R Square	
Standard Error	0.076736
Observations	11

ANOVA

	df	*SS*	*MS*	*F*	*Significance F*
Regression	3	0.004748	0.001583	0.40314	0.755446
Residual	8	0.047107	0.005888		
Total	11	0.051855			

	Coefficients	*Standard Error*	*t Stat*	*P-value*	*Lower 95%*	*Upper 95%*	*Lower 95.0%*	*Upper 95.0%*
Intercept	32.87303	0.146984	223.6504	1.79E-16	32.53408	33.21197	32.53408	33.21197
FG	0	0	65535	#NUM!	0	0	0	0
MG	-0.00187	0.002864	-0.65406	#NUM!	-0.00848	0.004731	-0.00848	0.004731
CG	-0.00118	0.001318	-0.89436	0.397238	-0.00422	0.00186	-0.00422	0.00186

SUMMARY OUTPUT

Regression Statistics	
Multiple R	0.882147
R Square	0.778184
Adjusted R Square	0.556368
Standard Error	0.047963
Observations	11

ANOVA

	df	*SS*	*MS*	*F*	*Significance F*
Regression	5	0.040352	0.00807	3.508237	0.097301
Residual	5	0.011502	0.0023		
Total	10	0.051855			

	Coefficients	*Standard Error*	*t Stat*	*P-value*	*Lower 95%*	*Upper 95%*	*Lower 95.0%*	*Upper 95.0%*
Intercept	27.11726	2.292936	11.82643	7.61E-05	21.22308	33.01144	21.22308	33.01144
SU	0.0571	0.023114	2.470363	0.056505	-0.00232	0.116516	-0.00232	0.116516
CC	0.05853	0.023653	2.474464	0.056221	-0.00227	0.119333	-0.00227	0.119333
LO	0.05336	0.022589	2.362168	0.064577	-0.00471	0.111428	-0.00471	0.111428
TA	0.053817	0.02239	2.403612	0.061346	-0.00374	0.111372	-0.00374	0.111372
FI	0.058805	0.022877	2.5705	0.050005	-1.9E-06	0.117612	-1.9E-06	0.117612

Contact nature

SUMMARY OUTPUT

Regression Statistics	
Multiple R	0.852821
R Square	0.727304
Adjusted R Square	0.545506
Standard Error	0.048546
Observations	11

ANOVA

	df	*SS*	*MS*	*F*	*Significance F*
Regression	4	0.037714	0.009428	4.000623	0.064525
Residual	6	0.014141	0.002357		
Total	10	0.051855			

	Coefficients	*Standard Error*	*t Stat*	*P-value*	*Lower 95%*	*Upper 95%*	*Lower 95.0%*	*Upper 95.0%*
Intercept	32.03444	0.269259	118.9725	2.38E-11	31.37559	32.6933	31.37559	32.6933
GG	0.006512	0.002562	2.541935	0.043966	0.000243	0.012781	0.000243	0.012781
GD	0.005679	0.002854	1.989522	0.093778	-0.00131	0.012663	-0.00131	0.012663
GT	0.007545	0.002901	2.601188	0.040598	0.000448	0.014643	0.000448	0.014643
GA	0.006203	0.001654	3.749186	0.009519	0.002155	0.010251	0.002155	0.010251

Packing

SUMMARY OUTPUT

Regression Statistics	
Multiple R	0.688263
R Square	0.473706
Adjusted R Square	0.248152
Standard Error	0.062439
Observations	11

ANOVA

	df	*SS*	*MS*	*F*	*Significance F*
Regression	3	0.024564	0.008188	2.100185	0.188672
Residual	7	0.027291	0.003899		
Total	10	0.051855			

	Coefficients	*Standard Error*	*t Stat*	*P-value*	*Lower 95%*	*Upper 95%*	*Lower 95.0%*	*Upper 95.0%*
Intercept	32.95251	0.106723	308.7657	9.87E-16	32.70015	33.20487	32.70015	33.20487
PD	-0.0004	0.000976	-0.41149	0.693022	-0.00271	0.001906	-0.00271	0.001906
PP	-0.00313	0.002612	-1.19832	0.269783	-0.00931	0.003047	-0.00931	0.003047
pcc	0.151023	0.294853	0.512199	0.624272	-0.54619	0.84824	-0.54619	0.84824

B2

SUMMARY OUTPUT

Regression Statistics	
Multiple R	1
R Square	1
Adjusted R Square	65535
Standard Error	0
Observations	11

ANOVA

	df	*SS*	*MS*	*F*	*Significance F*
Regression	15	1.36E-07	9.09E-09	#NUM!	#NUM!
Residual	0	0	65535		
Total	15	1.36E-07			

	Coefficients	*Standard Error*	*t Stat*	*P-value*	*Lower 95%*	*Upper 95%*	*Lower 95.0%*	*Upper 95.0%*
Intercept	0.938541	0	65535	#NUM!	0.938541	0.938541	0.938541	0.938541
FG	0	0	65535	#NUM!	0	0	0	0
MG	1.66E-05	0	65535	#NUM!	1.66E-05	1.66E-05	1.66E-05	1.66E-05
CG	-8.5E-07	0	65535	#NUM!	-8.5E-07	-8.5E-07	-8.5E-07	-8.5E-07
SU	-2.3E-05	0	65535	#NUM!	-2.3E-05	-2.3E-05	-2.3E-05	-2.3E-05
CC	0	0	65535	#NUM!	0	0	0	0
LO	3.9E-07	0	65535	#NUM!	3.9E-07	3.9E-07	3.9E-07	3.9E-07
TA	-2.6E-06	0	65535	#NUM!	-2.6E-06	-2.6E-06	-2.6E-06	-2.6E-06
FI	0	0	65535	#NUM!	0	0	0	0
GG	3.13E-05	0	65535	#NUM!	3.13E-05	3.13E-05	3.13E-05	3.13E-05

GD	7.8E-06	0	65535	#NUM!	7.8E-06	7.8E-06	7.8E-06	7.8E-06
GT	6.46E-05	0	65535	#NUM!	6.46E-05	6.46E-05	6.46E-05	6.46E-05
GA	0	0	65535	#NUM!	0	0	0	0
PD	-8.5E-06	0	65535	#NUM!	-8.5E-06	-8.5E-06	-8.5E-06	-8.5E-06
PP	-3.8E-06	0	65535	#NUM!	-3.8E-06	-3.8E-06	-3.8E-06	-3.8E-06
pcc	0	0	65535	#NUM!	0	0	0	0

TEX

SUMMARY OUTPUT

Regression Statistics	
Multiple R	0.332945
R Square	0.110852
Adjusted R Square	-0.23643
Standard Error	0.000123
Observations	11

ANOVA

	df	*SS*	*MS*	*F*	*Significance F*
Regression	3	1.51E-08	5.04E-09	0.49869	0.694839
Residual	8	1.21E-07	1.52E-08		
Total	11	1.36E-07			

	Coefficients	*Standard Error*	*t Stat*	*P-value*	*Lower 95%*	*Upper 95%*	*Lower 95.0%*	*Upper 95.0%*
Intercept	0.940907	0.000236	3990.09	1.74E-26	0.940363	0.941451	0.940363	0.941451
FG	0	0	65535	#NUM!	0	0	0	0
MG	-2.8E-06	4.59E-06	-0.60879	#NUM!	-1.3E-05	7.8E-06	-1.3E-05	7.8E-06
CG	-2E-06	2.11E-06	-0.96772	0.361524	-6.9E-06	2.83E-06	-6.9E-06	2.83E-06

CT

SUMMARY OUTPUT

Regression Statistics	
Multiple R	0.882826
R Square	0.779382
Adjusted R Square	0.558765
Standard Error	7.76E-05
Observations	11

ANOVA

	df	*SS*	*MS*	*F*	*Significance F*
Regression	5	1.06E-07	2.13E-08	3.532728	0.096137
Residual	5	3.01E-08	6.02E-09		

Total	10	1.36E-07

	Coefficients	*Standard Error*	*t Stat*	*P-value*	*Lower 95%*	*Upper 95%*	*Lower 95.0%*	*Upper 95.0%*
Intercept	0.932254	0.003708	251.3987	1.89E-11	0.922722	0.941787	0.922722	0.941787
SU	8.57E-05	3.74E-05	2.29185	0.070486	-1E-05	0.000182	-1E-05	0.000182
CC	8.77E-05	3.83E-05	2.292912	0.070393	-1.1E-05	0.000186	-1.1E-05	0.000186
LO	8.01E-05	3.65E-05	2.192995	0.079795	-1.4E-05	0.000174	-1.4E-05	0.000174
TA	8.06E-05	3.62E-05	2.226835	0.076469	-1.2E-05	0.000174	-1.2E-05	0.000174
FI	8.88E-05	3.7E-05	2.399172	0.061684	-6.3E-06	0.000184	-6.3E-06	0.000184

CN

SUMMARY OUTPUT

Regression Statistics	
Multiple R	0.881368
R Square	0.77681
Adjusted R Square	0.628017
Standard Error	7.12E-05
Observations	11

ANOVA

	df	*SS*	*MS*	*F*	*Significance F*
Regression	4	1.06E-07	2.65E-08	5.220737	0.037027

Residual	6	3.04E-08	5.07E-09	
Total	10	1.36E-07		

	Coefficients	*Standard Error*	*t Stat*	*P-value*	*Lower 95%*	*Upper 95%*	*Lower 95.0%*	*Upper 95.0%*
Intercept	0.939562	0.000395	2378.491	3.73E-19	0.938596	0.940529	0.938596	0.940529
GG	1.05E-05	3.76E-06	2.781461	0.031935	1.26E-06	1.97E-05	1.26E-06	1.97E-05
GD	8.71E-06	4.19E-06	2.078836	0.082868	-1.5E-06	1.9E-05	-1.5E-06	1.9E-05
GT	1.21E-05	4.26E-06	2.84643	0.029319	1.7E-06	2.25E-05	1.7E-06	2.25E-05
GA	1.02E-05	2.43E-06	4.202034	0.005673	4.26E-06	1.61E-05	4.26E-06	1.61E-05

PACKING

SUMMARY OUTPUT

Regression Statistics	
Multiple R	0.720616
R Square	0.519287
Adjusted R Square	0.313267
Standard Error	9.68E-05
Observations	11

ANOVA

	df	*SS*	*MS*	*F*	*Significance F*
Regression	3	7.08E-08	2.36E-08	2.520568	0.141577

Residual	7	6.56E-08	9.36E-09
Total	10	1.36E-07	

	Coefficients	*Standard Error*	*t Stat*	*P-value*	*Lower 95%*	*Upper 95%*	*Lower 95.0%*	*Upper 95.0%*
Intercept	0.94106	0.000165	5689.487	1.37E-24	0.940669	0.941451	0.940669	0.941451
PD	-3.4E-07	1.51E-06	-0.22255	0.830236	-3.9E-06	3.24E-06	-3.9E-06	3.24E-06
PP	-5.9E-06	4.05E-06	-1.46224	0.187071	-1.5E-05	3.65E-06	-1.5E-05	3.65E-06
pcc	0.000289	0.000457	0.631569	0.547731	-0.00079	0.001369	-0.00079	0.001369

B3

SUMMARY OUTPUT

Regression Statistics	
Multiple R	1
R Square	1
Adjusted R Square	65535
Standard Error	0
Observations	11

ANOVA

	df	*SS*	*MS*	*F*	*Significance F*
Regression	15	0.063941	0.004263	#NUM!	#NUM!
Residual	0	0	65535		

Total	15	0.063941

	Coefficients	*Standard Error*	*t Stat*	*P-value*	*Lower 95%*	*Upper 95%*	*Lower 95.0%*	*Upper 95.0%*
Intercept	-2.31017	0	65535	#NUM!	-2.31017	-2.31017	-2.31017	-2.31017
FG	0	0	65535	#NUM!	0	0	0	0
MG	0.020843	0	65535	#NUM!	0.020843	0.020843	0.020843	0.020843
CG	0.000559	0	65535	#NUM!	0.000559	0.000559	0.000559	0.000559
SU	-0.02401	0	65535	#NUM!	-0.02401	-0.02401	-0.02401	-0.02401
CC	0	0	65535	#NUM!	0	0	0	0
LO	-0.00015	0	65535	#NUM!	-0.00015	-0.00015	-0.00015	-0.00015
TA	-0.00063	0	65535	#NUM!	-0.00063	-0.00063	-0.00063	-0.00063
FI	0	0	65535	#NUM!	0	0	0	0
GG	0.025501	0	65535	#NUM!	0.025501	0.025501	0.025501	0.025501
GD	-0.00035	0	65535	#NUM!	-0.00035	-0.00035	-0.00035	-0.00035
GT	0.060689	0	65535	#NUM!	0.060689	0.060689	0.060689	0.060689
GA	0	0	65535	#NUM!	0	0	0	0
PD	-0.01027	0	65535	#NUM!	-0.01027	-0.01027	-0.01027	-0.01027
PP	0.005594	0	65535	#NUM!	0.005594	0.005594	0.005594	0.005594
pcc	0	0	65535	#NUM!	0	0	0	0

SUMMARY OUTPUT

Regression Statistics	
Multiple R	0.553553
R Square	0.306421

Adjusted R Square	0.008026
Standard Error	0.074455
Observations	11

ANOVA

	df	*SS*	*MS*	*F*	*Significance F*
Regression	3	0.019593	0.006531	1.767184	0.240669
Residual	8	0.044348	0.005544		
Total	11	0.063941			

	Coefficients	*Standard Error*	*t Stat*	*P-value*	*Lower 95%*	*Upper 95%*	*Lower 95.0%*	*Upper 95.0%*
Intercept	0.245814	0.142616	1.723613	0.123069	-0.08306	0.574687	-0.08306	0.574687
FG	0	0	65535	#NUM!	0	0	0	0
MG	-0.00192	0.002779	-0.69002	#NUM!	-0.00832	0.00449	-0.00832	0.00449
CG	0.000687	0.001279	0.537174	0.605762	-0.00226	0.003635	-0.00226	0.003635

SUMMARY OUTPUT

Regression Statistics	
Multiple R	0.722779
R Square	0.522409
Adjusted R Square	0.044819

Standard Error	0.078151
Observations	11

ANOVA

	df	*SS*	*MS*	*F*	*Significance F*
Regression	5	0.033404	0.006681	1.093843	0.461995
Residual	5	0.030538	0.006108		
Total	10	0.063941			

	Coefficients	*Standard Error*	*t Stat*	*P-value*	*Lower 95%*	*Upper 95%*	*Lower 95.0%*	*Upper 95.0%*
Intercept	-6.68227	3.736123	-1.78856	0.133713	-16.2863	2.921735	-16.2863	2.921735
SU	0.070777	0.037662	1.879285	0.118986	-0.02604	0.16759	-0.02604	0.16759
CC	0.070733	0.038541	1.835258	0.125913	-0.02834	0.169806	-0.02834	0.169806
LO	0.066755	0.036807	1.813645	0.129464	-0.02786	0.161371	-0.02786	0.161371
TA	0.067031	0.036482	1.837353	0.125574	-0.02675	0.160812	-0.02675	0.160812
FI	0.068665	0.037276	1.842071	0.124815	-0.02716	0.164485	-0.02716	0.164485

SUMMARY OUTPUT

Regression Statistics	
Multiple R	0.519898
R Square	0.270294
Adjusted R Square	-0.21618

Standard Error	0.088184
Observations	11

ANOVA

	df	*SS*	*MS*	*F*	*Significance F*
Regression	4	0.017283	0.004321	0.555622	0.703614
Residual	6	0.046658	0.007776		
Total	10	0.063941			

	Coefficients	*Standard Error*	*t Stat*	*P-value*	*Lower 95%*	*Upper 95%*	*Lower 95.0%*	*Upper 95.0%*
Intercept	0.044502	0.489106	0.090986	0.930465	-1.1523	1.241301	-1.1523	1.241301
GG	0.001876	0.004654	0.403174	0.700794	-0.00951	0.013263	-0.00951	0.013263
GD	-0.0014	0.005185	-0.27068	0.795711	-0.01409	0.011284	-0.01409	0.011284
GT	0.003771	0.005269	0.715665	0.501087	-0.00912	0.016664	-0.00912	0.016664
GA	0.000644	0.003005	0.214305	0.837407	-0.00671	0.007998	-0.00671	0.007998

SUMMARY OUTPUT

Regression Statistics	
Multiple R	0.595707
R Square	0.354867
Adjusted R Square	0.078381
Standard Error	0.076766

Observations	11

ANOVA

	df	*SS*	*MS*	*F*	*Significance F*
Regression	3	0.022691	0.007564	1.283492	0.352236
Residual	7	0.041251	0.005893		
Total	10	0.063941			

	Coefficients	*Standard Error*	*t Stat*	*P-value*	*Lower 95%*	*Upper 95%*	*Lower 95.0%*	*Upper 95.0%*
Intercept	0.08188	0.13121	0.62404	0.552387	-0.22838	0.392143	-0.22838	0.392143
PD	-0.00164	0.0012	-1.37022	0.212945	-0.00448	0.001193	-0.00448	0.001193
PP	0.001313	0.003212	0.408753	0.694937	-0.00628	0.008907	-0.00628	0.008907
pcc	0.197181	0.362505	0.543939	0.603368	-0.66001	1.054369	-0.66001	1.054369

B4

SUMMARY OUTPUT

Regression Statistics	
Multiple R	1
R Square	1
Adjusted R Square	65535
Standard Error	0

Observations	11

ANOVA

	df	*SS*	*MS*	*F*	*Significance F*
Regression	15	3.68E-05	2.45E-06	#NUM!	#NUM!
Residual	0	0	65535		
Total	15	3.68E-05			

	Coefficients	*Standard Error*	*t Stat*	*P-value*	*Lower 95%*	*Upper 95%*	*Lower 95.0%*	*Upper 95.0%*
Intercept	-0.04633	0	65535	#NUM!	-0.04633	-0.04633	-0.04633	-0.04633
FG	0	0	65535	#NUM!	0	0	0	0
MG	0.000432	0	65535	#NUM!	0.000432	0.000432	0.000432	0.000432
CG	-9.2E-06	0	65535	#NUM!	-9.2E-06	-9.2E-06	-9.2E-06	-9.2E-06
SU	-0.00044	0	65535	#NUM!	-0.00044	-0.00044	-0.00044	-0.00044
CC	0	0	65535	#NUM!	0	0	0	0
LO	4.85E-05	0	65535	#NUM!	4.85E-05	4.85E-05	4.85E-05	4.85E-05
TA	0.000111	0	65535	#NUM!	0.000111	0.000111	0.000111	0.000111
FI	0	0	65535	#NUM!	0	0	0	0
GG	0.000421	0	65535	#NUM!	0.000421	0.000421	0.000421	0.000421
GD	-0.00013	0	65535	#NUM!	-0.00013	-0.00013	-0.00013	-0.00013
GT	0.001109	0	65535	#NUM!	0.001109	0.001109	0.001109	0.001109
GA	0	0	65535	#NUM!	0	0	0	0
PD	-0.00018	0	65535	#NUM!	-0.00018	-0.00018	-0.00018	-0.00018
PP	0.00014	0	65535	#NUM!	0.00014	0.00014	0.00014	0.00014
pcc	0	0	65535	#NUM!	0	0	0	0

SUMMARY OUTPUT

Regression Statistics	
Multiple R	0.484811
R Square	0.235042
Adjusted R Square	-0.0812
Standard Error	0.001876
Observations	11

ANOVA

	df	*SS*	*MS*	*F*	*Significance F*
Regression	3	8.65E-06	2.88E-06	1.229044	0.36843
Residual	8	2.82E-05	3.52E-06		
Total	11	3.68E-05			

	Coefficients	*Standard Error*	*t Stat*	*P-value*	*Lower 95%*	*Upper 95%*	*Lower 95.0%*	*Upper 95.0%*
Intercept	0.003098	0.003594	0.861843	0.41386	-0.00519	0.011386	-0.00519	0.011386
FG	0	0	65535	#NUM!	0	0	0	0
MG	-3.7E-05	7E-05	-0.52718	#NUM!	-0.0002	0.000125	-0.0002	0.000125
CG	1.6E-05	3.22E-05	0.497149	0.632457	-5.8E-05	9.03E-05	-5.8E-05	9.03E-05

SUMMARY OUTPUT

Regression Statistics	
Multiple R	0.763201
R Square	0.582475
Adjusted R Square	0.16495
Standard Error	0.001753
Observations	11

ANOVA

	df	*SS*	*MS*	*F*	*Significance F*
Regression	5	2.14E-05	4.29E-06	1.395066	0.361883
Residual	5	1.54E-05	3.07E-06		
Total	10	3.68E-05			

	Coefficients	*Standard Error*	*t Stat*	*P-value*	*Lower 95%*	*Upper 95%*	*Lower 95.0%*	*Upper 95.0%*
Intercept	-0.03013	0.083828	-0.35945	0.733942	-0.24562	0.185354	-0.24562	0.185354
SU	0.000336	0.000845	0.397075	0.707695	-0.00184	0.002508	-0.00184	0.002508
CC	0.000281	0.000865	0.325224	0.758179	-0.00194	0.002504	-0.00194	0.002504
LO	0.000363	0.000826	0.439665	0.678533	-0.00176	0.002486	-0.00176	0.002486
TA	0.000389	0.000819	0.474906	0.654873	-0.00172	0.002493	-0.00172	0.002493
FI	0.000289	0.000836	0.345627	0.74369	-0.00186	0.002439	-0.00186	0.002439

SUMMARY OUTPUT

Regression Statistics	
Multiple R	0.765738
R Square	0.586354
Adjusted R Square	0.31059
Standard Error	0.001593
Observations	11

ANOVA

	df	*SS*	*MS*	*F*	*Significance F*
Regression	4	2.16E-05	5.4E-06	2.126291	0.195275
Residual	6	1.52E-05	2.54E-06		
Total	10	3.68E-05			

	Coefficients	*Standard Error*	*t Stat*	*P-value*	*Lower 95%*	*Upper 95%*	*Lower 95.0%*	*Upper 95.0%*
Intercept	0.015032	0.008837	1.701027	0.139841	-0.00659	0.036655	-0.00659	0.036655
GG	-0.00011	8.41E-05	-1.30151	0.24082	-0.00032	9.63E-05	-0.00032	9.63E-05
GD	-0.00017	9.37E-05	-1.85863	0.112438	-0.0004	5.51E-05	-0.0004	5.51E-05
GT	-7.6E-05	9.52E-05	-0.79749	0.45556	-0.00031	0.000157	-0.00031	0.000157
GA	-9.7E-05	5.43E-05	-1.79377	0.123009	-0.00023	3.55E-05	-0.00023	3.55E-05

SUMMARY OUTPUT

Regression Statistics	
Multiple R	0.517274
R Square	0.267573
Adjusted R Square	-0.04632
Standard Error	0.001963
Observations	11

ANOVA

	df	*SS*	*MS*	*F*	*Significance F*
Regression	3	9.85E-06	3.28E-06	0.85242	0.508167
Residual	7	2.7E-05	3.85E-06		
Total	10	3.68E-05			

	Coefficients	*Standard Error*	*t Stat*	*P-value*	*Lower 95%*	*Upper 95%*	*Lower 95.0%*	*Upper 95.0%*
Intercept	-0.00182	0.003355	-0.54157	0.604916	-0.00975	0.006116	-0.00975	0.006116
PD	4.45E-06	3.07E-05	0.144869	0.888897	-6.8E-05	7.7E-05	-6.8E-05	7.7E-05
PP	5.48E-05	8.21E-05	0.666778	0.526274	-0.00014	0.000249	-0.00014	0.000249
pcc	-0.00062	0.009269	-0.06702	0.948441	-0.02254	0.021296	-0.02254	0.021296

SUMMARY OUTPUT

Regression Statistics	
Multiple R	0.582683
R Square	0.33952
Adjusted R Square	0.174399
Standard Error	0.001744
Observations	11

ANOVA

	df	*SS*	*MS*	*F*	*Significance F*
Regression	2	1.25E-05	6.25E-06	2.056198	0.1903
Residual	8	2.43E-05	3.04E-06		
Total	10	3.68E-05			

	Coefficients	*Standard Error*	*t Stat*	*P-value*	*Lower 95%*	*Upper 95%*	*Lower 95.0%*	*Upper 95.0%*
Intercept	0.004454	0.001164	3.825575	0.00505	0.001769	0.007139	0.001769	0.007139
GD	-5.4E-05	5.58E-05	-0.96079	0.364792	-0.00018	7.5E-05	-0.00018	7.5E-05
GA	-6.4E-05	3.24E-05	-1.98647	0.082221	-0.00014	1.04E-05	-0.00014	1.04E-05

SUMMARY OUTPUT

Regression Statistics	
Multiple R	0.513134

R Square	0.263307
Adjusted R Square	0.181452
Standard Error	0.001736
Observations	11

ANOVA

	df	*SS*	*MS*	*F*	*Significance F*
Regression	1	9.7E-06	9.7E-06	3.216752	0.106475
Residual	9	2.71E-05	3.01E-06		
Total	10	3.68E-05			

	Coefficients	*Standard Error*	*t Stat*	*P-value*	*Lower 95%*	*Upper 95%*	*Lower 95.0%*	*Upper 95.0%*
Intercept	0.003533	0.000658	5.368423	0.000451	0.002044	0.005022	0.002044	0.005022
GA	-5.5E-05	3.09E-05	-1.79353	0.106475	-0.00013	1.45E-05	-0.00013	1.45E-05

B5

SUMMARY OUTPUT

Regression Statistics	
Multiple R	1
R Square	1
Adjusted R Square	65535

Standard Error	0
Observations	11

ANOVA

	df	*SS*	*MS*	*F*	*Significance F*
Regression	15	0.009658	0.000644	#NUM!	#NUM!
Residual	0	0	65535		
Total	15	0.009658			

	Coefficients	*Standard Error*	*t Stat*	*P-value*	*Lower 95%*	*Upper 95%*	*Lower 95.0%*	*Upper 95.0%*
Intercept	-0.34056	0	65535	#NUM!	-0.34056	-0.34056	-0.34056	-0.34056
FG	0	0	65535	#NUM!	0	0	0	0
MG	0.005437	0	65535	#NUM!	0.005437	0.005437	0.005437	0.005437
CG	-9.7E-05	0	65535	#NUM!	-9.7E-05	-9.7E-05	-9.7E-05	-9.7E-05
SU	-0.0041	0	65535	#NUM!	-0.0041	-0.0041	-0.0041	-0.0041
CC	0	0	65535	#NUM!	0	0	0	0
LO	0.001492	0	65535	#NUM!	0.001492	0.001492	0.001492	0.001492
TA	0.002608	0	65535	#NUM!	0.002608	0.002608	0.002608	0.002608
FI	0	0	65535	#NUM!	0	0	0	0
GG	0.003178	0	65535	#NUM!	0.003178	0.003178	0.003178	0.003178
GD	-0.00201	0	65535	#NUM!	-0.00201	-0.00201	-0.00201	-0.00201
GT	0.010593	0	65535	#NUM!	0.010593	0.010593	0.010593	0.010593
GA	0	0	65535	#NUM!	0	0	0	0
PD	-0.00237	0	65535	#NUM!	-0.00237	-0.00237	-0.00237	-0.00237
PP	0.000776	0	65535	#NUM!	0.000776	0.000776	0.000776	0.000776
pcc	0	0	65535	#NUM!	0	0	0	0

SUMMARY OUTPUT

Regression Statistics	
Multiple R	0.175016
R Square	0.030631
Adjusted R Square	-0.33671
Standard Error	0.034209
Observations	11

ANOVA

	df	*SS*	*MS*	*F*	*Significance F*
Regression	3	0.000296	9.86E-05	0.126395	0.941465
Residual	8	0.009362	0.00117		
Total	11	0.009658			

	Coefficients	*Standard Error*	*t Stat*	*P-value*	*Lower 95%*	*Upper 95%*	*Lower 95.0%*	*Upper 95.0%*
Intercept	0.028877	0.065525	0.440698	0.671097	-0.12222	0.179978	-0.12222	0.179978
FG	0	0	65535	#NUM!	0	0	0	0
MG	0.000626	0.001277	0.49065	#NUM!	-0.00232	0.00357	-0.00232	0.00357
CG	0.000187	0.000587	0.318131	0.758531	-0.00117	0.001542	-0.00117	0.001542

SUMMARY OUTPUT

Regression Statistics	
Multiple R	0.771459
R Square	0.595149
Adjusted R Square	0.190299
Standard Error	0.027964
Observations	11

ANOVA

	df	*SS*	*MS*	*F*	*Significance F*
Regression	5	0.005748	0.00115	1.470047	0.341378
Residual	5	0.00391	0.000782		
Total	10	0.009658			

	Coefficients	*Standard Error*	*t Stat*	*P-value*	*Lower 95%*	*Upper 95%*	*Lower 95.0%*	*Upper 95.0%*
Intercept	0.593403	1.336857	0.443879	0.675681	-2.8431	4.029903	-2.8431	4.029903
SU	-0.0057	0.013476	-0.42274	0.69005	-0.04034	0.028945	-0.04034	0.028945
CC	-0.00686	0.013791	-0.49735	0.640038	-0.04231	0.028591	-0.04231	0.028591
LO	-0.00439	0.01317	-0.33301	0.752636	-0.03824	0.02947	-0.03824	0.02947
TA	-0.00414	0.013054	-0.31692	0.764111	-0.03769	0.029419	-0.03769	0.029419
FI	-0.00472	0.013338	-0.35389	0.737852	-0.03901	0.029566	-0.03901	0.029566

SUMMARY OUTPUT

Regression Statistics	
Multiple R	0.876673
R Square	0.768556
Adjusted R Square	0.61426
Standard Error	0.019301
Observations	11

ANOVA

	df	*SS*	*MS*	*F*	*Significance F*
Regression	4	0.007422	0.001856	4.981054	0.040982
Residual	6	0.002235	0.000373		
Total	10	0.009658			

	Coefficients	*Standard Error*	*t Stat*	*P-value*	*Lower 95%*	*Upper 95%*	*Lower 95.0%*	*Upper 95.0%*
Intercept	0.436441	0.107052	4.076899	0.006525	0.174494	0.698389	0.174494	0.698389
GG	-0.00379	0.001019	-3.72125	0.009838	-0.00628	-0.0013	-0.00628	-0.0013
GD	-0.004	0.001135	-3.52094	0.012504	-0.00677	-0.00122	-0.00677	-0.00122
GT	-0.0035	0.001153	-3.03455	0.022963	-0.00632	-0.00068	-0.00632	-0.00068
GA	-0.00101	0.000658	-1.53049	0.176772	-0.00262	0.000603	-0.00262	0.000603

SUMMARY OUTPUT

Regression Statistics	
Multiple R	0.422427
R Square	0.178445
Adjusted R Square	-0.17365
Standard Error	0.033667
Observations	11

ANOVA

	df	*SS*	*MS*	*F*	*Significance F*
Regression	3	0.001723	0.000574	0.506808	0.689878
Residual	7	0.007934	0.001133		
Total	10	0.009658			

	Coefficients	*Standard Error*	*t Stat*	*P-value*	*Lower 95%*	*Upper 95%*	*Lower 95.0%*	*Upper 95.0%*
Intercept	0.123183	0.057545	2.140653	0.069567	-0.01289	0.259255	-0.01289	0.259255
PD	-0.0002	0.000526	-0.38059	0.714792	-0.00144	0.001044	-0.00144	0.001044
PP	0.000119	0.001409	0.084208	0.935249	-0.00321	0.003449	-0.00321	0.003449
pcc	-0.09342	0.158983	-0.58763	0.575241	-0.46936	0.282513	-0.46936	0.282513

SUMMARY OUTPUT

Regression Statistics	
Multiple R	0.82353
R Square	0.678201
Adjusted R Square	0.540287
Standard Error	0.021071
Observations	11

ANOVA

	df	*SS*	*MS*	*F*	*Significance F*
Regression	3	0.00655	0.002183	4.917568	0.038081
Residual	7	0.003108	0.000444		
Total	10	0.009658			

	Coefficients	*Standard Error*	*t Stat*	*P-value*	*Lower 95%*	*Upper 95%*	*Lower 95.0%*	*Upper 95.0%*
Intercept	0.300003	0.064705	4.636489	0.002379	0.147001	0.453006	0.147001	0.453006
GG	-0.00257	0.000692	-3.71524	0.007503	-0.00421	-0.00093	-0.00421	-0.00093
GD	-0.00281	0.000903	-3.10734	0.017145	-0.00494	-0.00067	-0.00494	-0.00067
GT	-0.00202	0.000688	-2.93807	0.021773	-0.00365	-0.00039	-0.00365	-0.00039

B6

SUMMARY OUTPUT

Regression Statistics	
Multiple R	1
R Square	1
Adjusted R Square	65535
Standard Error	0
Observations	11

ANOVA

	df	*SS*	*MS*	*F*	*Significance F*
Regression	15	0.002534	0.000169	#NUM!	#NUM!
Residual	0	0	65535		
Total	15	0.002534			

	Coefficients	*Standard Error*	*t Stat*	*P-value*	*Lower 95%*	*Upper 95%*	*Lower 95.0%*	*Upper 95.0%*
Intercept	-0.66445	0	65535	#NUM!	-0.66445	-0.66445	-0.66445	-0.66445
FG	0	0	65535	#NUM!	0	0	0	0
MG	0.00414	0	65535	#NUM!	0.00414	0.00414	0.00414	0.00414
CG	-1.4E-05	0	65535	#NUM!	-1.4E-05	-1.4E-05	-1.4E-05	-1.4E-05
SU	-0.00471	0	65535	#NUM!	-0.00471	-0.00471	-0.00471	-0.00471
CC	0	0	65535	#NUM!	0	0	0	0
LO	0.000694	0	65535	#NUM!	0.000694	0.000694	0.000694	0.000694
TA	1.46E-05	0	65535	#NUM!	1.46E-05	1.46E-05	1.46E-05	1.46E-05
FI	0	0	65535	#NUM!	0	0	0	0
GG	0.004671	0	65535	#NUM!	0.004671	0.004671	0.004671	0.004671
GD	-0.00043	0	65535	#NUM!	-0.00043	-0.00043	-0.00043	-0.00043
GT	0.011869	0	65535	#NUM!	0.011869	0.011869	0.011869	0.011869

GA	0	0	65535	#NUM!	0	0	0	0
PD	-0.00173	0	65535	#NUM!	-0.00173	-0.00173	-0.00173	-0.00173
PP	0.00112	0	65535	#NUM!	0.00112	0.00112	0.00112	0.00112
pcc	0	0	65535	#NUM!	0	0	0	0

SUMMARY OUTPUT

Regression Statistics	
Multiple R	0.493666
R Square	0.243707
Adjusted R Square	-0.07037
Standard Error	0.015476
Observations	11

ANOVA

	df	*SS*	*MS*	*F*	*Significance F*
Regression	3	0.000617	0.000206	1.288952	0.35066
Residual	8	0.001916	0.00024		
Total	11	0.002534			

	Coefficients	*Standard Error*	*t Stat*	*P-value*	*Lower 95%*	*Upper 95%*	*Lower 95.0%*	*Upper 95.0%*
Intercept	-0.16544	0.029644	-5.58095	0.000522	-0.2338	-0.09708	-0.2338	-0.09708
FG	0	0	65535	#NUM!	0	0	0	0

MG	-0.00028	0.000578	-0.48142	#NUM!	-0.00161	0.001054	-0.00161	0.001054
CG	0.000151	0.000266	0.567209	0.586132	-0.00046	0.000764	-0.00046	0.000764

SUMMARY OUTPUT

Regression Statistics	
Multiple R	0.793409
R Square	0.629498
Adjusted R Square	0.258996
Standard Error	0.013702
Observations	11

ANOVA

	df	*SS*	*MS*	*F*	*Significance F*
Regression	5	0.001595	0.000319	1.699041	0.287456
Residual	5	0.000939	0.000188		
Total	10	0.002534			

	Coefficients	*Standard Error*	*t Stat*	*P-value*	*Lower 95%*	*Upper 95%*	*Lower 95.0%*	*Upper 95.0%*
Intercept	-0.90615	0.655025	-1.38339	0.225126	-2.58995	0.77764	-2.58995	0.77764
SU	0.00757	0.006603	1.146494	0.303478	-0.0094	0.024544	-0.0094	0.024544
CC	0.007135	0.006757	1.05593	0.339327	-0.01023	0.024505	-0.01023	0.024505
LO	0.007742	0.006453	1.199687	0.284002	-0.00885	0.02433	-0.00885	0.02433

TA	0.007521	0.006396	1.175908	0.292567	-0.00892	0.023963	-0.00892	0.023963
FI	0.007107	0.006535	1.087501	0.326437	-0.00969	0.023907	-0.00969	0.023907

SUMMARY OUTPUT

Regression Statistics	
Multiple R	0.727857
R Square	0.529776
Adjusted R Square	0.216293
Standard Error	0.014091
Observations	11

ANOVA

	df	*SS*	*MS*	*F*	*Significance F*
Regression	4	0.001342	0.000336	1.689969	0.269216
Residual	6	0.001191	0.000199		
Total	10	0.002534			

	Coefficients	*Standard Error*	*t Stat*	*P-value*	*Lower 95%*	*Upper 95%*	*Lower 95.0%*	*Upper 95.0%*
Intercept	-0.11481	0.078154	-1.46897	0.192229	-0.30604	0.07643	-0.30604	0.07643
GG	-0.00046	0.000744	-0.61931	0.558481	-0.00228	0.001359	-0.00228	0.001359
GD	-0.00112	0.000829	-1.35264	0.224919	-0.00315	0.000907	-0.00315	0.000907
GT	-1.3E-05	0.000842	-0.01589	0.98784	-0.00207	0.002047	-0.00207	0.002047

GA	-0.00041	0.00048	-0.86175	0.421923	-0.00159	0.000761	-0.00159	0.000761

SUMMARY OUTPUT

Regression Statistics	
Multiple R	0.463042
R Square	0.214407
Adjusted R Square	-0.12228
Standard Error	0.016862
Observations	11

ANOVA

	df	*SS*	*MS*	*F*	*Significance F*
Regression	3	0.000543	0.000181	0.636824	0.614764
Residual	7	0.00199	0.000284		
Total	10	0.002534			

	Coefficients	*Standard Error*	*t Stat*	*P-value*	*Lower 95%*	*Upper 95%*	*Lower 95.0%*	*Upper 95.0%*
Intercept	-0.20426	0.028821	-7.0871	0.000196	-0.27241	-0.13611	-0.27241	-0.13611
PD	6.63E-05	0.000264	0.251501	0.808651	-0.00056	0.00069	-0.00056	0.00069
PP	-3E-05	0.000705	-0.0429	0.966978	-0.0017	0.001638	-0.0017	0.001638
pcc	0.05399	0.079626	0.678046	0.519519	-0.1343	0.242277	-0.1343	0.242277